CONTENTS

ORIGINAL ARTICLES

APPLICATION OF AI-BASED WELDING PROCESS MONITORING FOR QUALITY CONTROL IN PIPE PRODUCTION

S. Gook[1], B. El-Sari[1], M. Biegler[1], M. Rethmeier[2,1,3]

[1]Fraunhofer Institute for Production Systems and Design Technology IPK, Berlin, Germany
[2]Chair of Joining, Technische Universität Berlin, Germany
[3]Bundesanstalt für Materialforschung und -Prüfung (BAM), Berlin, Germany

ABSTRACT

The paper presents the experimental results into the development of a multi-channel system for monitoring and quality assurance of the multi-wire submerged arc welding (SAW) process for the manufacture of large diameter pipes. Process signals such as welding current, arc voltage and the acoustic signal emitted from the weld zone are recorded and processed to provide information on the stability of the welding process. It was shown by the experiments that the acoustic pattern of the SAW process in a frequency range between 30 Hz and 2.5 kHz contains the most diagnostic information. The on-line quality assessment of the weld seam produced is carried out in combination with methods of artificial intelligence (AI). From the results obtained, it can be concluded that the use of the latest concepts in welding and automation technology, combined with the high potential of AI, can achieve a new level of quality assurance in pipe manufacturing.

KEYWORDS: submerged arc welding, high-strength fine-grain steels, pipe production, artificial intelligence, acoustic signals, quality control

INTRODUCTION

Submerged arc welding (SAW) makes a significant contribution to cost-effective production in industrial manufacturing. Numerous construction units and components from various sectors of industry, such as the oil and gas industry, shipbuilding, petrochemical industry, hydroelectric and offshore wind energy plants, use SAW. SAW guarantees a continuous production cycle and is characterized by high efficiency, which is primarily due to the high deposition rate of this welding process. In practice, single-wire SAW is usually used for component wall thicknesses of up to approx. 10 mm. Parts with a larger thickness, require an increased deposition rate, which can be achieved through the application of multiple wire SAW [1]. Especially, multi-wire SAW processes with up to five electrodes have been proven successfully [2]. Multi-wire SAW techniques are known where a cold wire is added to the welding zone to increase the deposition rate, adjust the welding temperature cycle, and thereby improve the properties of the welded joint [3]. Thick-walled large pipes for transporting oil and gas, foundations and towers for wind turbines are examples of structures where the advantages of multiple wire SAW can be utilized [4]. The Arctic offshore shipbuilding industry also requires a safe and efficient welding process for joining thick steel plates [5]. In these applications, welded constructions must guarantee safe operation of the systems even after years of extreme stress. The welded joints must therefore be of a correspondingly high quality.

In welding practice, it is generally known that the submerged arc welding process is characterized by a relatively high level of robustness. However, it should be noted that due to the increasing demand for welded steel structures in the energy sector and the existing competition, companies are aiming to increase the throughput in the manufacture of their products. This means that welding processes are reaching their limits, which can lead to an increased defect and scrap rate [6, 7]. This problem also applies to multi-wire SAW, in which the consumable welding wires form a common weld pool and each wire electrode is controlled individually. The quality of individual weld seams cannot always be guaranteed in multi-wire SAW. Interaction between the welding wires if the parameter settings are not optimized, for example, can lead to a disrupted welding process. The reproducibility of optimum welding process parameters and technological conditions, particularly with regard to a competitive and consistent high level of production quality, is essential [8].

In welding production, the quality of the products is ensured by the expertise of the personnel and the application of process parameters that have been determined through many years of manufacturing experience. Increased automation of welding does not exclude the possibility of welding defects. Surface defects can be easily recognized, while defects such as slag inclusions, lack of fusion or pores can only be detected by radiographic or ultrasonic testing of the weld seam.

Ensuring that the actual parameters of the ongoing welding process match the set target parameters can be guaranteed by using suitable measuring and moni-

Figure 1. Five-wire SAW test stand for welding sheets and tubes at Fraunhofer IPK in Berlin (left) and multi-wire SAW welding head (right)

toring systems [9, 10]. The most important parameters to be monitored are usually welding current, voltage, welding speed and filler wire feed speed. Such signal recordings provide the operator of the welding system with qualitative information about the stability of the welding process. The decision on the quality of the weld seam is made subjectively.

For reliable quality control with logging and traceability of data, the use of testing methods such as metallographic examinations, ultrasound and X-ray examinations is necessary. The use of the latest concepts in welding and automation technology in combination with the high potential of artificial intelligence (AI), on the other hand, enables a new level of quality assurance for welded products by combining various sensor signals [11].

In contrast to empirical and statistical models, AI models do not require any assumptions or prior knowledge regarding the physical phenomena of a relationship to be modelled, which is why AI models are referred to as data-driven models [12]. This approach enables AI models to capture very complex, highly non-linear relationships [13]. Recent studies have investigated the applicability of various nonlinear methods with AI capabilities in the field of welding, such as the Taguchi method, response surface method (RSM), artificial neural networks (ANN), genetic algorithms (GA), fuzzy logic systems, adaptive neuro-fuzzy inference systems (ANFIS), decision tree methods and particle swarm optimization (PSO) [14–16].

The aim of this study was to investigate the feasibility of AI-based process monitoring in SAW based on process signals such as welding current and voltage, as well as acoustic signals. The results will be used to develop a knowledge-based expert system to assist the operator in determining the optimum parameters for the selected welding task, and to monitor and record these during production.

WELDING EQUIPMENT AND MATERIALS

The welding experiments were conducted on a full-scale industrial welding system (SMS group GmbH) for longitudinal five-wire SAW on large-diameter pipes. The arcs are supplied with current by five electronically controlled current sources of type PERFECTarc® 1500 AC/DC (SMS group GmbH) with a total current of up to 7500 A. The resulting advantages are not limited to high deposition rates and welding speeds. With a programmable waveform for current and voltage, the welding result can be modeled with respect to various factors (e.g. weld geometry) [17]. Both, flat specimens with a length of two meters and large pipes with a length of up to six meters can be welded on the system. The transport carriage with the component to be welded can be moved at a speed of up to 6 m/min. The five-wire SAW system is shown in Figure 1.

Welding tests were carried out on sheets of pipeline steel grade X70 according to API 5L or L485MB according to DIN EN 10208-2 (material no. 1.8977). The welding consumables used were solid wire BA
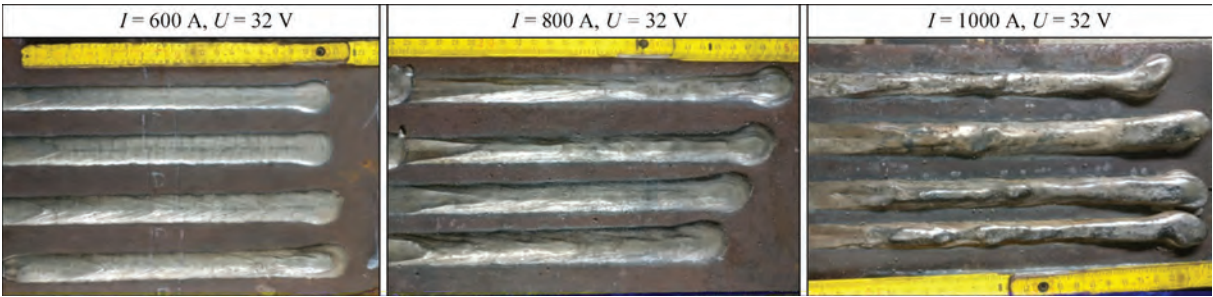
Figure 2. Outer appearance of bead on plates SAW welds produced with different parameters
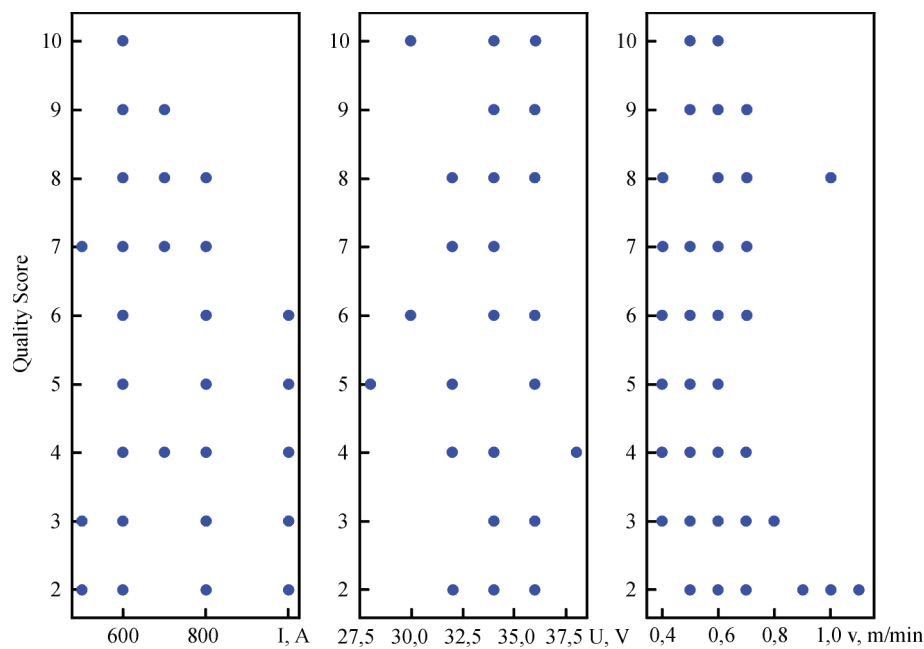
Figure 3. Subjective quality score. Scores are plotted against current (*I*), voltage (*U*) and welding speed (*v*)

S2Mo according to EN ISO 14171-A (EN 756) and an agglomerated welding powder of type BF 5.1.

RESULTS AND DISCUSSION

As a first step, a series of experiments were produced with a single-wire SAW process as bead on plate welds. Parameters such as welding current (*I*), welding voltage (*U*) and welding speed (*v*) were varied. These tests were used to teach the AI model and to analyse the correlation between the welding parameters and the welding result. Examples of bead on plate welds for different welding parameters are shown in Figure 2.

To quantify the weld quality of each specimen, a subjective quality rating was implemented. The rating was measured on a ten-point scale ranging from 1 (unacceptable) to 10 (excellent). The welds were visually inspected by eye to identify any surface discontinuities. These include surface cracking, porosity, undersized welds, undercutting and excessive and uneven reinforcement. Approximately 40 weld seams were characterised. The results of the subjective quality judgement are shown in Figure 3. It is worth noting that increasing the welding current and welding speed above a certain limit decreases the weld quality. This statement is in line with practical welding experience. A single-wire SAW process with a 4 mm thick wire is typically performed with welding currents in the range of 500 to 600 A and welding speeds of 0.4 to 0.6 m/min. As expected, higher values of these process parameters lead to process instabilities and a loss in seam quality.

To assess the internal quality of the welds, metallographic cross sections were taken. A selection of cross sections for welds made with different welding parameters is shown in Figure 4. Although no internal defects such as pores, cracks and slag inclusions were detected, external weld irregularities were confirmed for not optimal welding parameters.

A process signal recording was performed to document the welding tests. All relevant process data such as welding current, voltage, welding speed and wire feed speed (v_f) were recorded during welding and used for further analysis of the welding process. In particular, these recordings were necessary to determine the correlation between signal progression and weld quality. The recorded data of the welding process are shown as an example in Figure 5. The signal curves were ana-
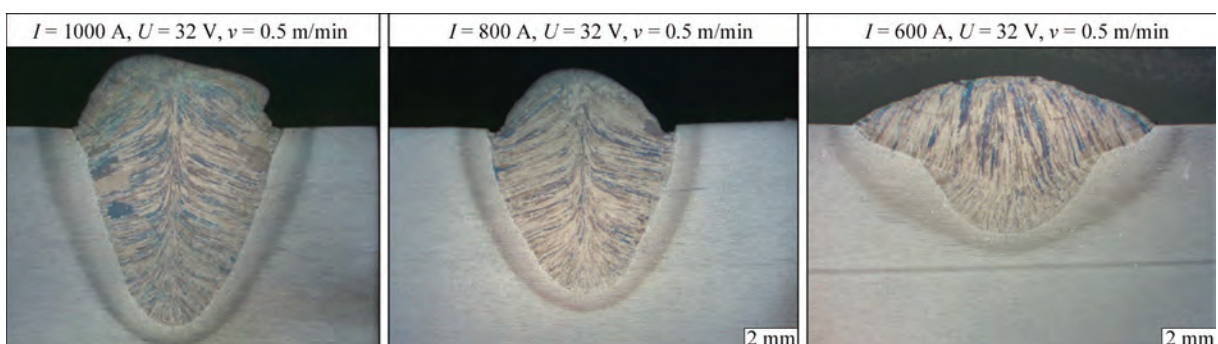
Figure 4. Cross sections of the welds made with different welding parameters
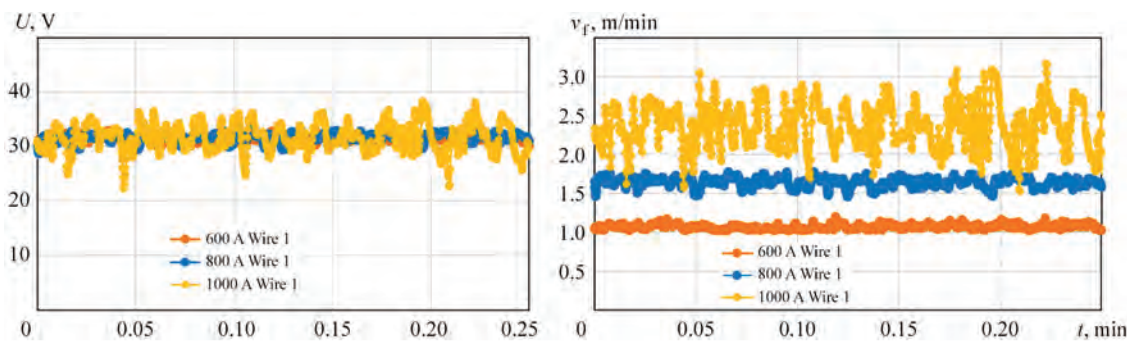
Figure 5. Progressions for the welding voltage and wire feed speed for different welding currents at constant welding speed of the single-wire SAW process

lyzed and a standard deviation was determined for the recorded values. It was found that the higher the welding current, the greater the variation in welding voltage and wire feed speed. The smooth progressions of the welding voltage and wire feeding signals for 600 and 800 A welding current indicate that the welding process is stable. The relatively high fluctuations in welding voltage (31.6±2.6 V) and wire feed speed (2.4±0.6 m/min) at a welding current of 1000 A indicate that the process is leaving the stability range.

The physical explanation for the relationship between the welding voltage and the wire feed speed lies in the control concept of submerged arc welding.

The welding current is constant during the welding process. In the case of process faults, the voltage and therefore the wire feed speed is regulated in order to keep the arc length constant. For this reason, the level of voltage signal fluctuation can be used as a diagnostic feature for evaluating process stability.

The next step in signal acquisition was to record the acoustic signals of the welding process. This method is based on the assumption that each type of welding has its own noise, and this noise can indicate quality problems. For example, metal transfer during welding is a key element of weld quality, and welders use the "noise" of metal transfer to make fine adjustments to
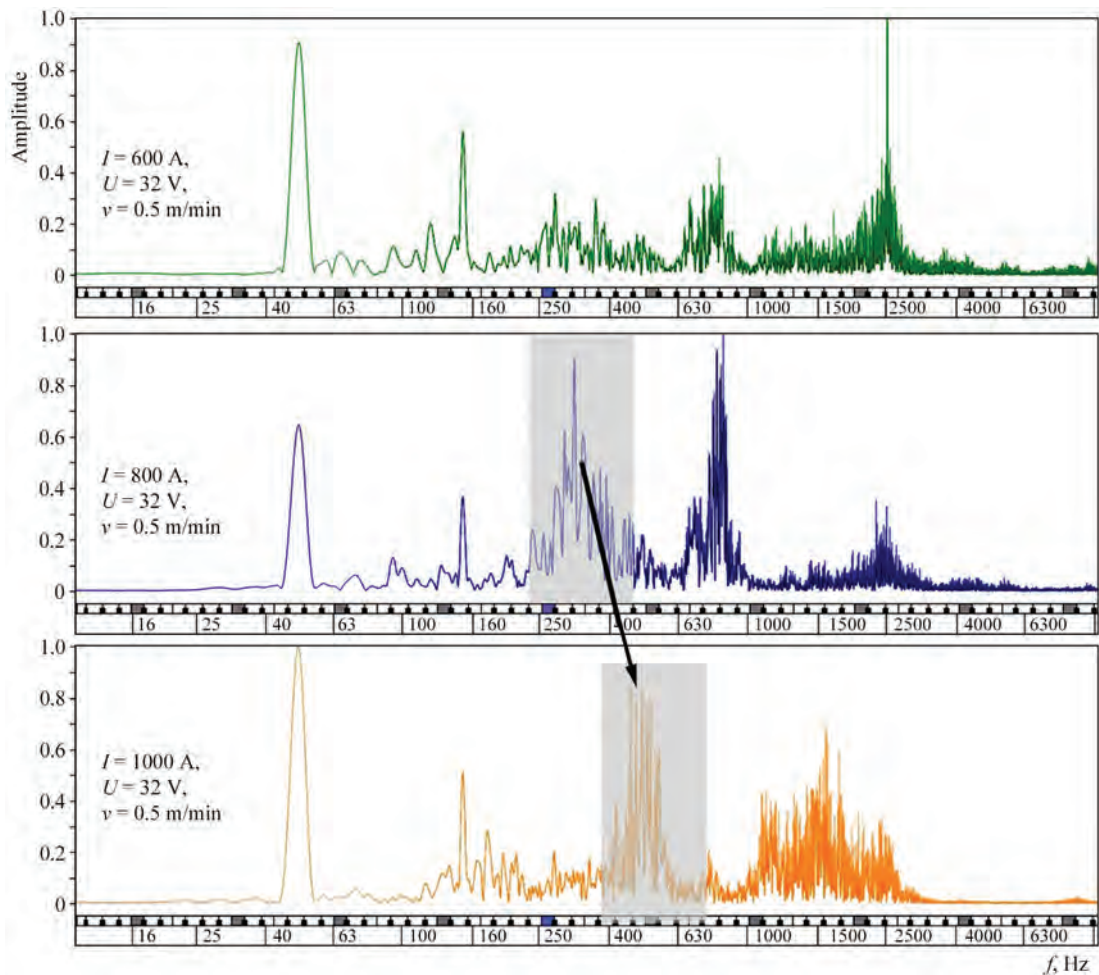
Figure 6. Frequency spectrum of the acoustic signals during submerged arc welding

Table 1. Calculated features and descriptions

Feature name	Description
Mean	Mean frequency in kHz
Standard deviation	Standard deviation of frequency
max v	Maximum fundamental frequency measured across acoustic signal
min v	Minimum fundamental frequency measured across acoustic signal
Median	Median frequency in kHz
Skew	Skewness (measure of asymmetry)
Kurt	Kurtosis (describes the availability of peaks in a distribution)
Q1	First quantile in kHz
Q3	Third quantile in kHz
IQR	Interquantile Range in kHz

welding parameters. However, in mechanized and automated systems, welding often takes place far from the operator and in noisy environments, so this process noise cannot be heard. In these situations, a welding microphone, for example, can provide operators with the sound they need to monitor and control arc stability and even predict when welding problems are occurring.

In this study, the acoustic signals were recorded with a piezoelectric vibro-acoustic sensor attached to the welding torch. The analog signal was converted into a digital form using an analog-to-digital converter. The sampling rate was selected so that the signal could be analyzed in the acoustically audible frequency range. By converting a time signal into its frequency components, it was possible to identify the dominant frequencies in a signal, detect unwanted noise and analyze harmonics. The recorded acoustic signals for various welding parameters were converted into a frequency spectrum (Figure 6).

The analysis of the frequency spectrum shows that the acoustic profile of the welding process tends to be in the low and medium frequency range from approx. 30 to 2.5 kHz. It is worth noting that increasing the welding current from 600 to 800 A results in a visible change in the spectrum. The frequency amplitudes in the range between 270 Hz and 430 Hz increase significantly. A further increase in the welding current up to 1000 A resulted in the amplitudes shifting to the 550–600 Hz range. Such changes in the spectrum of the acoustic signal allow the assumption that the acoustic profile of the welding process clearly depends on the welding parameters applied. In addition, it is assumed that both defect-free and defective weld seams can be identified using the acoustic weld signal.

The welding data from around 40 welds were evaluated in an attempt to classify defective and defect-free seams. The subjective quality points were considered as a reference (see Figure 2). Welds with quality points of five and less were considered defective.

The distribution of the frequency and its amplitude from the spectrum were evaluated using an approach
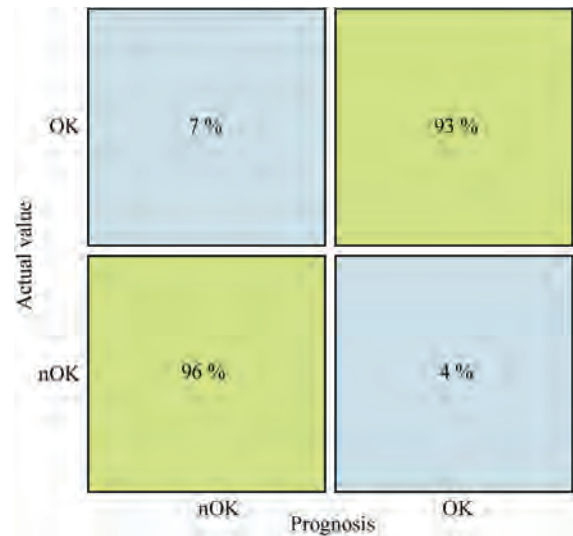
Figure 7. Confusion matrix for precision and accuracy assessment

from the field of AI based voice recognition in Python [18]. The author was able to determine the gender based on the voice with an accuracy of 99 %. The method calculates several statistical features from the frequencies of each signal. The calculated features are listed in Table 1. Preliminary tests have shown that these features are significant for the application in the present use case of this paper. Therefore, the features were extracted from the signals that served as input variables for the AI model.

The AI algorithm was designed to classify the joining quality as "OK"/"nOK" based on the features. A decision tree algorithm was implemented and its predictive capability was investigated using a confusion matrix. The algorithm was trained using 90% of the available data and validated with the rest.

It was shown that the algorithm can predict both classes "OK" and "nOK" equally well (Figure 7). If the prediction is "OK", then the prediction is correct in 93 % of all cases and if the prediction is "nOK", then the prediction is correct in 96 % of all cases.

The results confirm that the algorithm used can predict the joining quality with a high level of precision and accuracy.

CONCLUSIONS

Submerged arc welding (SAW) offers high deposition rates and is widely used in the production of thick-walled large pipes. Since the multi-wire SAW processes reach their limits, there is a high risk of welding defects and rejects. For this reason, it is necessary to introduce process monitoring in order to reduce reject rates and to maintain a constant high level of pipe manufacturing quality. A multi-channel system for monitoring and quality assurance of SAW process offers a solution to this task. The system keeps records of welding current, voltage and wire feed curves, which serve as the basis for process and quality control. In addition, acoustic signals generated by the SAW welding process are recorded. Through the subsequent signal processing, features can be extracted from the signals, which served as input variables for the AI model.

With the proposed AI algorithm using a decision tree, good precision and accuracy in predicting the weld quality could be achieved. The results will be used to develop a knowledge-based expert system to assist the operator in determining the optimum parameters for the selected welding task, and to monitor and record these during production.

REFERENCES

1. Brensing, K.H., Sommer, B. *Herstellverfahren für Stahlrohre*. Salzgitter Großrohre GmbH. www.wv-stahlrohre.de/fileadmin/pdf/Stahlrohre_Herstellverfahren.pdf
2. Moeinifar, S., Kokabi, A.H., Hosseini, H.M. (2011) Role of tandem submerged arc welding thermal cycles on properties of the heat affected zone in X80 microalloyed pipe line steel. *J. of Materials Processing Technology*, 211(**3**), 368–375
3. Feinberg, L.J., Shchegol, V.V., Honcharenko, L.V. (2022) Two-wire submerged-arc welding with cold wire application. *The Paton Welding J*., **1**, 3–8. DOI: https://doi.org/10.37434/tpwj2022.01.01
4. Hochhauser, D.I.F., Rauch, M.R. (2012) Influence of the soft zone on the strength of welded modern HSLA steels. *Welding in the World*, 56(**5–6**), 77–85.
5. Layus, P., Kah, P., Martikainen, J. et al. (2014) Multi-wire SAW of 640 MPa arctic shipbuilding steel plates. *Inter. J. Adv. Manuf. Technol.*, 75(**5–8**), 771–782.
6. Hölbling, W. (2018) TM-Bleche im Extremeinsatz: Schweißen thermomechanisch gewalzter Bleche (TM-Bleche) für Offshore-Gründungen. *Der Praktiker*, Ausgabe 4.
7. Barot, R.S., Patel, V.J. (2021) Process monitoring and internet of things feasibility for submerged arc welding: State of art. *Materials Today: Proc.*, **45**, 4441–4446.
8. Neidel, A., Riesenbeck, S., Giller, M. (2022) Excessive lack of fusion in welds of limited accessibility. *Practical Metallography*, 59(**3**), 164–173.
9. Benakis, M., Du, C., Patran, A., French, R. (2019) Welding process monitoring applications and industry 4.0. In: *Proc. of 15th Inter. Conf. on Automation Science and Engineering, August, 2019*, 1755–1760.
10. Huot, P. (2015) The basics of weld and process monitoring. Quality, 6NDT.
11. Cheng, Y., Yu, R., Zhou, Q. et al. (2021) Real-time sensing of gas metal arc welding process – A literature review and analysis. *J. of Manufacturing Processes*, **70**, 452–469.
12. Chen, C., Lv, N., Chen, S. (2018) Data-driven welding expert system structure based on internet of things. *Transact. on Intelligent Welding Manufacturing*, I(**3**), 45–60).
13. Wang, B., Hu, S.J., Sun, L., Freiheit, T. (2020) Intelligent welding system technologies: State-of-the-art review and perspectives. *J. of Manufacturing Systems*, **56**, 373–91.
14. Gyasi, E.A., Handroos, H., Kah, P. (2019) Survey on artificial intelligence (AI) applied in welding: A future scenario of the influence of AI on technological, economic, educational and social changes. *Procedia Manufacturing*, **38**, 702–714.
15. Panda, B.N., Babhubalendruni, M.V.A.R., Biswal, B.B., Rajput, D.S. (2015) Application of artificial intelligence methods to spot welding of commercial aluminum sheets (B.S. 1050). In: *Proc. of Fourth Inter. Conf. on Soft Computing for Problem Solving, New Delhi 2015*. Eds by K.N. Das, K. Deep, M. Pant et al.
16. Ahmed, F., Kim, K.-Y. (2017) Data-driven weld nugget width prediction with decision tree algorithm. *Procedia Manufacturing*, **10**, 1009–19.
17. Wietrzniok, H., Lichtenthäler, F. (2014) Moderne Großrohrfertigung — Neue Hochleistungs-, Schweißstromquelle für alle Lichtbogenschweißverfahren, DVS Berichte, Band 306, 19–25, DVS-Verlag, Düsseldorf.
18. Subhash, S., Srivatsa, P.N., Siddesh, S. et al. (2020) Artificial intelligence-based voice assistant. In: *Proc. of Fourth World Conf. on Smart Trends in Systems, Security and Sustainability (WorldS4), July, 2020*, 593–596.

ORCID

S. Gook: 0000-0002-4350-3850

CONFLICT OF INTEREST

The Authors declare no conflict of interest

CORRESPONDING AUTHOR

S. Gook
Fraunhofer Institute for Production Systems and Design Technology IPK, Berlin, Germany.
E-mail: sergej.gook@ipk.fraunhofer.de

JOURNAL HOME PAGE

https://patonpublishinghouse.com/eng/journals/tpwj

DEVELOPMENT OF DETONATION GAS SPRAYING TECHNOLOGY OF COATINGS AT THE E.O. PATON ELECTRIC WELDING INSTITUTE OF THE NASU (OVERVIEW)

O.V. Kolisnichenko[1], V.M. Korzhyk[1], P.D. Stukhlyak[2], A.I. Kildiy[1], R. Tovbin[3], M. Shynlov[3], V. Mudrichenko[2]

[1]E.O. Paton Electric Welding Institute of the NASU
11 Kazymyr Malevych Str., 03150, Kyiv, Ukraine
[2]Paton Research Institute of Welding Technologies in Zhejiang Province:
PRC, Zhejiang Province, Hangzhou City, Xiaoshan District, St. Shixing Beilu 857, office. 426
[3]Sputtek Inc. 110 Share Road, Vaughan, Ontario, Canada, L4L 8P4

ABSTRACT

Despite the fact that the detonation gas spraying method is a high-tech process that allows high-quality coatings deposition on products, it has some disadvantages that may limit its widespread use in industry, compared to other thermal coating methods. Such disadvantages include increased safety requirements, low productivity and reliability of structures. However, the use of the latest component base, accumulated technological experience, modern research in the field of detonation processes, and new approaches to the design of detonation units allow us to hope that the detonation gas method will become widespread along with such methods as plasma or High Velocity Oxygen Fuel spraying. The paper shows the leading role of Ukrainian scientists and engineers in the development and implementation of detonation gas spraying of coatings. Particular attention is paid to the work carried out at the E.O. Paton Electric Welding Institute of the NAS of Ukraine. The concepts and development stages of design from classic detonation guns to valveless multi-chamber guns operating at high frequencies are shown. Automated industrial complexes have been created on their base with application of modern components and equipment that allow effective use of the advantages of detonation gas spraying.

KEYWORDS: detonation, coatings, detonation gas unit, valveless design, combustion chamber, production area

INTRODUCTION

High fuel combustion velocity, supersonic velocity of the process, high temperature and higher pressure of combustion products determine the fields of technical application of gas detonation. One of the first most important and currently well-developed accompanying processes for gas detonation is deposition of wear-resistant, thermal protection, corrosion-resistant and other kinds of powder coatings on the surface of various purpose parts. The essence of the method consists in heating and transportation of powder particles to the surface being sprayed using gas detonation.

Development of detonation spraying method is promising in the context of peculiarities, characteristic only for this technology, compared to other numerous thermal coating methods. The cyclic nature of the process, effectiveness of application of the energy of combustion of a flammable mixture, relative simplicity of detonation unit design, etc., allow implementation of the main advantages of detonation spraying method, namely:

● at the same quantity of sprayed powder, the loss of the components of the flammable gas mixture will be smaller at application of detonation combustion mode, compared to deflagration mode;

● detonation spraying units do not require any costly cooling systems;

● low energy consumption. The detonation gun consumes 100 kW, that is sufficient to generate a spark, instead of, for instance, thousands Ws for plasma spraying units;

● detonation complexes can use a standard inexpensive gas feed system with standard hoses, where the pressure in the lines is not higher than 0.3 MPa. In systems of high-velocity oxy-fuel (HVOF) it can be 1 MPa and higher;

● possibility of performing more complex tasks, for instance spraying of coatings without product overheating. The sprayed object is heated up to a temperature not higher than 250 °C, which allows avoiding thermal deformations of different parts, or applying coatings on thin-walled products.

However, the most important point is that when choosing the detonation spraying method, the determinant factor is the quality of the produced coatings, namely:

● high density (porosity < 1 %), due to higher particle velocity;

● increased wear resistance due to harder and stronger coatings;

● higher hardness due to less decomposition of the carbide phases at spraying of metal ceramic coatings;

● improved corrosion protection, due to reduction of through-thickness porosity;

● higher strength of adhesion to the base and increased cohesion strength of the coating;

● lower oxide content due to a shorter time of flight and heating by the products of the spraying powder combustion;

● preservation of the powder chemical composition due to shortening of the time of staying at a high temperature;

● low level of residual stresses;

● lower roughness of the sprayed surface due to a higher impact velocity and smaller particle size of the powder.

A high value of the jet kinetic energy relative to the thermal component kinetic energy make this method better for such applications as spraying wear resistant coatings from metal ceramics, where lower process temperatures prevent decarbonization, and high velocities create practically poreless coatings in a state with minimal residual stresses, making them less prone to cracking.

DEVELOPMENT OF TECHNOLOGICAL DETONATION-GAS SPRAYING UNITS

The question of application of detonation to obtain useful work in energy installations was first raised by Ya.B. Zeldovich in 1940. According to his paper "On the question of energy use of detonation combustion" [1] the thermodynamic effectiveness of detonation units is much higher than the efficiency of units with deflagration combustion of fuel. This is due to the fact that the detonation products have smaller entropy, compared to the products of regular burning, and at isentropic expansion a large portion of chemical energy goes into useful work. As a result, use of the detonation gun will be somewhat more cost-effective, compared to HVOF.

The detonation gas unit for spraying was first developed and patented in the USA by "Union Carbide Corp" in 1955 [2]. The initial stage of studying the method and development of the units for its realization is described in detail in [3, 4]. Creation of this invention was related to investigation of acetylene detonation to look for safe methods of its storage and transportation, conducted at the end of 1940s by Linde Company. Investigation results showed for the first time that the destructive force of gas detonation can be used to perform useful work. The researchers' efforts were aimed at development of the process of deposition of a layer of hard coatings with improved properties, compared to coatings, produced by other spraying methods. This technology, known as Detonation Gun process, became the base of commercial-industrial activities of Linde Division. Development of the method and first unit for detonation gas spraying ensured creation of top quality products. The firm established a wide network of specialized plants for deposition and processing of coatings, located in Japan, Germany and Canada, Great Britain and Switzerland, and for a long time maintained a monopoly for the unique technology.

Many of the advantages of detonation spraying were obvious for specialists immediately after appearance of the first information about the new technology. However, no one was able to reach this level of properties by other methods, although such attempts were made by numerous researchers in many countries of the world. Such a situation was explained in many ways by the monopoly of Praxair Company (former name is Union Carbide Corporation) and no possibility to purchase its equipment.

In 1960s the work on mastering the technology of detonation gas spraying began at the Institute for Problems of Materials of AS of the Ukr.SSR under the leadership of academician G.V. Samsonov [5, 6]. At this moment there was practically no information about the physical fundamentals of the process, and numerous publications in Western media were mostly of promotional nature. Investigations also began at Dnipropetrovsk Chemico-Technological (O.D. Kornev, V.I. Shynkarenko and oth.), metallurgical (T.P. Shmyrjova, G.M. Vorobjov) Institutes, Voroshilovgrad Mechanical Engineering Institute (Yu.O. Kharlamov, B.L. Ryaboshapko and oth.), PA "Kyivarmatura" (O.I. Zverev, V.I. Shesternenkov), CDB "Leninska Kuznya" (Kyiv), E.O. Paton Electric Welding Institute of AS of the Ukr.SSR (Kyiv), OJSC "Motor-Sich" (Zaporizhzhya) and at other organizations. Later on Kharkiv Aviation Institute, Research Institute of Mechanical Engineering Technology (Kharkiv), G.V. Karpenko Physico-Mechanical Institute (Lviv) joined the research. Investigations were focused on studying the stationary gas detonation processes. Gas dynamic parameters of the spraying process were studied, assessment of the energy state of sprayed material particles and clarification of the mechanism of coating layer formation were performed.

The coating deposition processes was performed using detonation units, which included: a combustion chamber in the form of a cylindrical barrel, gas-distribution device, ignition system, powder doser and system of unit control by the specified cyclogram.

For unit operation, oxygen was used as oxidizer, and acetylene was the flammable gas . This way the first local detonation gas units (DGU) appeared: first experimental samples "Soyuz" and "Blyskavka", and then the first production GDU — ""Dnipro" (IMP of AS of the Ukr.SSR), etc. In 1990s the detonation gas units ADM-2 and ADM-4 were created with the participation of specialists of IMP of AS of the Ukr.SSR.

Despite the fact that all the traditional detonation units are designed by the same principle, they differ by the method of introducing the spraying material: axial or radial feed, by the method of feeding the combustible mixture: chambers of direct or preliminary mixing; by the method of detonation initiation: direct or forechamber ignition.

DEVELOPMENT OF THE TECHNOLOGY OF DETONATION SPRAYING AT PWI

Investigations of the process of detonation-gas spraying began to be conducted at PWI since 1980s under the leadership of E.A. Astakhov [7–10]. Taking into account the main postulates of gas detonation theory, a complex of theoretical and experimental investigations were conducted as to selection and development of optimal designs of DGU components. The requirements to the unit main components and gas distribution and control systems, and the main principles of development of detonation equipment were defined. Allowing for powder characteristics and properties (density, dispersity, specific surface, bulk mass, gas permeability, etc.), powder feeders for DGU were developed, which operate with the firing rate of 1–8 Hz. The influence of the method of powder injection (transverse, axial, pulsed, continuous) on ensuring a stable density of the gas-powder mixture along the barrel length was studied. A comprehensive investigation of coatings from different powders was performed. DGU designs developed at the Institute for Problems of Materials of AS of the Ukr.SSR were taken as the base. The work related to mastering detonation spraying of coatings by industry was conducted at the same time. PWI and the Institute of Superhard Materials of the NAS of Ukraine developed units of "Perun" series, and SPA "Orgtekhavtomatizatsia" (Simferopol, Ukraine) mastered their pilot-production. The units have sufficiently different design and operating conditions, but most of the unit components were unified. It allowed producing equipment components in different block combinations. Automated detonation complex (ADC) "Perun-C" [11] is one of the characteristic representatives of this class of units. It has the following fundamental technological capabilities:

● operation of the developed equipment is possible at application of different working gases (propane-butane or hydrogen can be used as fuel, alongside acetylene), and it is allowed to use both nitrogen and compressed air transportation of powder, blowing the coil and barrel, and dilution of explosive mixture;

● control of the properties of sprayed coatings due to the change of spayed particles temperature and velocity in a broad range at the moment of coating layer formation and influence on the degree of their oxidation and change of the chemical and phase composition;

● spraying of a coating on large surfaces with minimal allowance for treatment, which is provided by stable operation of the doser (change of the injected powder dose during operation is not more than 8%) and application of a computer program for unit movement;

● fitting of the unit with two independently controlled powder feeders, which provide a transition from the mode of detonation-abrasive treatment to the mode of coating deposition without switching off the unit; performance of the process of abrasive treatment and spraying in one cycle; spraying a two-component coating without preliminary preparation of powder mixtures and adjustment of their percentage.

Similar to all classical detonation units, "Perun-C" complex uses a cylindrical barrel of a constant diameter for realization of the mode of stationary detonation and further heating and acceleration of the powder. Similar to the majority of the known DGU, electromechanical valves are used in the unit for periodical feeding of the combustible mixture and powder material. Figure 1 shows the design of "Perun-C" detonation gun. Pulsed-axial powder feed through assembly *1* by a preset cyclogram for each pulse is realized in the unit. Combustible hydrocarbon gas and oxygen are fed under pressure of 1.2 atm by supply line *2*, located inside the cooling jacket *3*. After filling of cylindrical barrel *4* up to the set level with the combustible mixture, its ignition by spark plug *5* is performed. It results in heating and acceleration of powder portion already fed into the barrel. Then the detonation unit is blown with nitrogen or air by a preset cyclogram supplied under the pressure of 3 atm. Higher pressure allows blocking the lines of flammable gas and oxygen during the unit blowing and using an electromechanical valve only in the blowing gas line.

"Perun-S" detonation unit is a highly-productive stationary complex, the effectiveness of industrial application of which was manifested particularly at mass and large-scale fabrication of coated products. Technical characteristics of "Perun-S" complex are given below.

Parameter	Value
Frequency of working cycles, Hz	3.3– 6.6
Coating area per cycle, mm^2	320
Coating thickness per cycle, μm	3–10
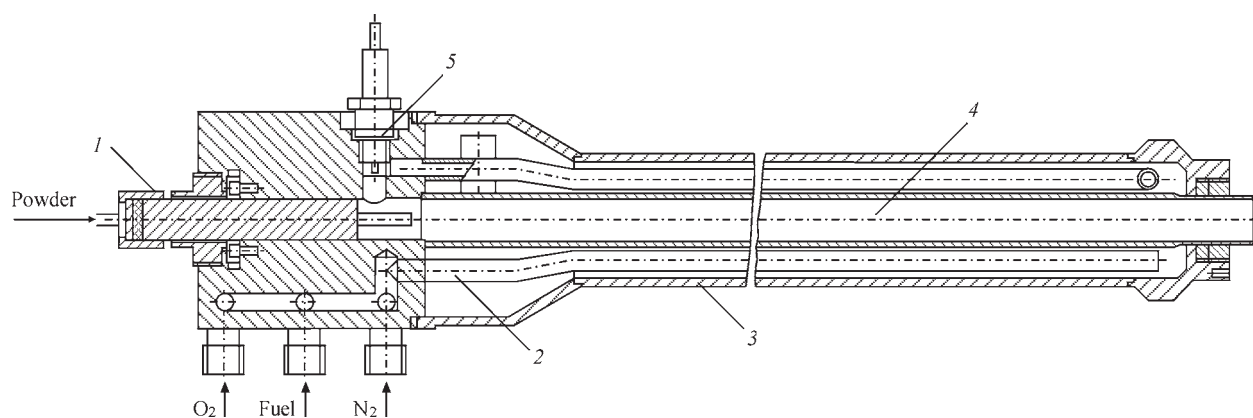
Figure 1. Perun-C detonation gun

Powder spraying productivity, kg/h 1–3
Powder utilization coefficient, % 30–60
Working gas flow rates, m³/h:
    acetylene. 0.65–1.20
    propane-butane 0.6–1.1
    hydrogen. 2.0–3.6
    oxygen 1.3–4.0
    nitrogen. 4.6–5.2
    compressed air 4.6–5.2
Power, kW. 2
Supply voltage, V 220, 380
Frequency, Hz 50
Three-coordinate manipulator movement range, m:
    right–left 1.6
    forward–backward 0.85
    upward–downward 0.20

As shown by practice, electromagnetic valves are operating with success in units with up to ten Hz frequency of detonation wave generation in gas mixtures. At operation at higher frequencies, however, the valve system creates great difficulties. Now, increase of DGU operating frequency allows improving the efficiency and coefficient of powder utilization. As a result, in parallel with studying detonation spraying in DGU classical designs, in order to increase process efficiency, work on designing valveless detonation units, as well as investigation of the possibilities of using nonstationary overcompressed detonation for coating deposition began at PWI under the leadership of Yu.M. Tyurin [12–17].

Figure 2 shows a drawing of one of the first variants of valveless detonation devices. Use of forechamber *4* allows initiation of gas mixture detonation by car spark plug *7*. When leaving holes *5* uniformly
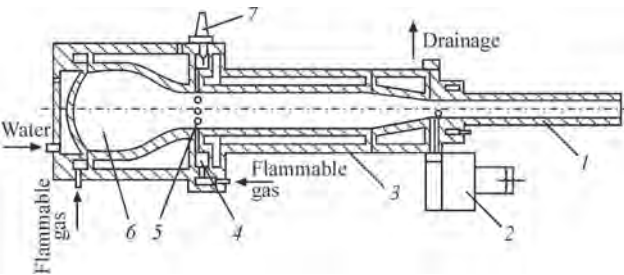
Figure 2. Valveless detonation unit

distributed around a circle, detonation is developing mainly in the main volume *6* of the detonation unit. Diameter of barrel *1* is smaller than that of the adjacent combustion chamber. It allows realizing an overcompressed detonation mode. Powder was fed radially into the barrel by pulsed powder feeder *2*. The device had water cooling *3*.

Despite a large number of experimental designs of valveless DGU developed at PWI, their operation is based on the same principle. Operation of valveless units in the pulsed mode is realized due to gas-dynamic processes in fuel and oxidizer supply lines, which result in interruption with a certain frequency of fuel and oxidizer supply into the detonation combustion chamber (DCC) and prevention of uncontrolled ignition of a new portion of combustible mixture by the combustion products from the previous cycle. The process proper consists in the following. A combustible mixture forms in the chamber. Mixture ignition leads to appearance of a detonation wave (DW) and, hence, to increased pressure in the DCC. At the moment, when the pressure in DCC begins to exceed the pressure in the supply lines, which usually is not higher than 300 kPa, flowing of the combustion products into the respective lines takes place. This way, supply of fresh fuel and oxidizer into DCC is interrupted. In other words, the "gas-dynamic valve" is closed. The detonation products are cooled, when moving in the gas lines. For stable operation and prevention of self-ignition the supply line length and diameter are selected experimentally. After DW has left the combustion chamber, a rarefaction wave starts propagating inside the latter towards the detonation product flow. Having reached the fuel and oxidizer supply lines, it propagates through the channels, and after some time, the pressure in the combustion products decreases, causing a reverse gas motion in the supply lines. Thus, "gas-dynamic valves" are opened. The backflow of the already cooled combustion products into the chamber begins. It is similar to the process of chamber blowing with inert gas, which takes place

at operation of valve detonation systems. This is followed by DCC filling by a new gas mixture. Here, the cooled combustion products are located between the combustible mixture and hot combustion products, the temperature of which exceeds that of combustible mixture self-ignition, thus preventing ignition of the supplied fresh gas mixture. DCC filling is followed by the next detonation initiation and the cycle is repeated. The period of time during which the DCC is again filled with fresh mixture after combustible mixture ignition includes the total time of: deflagration transition into detonation; DW propagation into DCC; outflowing of the combustion products from DCC into the ambient space; outflowing of the cooled combustion products from the fuel and oxidizer supply lines into the DCC; and DCC filling with the combustible mixture.

In the general case, the maximal frequency of the unit operation depends on combustion chamber length, its diameter, length of fuel and oxidizer supply lines, their diameter, pressure in them, kind of fuel and oxidizer and their proportion. Knowing all these parameters, it is possible to assess the limit frequency of DCC operation. Modern valveless DU for coating spray-deposition, allow operating with up to 100 Hz and higher frequency. Note for instance, the device design, using high-frequency pulsed detonation (HFPD) process [18, 19]. A number of detonation units were developed on their base which allow deposition of sound coatings with a high efficiency. In particular, HFPD-PK 200 modification of Aerostar Coatings (Spain) for deposition of metal powders, oxides and metal ceramics proved itself well [20]. At present in the market of thermal spraying equipment the Tecnalia Center of applied research and technological development (Spain) proposes HFPDneo system, which provides increased productivity and possibility of operation, using various combustible gas mixtures in a broad frequency range (up to 100 Hz and higher). Investigations and practical results in the field of creation of pulse detonation engines were the impetus

for development of new generation valveless detonation guns, operating at high frequency. As an example, we should note the developments of Hiroshima University [21]. The high-frequency detonation gun developed by them allows deposition of coatings with the frequency of 150 Hz [22]. Stable operation of the detonation gun in this case is ensured due to feeding the combustible mixture in the mode of detonation chamber blowing by inert gas or in the mode of blowing by vapours of the injected liquid [23]. Work on increasing the frequency, optimization of combustible mixture feeding and designs of detonation chambers of this class of devices is going on.

Controlled reliable ignition of detonation in the combustion chamber should be regarded as one of the main problems, associated with development of units, using the detonation phenomenon. In technical terms, of greatest interest when designing detonation units used for coating spray-deposition, is the initial ignition of the combustible mixture by a weaker energy source with the possibility of further realization of combustion transition into detonation (CTD). A method of initiation of accelerated CTD often used for this purpose is detonation formation as a result of flame acceleration in a separate channel (forechamber) and its guiding into the main volume of the combustion chamber.

Special attention should be paid to this assembly during design. The authors developed several forechamber designs which allows implementation of the detonation combustion mode in connected DCC of different geometry. As an example, Figure 3 shows a drawing of the working laboratory set up with air cooling of DCC. To avoid overheating, the maximal detonation frequency in the considered DGU is not higher than 12 Hz. The flammable gas (propane in this case) is supplied through nozzle *1* into forechamber *2*. Small-diameter holes are drilled in the nozzle for fuel gas feeding in the radial direction. Oxidizer (oxygen or a mixture of oxygen with air) is fed radially along a tangent to the internal cylindrical surface of
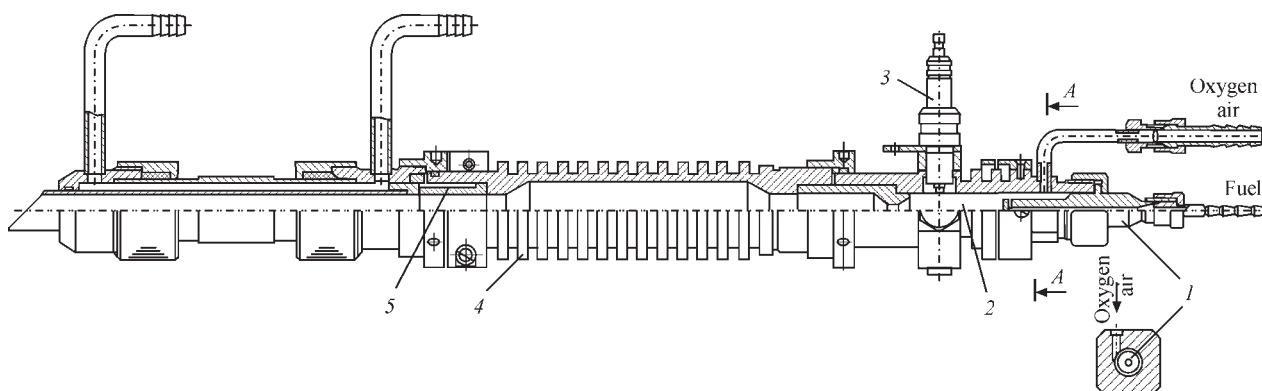

Figure 3. Valveless detonation unit with cylindrical forechamber

the forechamber, thus imparting an angular velocity to this flow. Such feeding of the combustible mixture components allows performing their uniform mixing. Spark plug *3* is located closer to the forechamber outlet. In order to create the conditions for detonation, the forechamber has a narrowing at the end. After ignition and detonation the shock wave front leaves the forechamber and detonation propagates in the adjacent DCC *4*. In this design the overcompression mode is realized at DCC outlet due to narrowing of the chamber cross-sectional area (30 mm diameter) to that of the cylindrical barrel (16 mm diameter) at 35° angle of inclination of the formed cone. As the overcompressed wave transforms into stationary Champan–Jouguet (ChJ) DW at the distance of several calibres in the cylindrical barrel, for effective acceleration and heating of the powder, it is desirable to feed it at the beginning of the barrel cylindrical part, whish is exactly what was realized in the considered design. Powder, which is heated and accelerated by the gas region with increased velocity head, is radially fed through special assembly *5*, directly at the beginning of the barrel.

In DCC of a variable cross-section the degree of DW overcompression α is determined by the following ratio: $\alpha = D_*/D_{ChJ}$, where D_* and D_{ChJ} are the velocities of overcompressed DW and ChJ detonation, respectively. As shown by calculations [24], already a slight increase of DW velocity leads to an abrupt increase of such characteristics of detonation products as pressure p_*, density ρ_*, mass velocity u_* Although the rise of detonation product temperature is partially compensated by dissociation processes, it is still noticeable. Therefore, overcompressed DWs can be the source of pulsed flows of the detonation products with parameters, noticeably exceeding those, which can be obtained at ChJ detonation that is exactly what deter-

mines the area of their possible application at powder coating deposition by the gas detonation method.

The estimate of pressure and density at the overcompressed DW front and velocity of detonation products, depending on the degree of overcompression can be derived from the ratios given in [25]. For DCC of the detonation gun shown in Figure 3, the overcompression degree α = 1.043. At application of a combustible mixture with molar ratio of the components (oxygen to propane), equal to 4.2, which contains 5 % nitrogen, the ChJ detonation parameters will be approximately as follows: $D_{ChJ} = 2400$ m/s, $p_{ChJ} = 34$ atm, $\rho_{ChJ} = 2.59$ kg/m^3, $u_{ChJ} = 1100$ m/s. Then, in this unit, in keeping with dependencies from [25] the following maximal parameters can be achieved due to overcompression: $p_* = 47$ atm, $\rho_* = 3.62$ kg/m^3, $u_* = 1470$ m/s. Here, dynamic head of overcompressed detonation products $\rho_* u_*^2/2$ will be 2.5 times higher than that of ChJ detonation.

Evaluation calculations are in agreement with numerical modeling of the detonation process in the considered DCC, performed using ANSYS program package.

Figure 4 shows time distribution of pressure on DCC walls and in the barrel. In DCC the detonation parameters correspond to ChJ parameters. The overcompressed detonation region, after which the detonation again changes to stationary ChJ, is located in the narrowing zone and at the distance of approximately two calibers directly in the barrel.

Multisection chambers can also be used in the detonation units, in order to ensure effective energy exchange and the required transformations in the initial powder material. Therefore, development of valveless DGU at PWI is currently focused on designing and studying the multichamber structures. At present, a series of laboratory multichamber units for detonation spraying have been developed. In this type of units, DW propagates in cylindrical and in annular combustion chambers, which enclose them, that ensures multiple reflection of the wave from the walls, their collision and combining into one jet of combustion products. As a result, an essential difference of this type of unit, is that a combination of the energy of the process of combustible mixture detonation from several, specially profiled detonation chambers, is realized. This ensures formation of a jet of the combustion products, having a high velocity and temperature, which allows effectively spraying different powder materials, using a combustible mixture based on hydrocarbon flammable gas.

Figure 5 shows a drawing of one of the experimental samples of a multichamber detonation unit (MCDU). In MCDU the design of forechamber *1* for
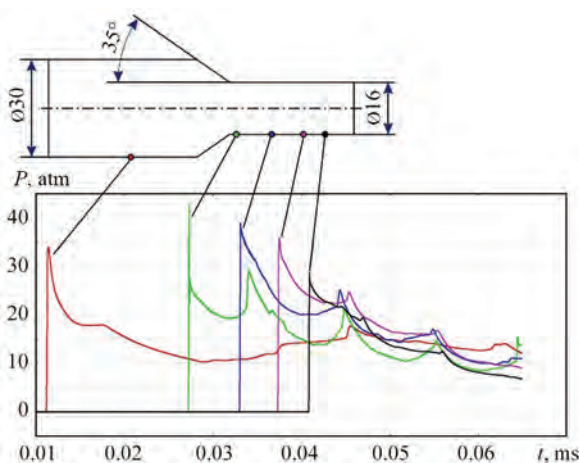

Figure 4. Numerical modeling of time distribution of pressure on the walls of detonation combustion chamber and barrel at different distance from the narrowing
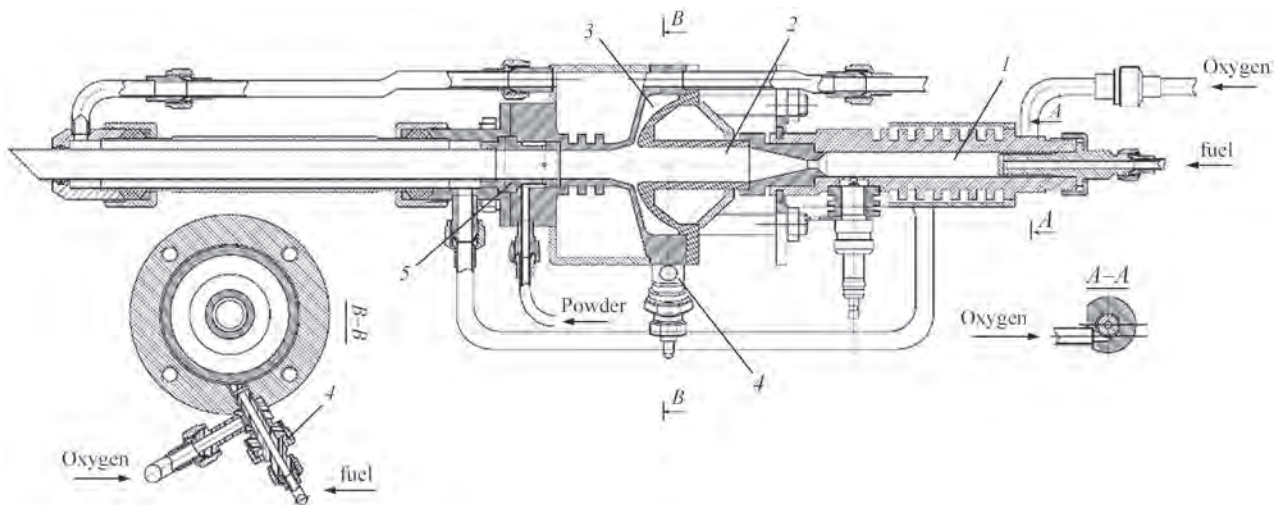
Figure 5. Multichamber detonation unit

detonation initiation was left unchanged, similar to DGU, shown in Figure 3. Propane-butane, propylene, methane, ethylene, and propylene-propane-methylaceneal (MAF) can be used as flammable gas. Oxygen or a mixture of oxygen with air is used as an oxidizer. The degree of combustible mixture dilution by air both depends on the properties of the sprayed powder, and is selected experimentally based on multifactorial experiment planning.

Flammable gas is fed through the nozzle into forechamber *1* of a similar design, as that of DGU, shown in Figure 3. The spark plug is located at the forechamber outlet. Main cylindrical detonation chamber *2* is filled with combustible mixture after forechamber filling. Annular DCC *3* is located around the cylindrical DCC. The annular chamber volume filling is performed through mixer *4*. Feeding the combustible mixture components into the mixer and their mixing are organized as in the forechamber. The spraying powder is fed into DU barrel radially through cylindrical insert *5* with holes uniformly drilled in a circle. There are no electric valves either in the gas or powder supply lines. The unit operates "quasicontinuously" at the frequency of 20 Hz and higher, that ensures the possibility of using standard devices and components for feeding powders and gases. Continuous feed of powder and combustible mixture simplifies the design and lowers the equipment cost, improves the reliability of its operation, and application of hydrocarbon fuel (except for acetylene) ensures the safety and efficiency of the technology.

Flow rates of the combustible mixture components can vary in the following range, m³/h: 0.8–2.0 of propane, 5–10 of oxygen and 0–5 of air. The detonation combustion mode develops in main cylindrical chamber *2*. Annular chamber *3* with slot exit into the cylindrical barrel is used for compression of the combus-

tion products and creation of an additional jet, which "back up" the detonation products in the cylindrical barrel from the main chamber. A dose of powder is fed into the barrel for acceleration and heating. The barrel can have an inner diameter of 16–20 mm, and length of 300–520 mm, and it is selected, depending on the properties of the sprayed powder material. Narrowing of the working volume of the cylindrical chamber of 26 mm diameter to barrel diameter of 16 mm ensures overcompression of detonation combustion mode. Further compression of the combustion products occurs owing to the annular chamber. Gas-dynamic process of detonation initiation in the annular chamber ensures collapse of combustion products along the barrel axis, which significantly increases their velocity, pressure and density. MCDU allows stretching the detonation products along the barrel length and thus enlarging the heating and acceleration zone, and, hence, also the time of the powder portion staying in this zone. This has a positive effect on material utilization coefficient.

EXPERIENCE OF DEVELOPMENT OF PRODUCTION AREAS OF DETONATION GAS SPRAYING

PWI staff developed several MCDU designs for coating deposition, and the best of them, in addition to scientific-laboratory experiments, have passed industrial trials. Figure 6 shows one of the modifications of such guns.

MCDU main parameters are given below.

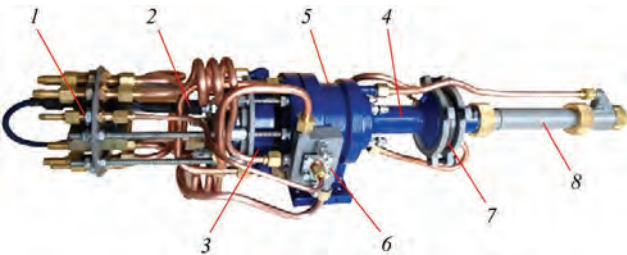| Parameter	Value
Overall dimensions (300 mm barrel length), m	0.8×0.2×0.15
Weight, kg	15
Consumed power (ignition system), W	< 100
Total volume of combustion chambers, cm³	150
Barrel diameter, mm	16–18
Frequency of pulse generation, Hz	10–30
System of powder feed and combustible	

Figure 6. Multichamber detonation unit for coating spray-deposition: *1* — assembly of combustible mixture component feeding; *2* — spark plug; *3* — forechamber; *4* — main DCC; *5* — annular DCC of the mixture; *6* — gas mixer; *7* — powder feeding assembly; *8* — barrel

mixture supply . . . . .Valveless
Pressure in gas lines, atm 1.2–3.0
Used fuel . . . . .LPG, propylene, MAF, methane
LPG flow rate, m³/h 1.0–1.6
Oxygen flow rate, m³/h 5.0–8.5
Air flow rate, m³/h. 0.3–3.5
Coolant flow rate (water), l/min 7
Productivity, kg/h:
   ceramics 0.5–1.0
   cermet 1.0–2.0
   metal 1.0–3.0
Powder utilization coefficient, %:
   ceramics 40–60
   cermet 70–80
   metal 70–90

The production areas for MCDU were set up mostly using standard equipment, widely applied for other thermal spraying methods. As regards the cost of the detonation unit proper, it is usually low, owing to relatively small production expenses and low material consumption. As a result, the cost of the detonation gun is equal to a tiny portion of the overall capital expenditures for the area and its infrastructure. Thus, in the feasibility study for establishing the production area the main attention was focused on the level of equipment automation and quality of its components.

Small dimensions of the spraying unit, low pressure (up to 0.3 MPa) in the gas supply lines and continuous feeding of the components of the flammable gas mixture and powders provide the conditions for technological manipulation at application of standard automated units and robots. Here, it is possible to use

standard boxes and noise neutralization systems, as well as powders feeder, gas cylinder systems of gas feeding, control panels and systems of control of spraying technology and coating quality.

The detonation spraying section (Figure 7) consists of three parts:

I — Operator's room for control and monitoring of the technological process.

II — Soundproof shelter, where the gun is installed on a manipulator, and coating deposition proper is performed.

III — Gas compartment accommodating the oxygen manifold, nitrogen and propane-butane cylinders, as well as compressor and cooling block.

A technological section for detonation spraying of metal wear-resistant coatings based on tungsten carbide on product surface was established in 2016 at Sputtek Advanced Coating Technologies Company (GTA, Ontario, Canada). Its main component is MCDU installed horizontally on a stationary bedplate and robotic manipulator for movement of sprayed products relative to the detonation unit nozzle. A programmed controller allows performing deposition of coatings of the specified thickness on parts of both flat and cylindrical shape. An integral part of technological equipment is a soundproof room of 36 m³ volume, which allows lowering the noise level to 90 dB and lower. A high-efficient exhaust ventilation system (up to 200 and higher m³/min) is envisaged, in order to lower the dust level in the working zone. Figure 8 shows the soundproof block with the control panel and operator's console. Process monitoring is performed remotely, using TV cameras. The system of supplying such gases as nitrogen, propane-butane mixture and oxygen, incorporates the required regulators of pressure, stop valves and a set of fire barriers. The technological section is fitted with equipment for part preparation for the spraying process, as well as quality control (surface roughness, coating thickness and its adhesion).

An important factor of technology development now is the degree of its automation. A robotic complex
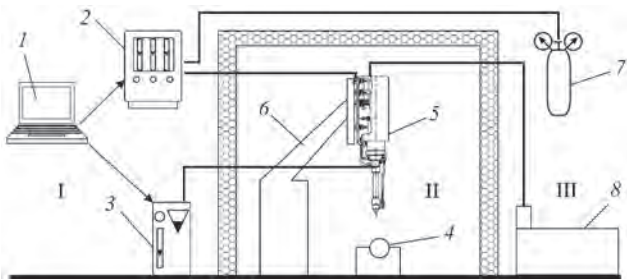

Figure 7. Scheme of detonation spraying area: *1* — system of technological process control and monitoring; *2* — low-pressure gas panel for feeding oxygen, propane-butane and air; *3* — powder feeder; *4* — sprayed product; *5* — multichamber detonation unit; *6* — manipulator; *7* — gas manifold; *8* — dealer

with an intelligent control system (Figure 9) for detonation gas spraying with realization of cumulative energy effect in the mulitchamber unit, manufactured at the production facilities of "Scientific and Production Center PLAZER" LTD (Kyiv) can be an example of complete automation of the process. The soundproof box (overall dimensions of 6540×6280×5200 mm) was developed, proceeding from the requirements of sanitary norms. The room is explosion-proof, and its sound insulation allows lowering the noise level in the operator work zone to the level of ~90 dB. In order to clean the air from combustion products, aerosols and micropowders, the ventilation installation is fitted with cyclone apparatus of the capacity of not less than 9000 m^3/h and mechanical filter. The gun proper is installed on a programmable anthropomorphous 6-axis robot for unit movement along a preset trajectory or in the manual mode by operator's commands from the remote panel of the control system. The following

Figure 8. Section for detonation spraying of coatings

components are located outside the soundproof box: modules of the programmed system of automated control of the equipment and technology (including: cabinet for gas preparation and gas flow rate control;
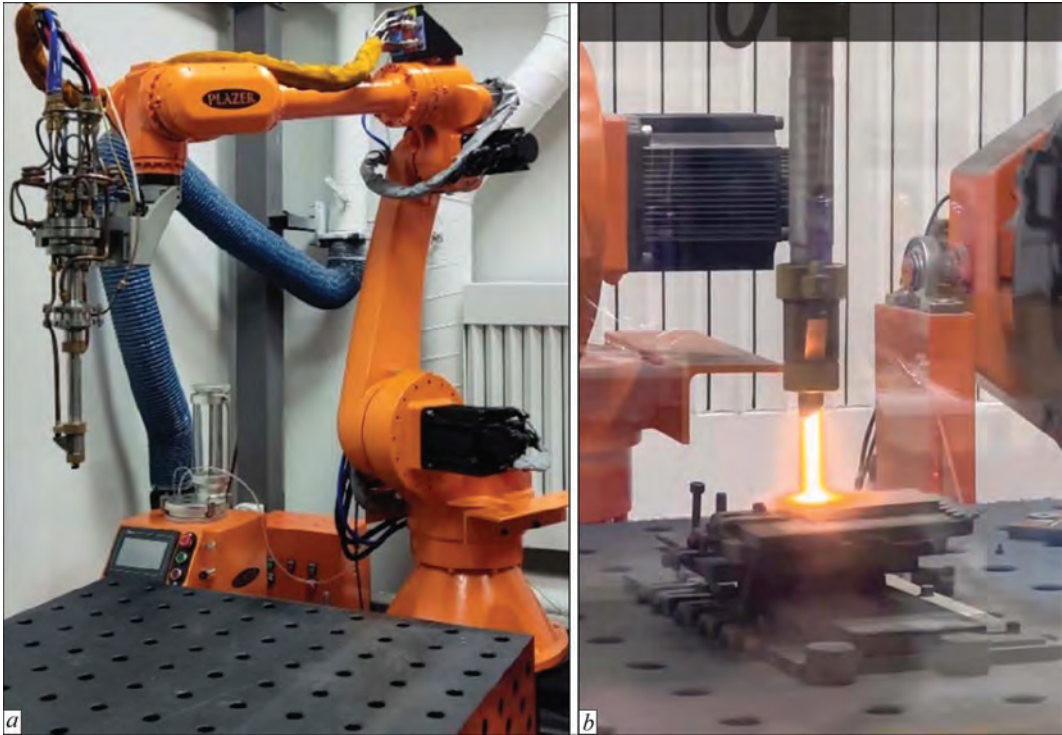
Figure 9. Robotic equipment (*a*) and process (*b*) of detonation gas spraying with realization of cumulative energy effect in MCDU, production of which was set up at "Scientific and Production Center "PLAZER" LTD. (Kyiv)

Figure 10. Rotobotic section of detonation gas spraying with realization of cumulative energy effect in MCDU, fitted with 6 axis robot with maximal arm range of 2238 mm and two-axis manipulator for rotation of the sprayed parts

mobile panel of the control system with PLC controller and CCTV module monitor; display of the module for remote measurement of the part temperature; controller of spraying robot); block of MCDU forced autonomous cooling, integrated with automatic control system; cylinder manifold. In order to avoid emergency situations, special attention was given to development of a safety system. Figure 10 shows an example of such a robotic section, set up at the Paton Research Institute of Welding Technologies in Zhejiang Province (PRC).

Application of such automated complexes allows performing operator training in a short time and introducing the technology and equipment in production.

CONCLUSIONS

The paper provides information about the work on development of detonation gas spraying technology, conducted at PWI. Traditional DGU of "Perun" class and coatings produced in them, were studied in detail by the Institute staff, beginning from 1980s. Despite the fact that acetylene is the best studied fuel, convenient for detonation combustion, and acetylene-oxygen explosive mixtures feature the highest temperature and high dynamic head of detonation products, use of acetylene requires compliance with increased safety measures. Now, application of a safer combustible mixture based on methane, propane-butane or MAF allowed the developers significantly enhancing the capabilities at detonation gun design and considering the possibility of using valveless systems, operating at higher frequencies. This way, it became possible to increase system reliability, efficiency and productivity of the process. Operation in the pulsed mode of valveless DGU, developed by PWI staff, is ensured due to gas-dynamic processes in the fuel and oxidizer supply lines. This principle is ever more often used when designing the detonation guns also in other research organizations.

At present the possibility of using nonstationary overcompressed detonation for coating deposition is actively studied. All these problems were addressed by PWI staff also when designing MCDU. Unlike the traditional detonation units for coating deposition, in MCDU an overcompressed mode of detonation combustion of flammable gas mixtures and valveless supply of combustible mixture and powder are used. More over, application of cumulative energy in specially profiled chambers enables creation of a multifrontal flow of detonation combustion products, which ensures enhanced influence on the dispersed particles of sprayed material. This significantly enhances the effectiveness of energy transfer and ensures its saving. Burning of combustible mixtures in specialized chambers provides wide possibilities for controlling the velocity, temperature and composition of combustion products, which allows creating technological conditions for spraying, which are realized, for instance, by such technologies as Cold Spray, HVAF or HVOF. The high frequency of combustion initiation (20 Hz and higher) will ensure quasicontinuous flow of the combustion products, that allows using this technology for coating deposition on product surfaces at the level with known HVOF, HVAF and Cold Spray spraying processes. The technology based on MCDU has several advantages, compared to the high-velocity thermal methods, which are widely applied. High-quality coatings are produced at much lower material and energy expenditures, and easy selection of spraying parameters ensures a wide range of coating properties. The unit design allows working with a high efficiency and reliability using various hydrocarbon mixtures in a broad range of adjustment of the combustion product temperature. The unit is safely operating with different fuel, for instance, propane, propane-butane, propylene, MAF and natural gas. Low pressure infrastructure is used for gas supply. Automated system of control (monitoring) of the process and modular concept allow easily integrating the technology with the already available material and technical base for thermal spraying in the enterprises.

The concept of development of valveless, multichamber detonation guns operating at frequencies of 20 Hz and higher, has high potential in terms of improvement of the effectiveness of coating deposition method proper. At present PWI is actively conducting work on studying the process and introduction of the already available unit designs for their practical application in different industries.

REFERENCES

1. Zeldovich, Ya.B. (1940) On the issue of energy use of detonation combustion. *ZhTF*, 10(**17**), 1453–1461 [in Russian].
2. Poorman, R.M., Sargent, H.B., Lamprey, H. (1955) *Method and apparatus utilizing detonation waves for spraying and other purposes*. Pat. US 2714563A. Publ. 08.02.1955.
3. Zverev, A.I., Sharivker, S.Yu., Astakhov, E.A. (1979) *Detonation spraying of coatings*. Leningrad, Sudostroenie [in Russian].
4. Bartenev, S.S., Fedko, Yu.P., Grigoriev, A.I. (1982) *Detonation coatings in mechanical engineering*. Leningrad, Mashinostroenie [in Russian].
5. Shesternenkov, V.I. (1968) Detonation coating. *Poroshkovaya Metallurgiya*, 1, 37–46 [in Russian].
6. Samsonov, G.V., Sharivker, S.Yu. (1977) *Detonation coatings*: Encyclopedia of Inorganic Materials. Vol. 1. Kyiv, Main Edition of the Ukrainian Soviet Encyclopedia [in Russian].
7. Yushchenko, K.A., Astakhov, E.A., Klimenko, V.S., Borisov, Yu.S. (1990) Detonation spraying of hardening coatings and ways of its development. In: *Proc. of Conf. on New Processes and Equipment for Gas-Thermal and Vacuum Coating, Kyiv, PWI*, 26–32 [in Russian].

8. Astakhov, E.A. (2005) *Scientific and technological basis for controlling the properties of detonation coatings*: Syn. of Thesis for Dr. of Tech. Sci. Degree. Kyiv, PWI [in Russian].

9. Borisov, Yu.S., Astakhov, E.A., Korzhyk, V.N. et. al. (1993) Influence of the composition of the detonating medium on the formation of amorphous-crystalline coatings. *Avtomatich. Svarka*, **6**, 83–93 [in Russian].

10. Borisov, Yu.S., Astakhov, E.A., Murashov, A.P. et. al. (2015) Investigation of structure and properties of thermal coatings of WC–Co–Cr system produced by high-velocity methods of spraying. *The Paton Welding J.*, **10**, 25–28. DOI: https://doi.org/10.15407/tpwj2015.10.04

11. Astakhov, E.A. (2003) Detonation system "Perun-S" for deposition of protective coatings. *The Paton Welding J.*, **2**, 36–40.

12. Tyurin, Yu.M., Kolisnichenko, O.V. (2008) *Method of detonation spraying of coatings and device for its realization*. Pat. Ukraine 8383.

13. Tyurin, Yu. N., Pogrebnjak, O.D., Kolisnichenko, O.V. (2009) Comparative analysis of an efficiency of cumulative-detonation and HVOF devices, which are applied for gas-thermal deposition of coatings. *Fizicheskaya Inzheneriya Poverkhosti*, 7(**1–2**), 39–45 [in Russian]. DOI: http://dspace.nbuv.gov.ua/handle/123456789/7948

14. Kolisnichenko, O.V., Tyurin,Yu.N., Tovbin R. (2017) Efficiency of process of coating spraying using multichamber detonation unit. *The Paton Welding J.*, **10**, 18–23 DOI: https://doi.org/10.15407/tpwj2017.10.03

15. Vasilik, N. J., Tyurin, Yu.N., Kolisnichenko, O.V. et. al. (2013) Properties, peculiarities and applications of powder coatings formed by multi-chamber detonation sprayer. *Applied Mechanics and Materials*, **467**, 179–184. DOI: https://doi.org/10.4028/www.scientific.net/amm.467.179

16. Markashova, L.I., Tyurin, Yu.N., Kolisnichenko, O.V. et al. (2017) Effect of structure on properties of Al_2O_3 and Al (or Ti) mechanical mixture coatings produced by multichamber detonation spraying method. *The Paton Welding J.*, **9**, 27–32. DOI: https://doi.org/10.15407/tpwj2017.09.05

17. Kolisnichenko, O.V., Tyurin, Yu.M. (2023) Properties of WC–Co–Cr coatings, deposited by multichamber detonation device and their application. *The Paton Welding J.,* **9,** 47–52. DOI: https://doi.org/10.37434/tpwj2023.09.08

18. Fagoaga, I., Barykin, G., De Juan, J. et al. (1999) The high frequency pulse detonation (HFPD) spray process. Thermal Spray 1999. In: *Proc. of the United Thermal Spray Conf., Dusseldorf, Germany,* 282–287. DOI: https://doi.org/10.31399/asm.cp.itsc1999p0282

19. Parco, M., Barykin, G., Fagoaga, I., Vaquero, C. (2008) Development of wear resistant ceramic coatings by HFPD. ITSC 2008. In: *Proc. of the 2008 Int. Thermal Spray Conf., June 2–4, 2008, Maastricht, The Netherlands*, 130–134. DOI: https://doi.org/10.31399/asm.cp.itsc2008p0130

20. Higuera, V., Belzunce, F. J., Riba, J. (2006) Influence of the thermal-spray procedure on the properties of a CoNiCrAlY coating. *Surf. and Coat. Technol.,* 200(**18–19**), 5550–5556. DOI: https://doi.org/10.1016/j.surfcoat.2005.07.070

21. Matsuoka, K., Muto, K., Kasahara, J. et al. (2016) Development of high-frequency pulse detonation combustor without purging material. *J. of Propulsion and Power,* 33(**1**), 1–8. DOI: https://doi.org/10.2514/1.B36068

22. Endo, T. (2020) Pulse-detonation thermal spray. *J. of the Combustion Society of Japan,* 200(**62**), 103–115. DOI: https://doi.org/10.20619/jcombsj.62.200_103

23. Endo, T., Obayashi, R., Tajiri, T. et. al. (2016) Thermal spray using a high-frequency pulse detonation combustor operated in the liquid-purge mode. *J. of Thermal Spray Technology,* **25**, 494–508. DOI: https://doi.org/10.1007/s11666-015-0354-8

24. Nikolaev, Yu.A., Topchiyan, M.E. (1977) Calculation of equilibrium flows in detonation waves in gases. *Fizika Goreniya i Vzryva,* 13(**3**), 393–404 [in Russian].

25. Prokhorov, E.S. (2011) Approximate calculation of overdriven gaseous detonation in convergent channels. *Vestnik NSU. Series: Physics*, 6(**2**), 5–9 [in Russian]. DOI: https://doi.org/10.54362/1818-7919-2011-6-2-5-9

ORCID

O.V. Kolisnichenko: 0000-0003-4507-9050,

V.M. Korzhyk: 0000-0001-9106-8593,

P.D. Stukhlyak: 0000-0001-9067-5543,

A.I. Kildiy: 0000-0001-8133-8705,

M. Shynlov: 0009-0003-2679-9850,

V. Mudrichenko: 0009-0005-8311-2685

CONFLICT OF INTEREST

The Authors declare no conflict of interest

CORRESPONDING AUTHOR

O.V. Kolisnichenko
E.O. Paton Electric Welding Institute of the NASU
11 Kazymyr Malevych Str., 03150, Kyiv, Ukraine.
E-mail: okolis@i.ua

JOURNAL HOME PAGE

https://patonpublishinghouse.com/eng/journals/tpwj

STEAM PLASMA GASIFICATION OF BIOMASS USING ELECTRODELESS PLASMATRONS

S. Petrov[1], P. Stukhlyak[2], S. Bondarenko[3], S. Roshanpour[4], M. Ganczarski[5]

[1]The Gas Institute of the NASU
39 Degtyarivska Str., 03113, Kyiv, Ukraine
[2]Paton Research Institute of Welding Technologies in Zhejiang Province. People's Republic of China, Zhejiang Province, Hangzhou City, Xiaoshan District, St. Shixing Beilu 857, Office 426
[3]National Technical University of Ukraine "Igor Sikorsky Kyiv Polytechnic Institute"
37 Prosp. Beresteiskyi, 03056, Kyiv, Ukraine
[4]Plasma Dynamics srl
11/13, Via del Progresso, Vicenza, Italy, 36100
[5]HYDROGENIUM p.s.a.
5/35, Gliniana, Lublin, Poland, 20-616

ABSTRACT

The use of plasma processes in the production of biohydrogen opens up the possibility of replacing fossil fuels with an environmentally friendly energy source from biomass. The work examines the process of plasma processing of biomass (based on the example of sunflower husks), using an electrodeless discharge to produce highly productive synthesis gas with a high hydrogen content. The use of CFD modeling made it possible to determine the parameters of a steam plasma reactor for the gasification process. The operation of the reactor is based on the principle of gasification using steam-water plasma with oxygen. The use of plasma blast allows increasing the process temperature, the rate of physical and chemical transformations, the degree of conversion of raw materials, the residence time of gases in the reaction volume, the content of hydrogen and carbon monoxide in the synthesis gas, the thermal intensity of the reaction volume and specific productivity. It has been experimentally established that plasma power affects the energy balance of the entire gasification process, and also directly affects the temperature profile, synthesis gas composition, resin yield and stability of the gasification process. The influence of such parameters as the plasma energy to waste energy ratio (PER), equivalence ratio (ER) and steam to oxygen mass ratio (SOMR) on the gasification process was studied. It has been found that increasing PER raises the average temperature of the supplied steam-oxygen mixture and increases the heat input for gasification. A dual influence of ER on the gasification process has been noted: on the one hand, a higher ER provides more chemical heat during combustion, which has a beneficial effect on the synthesis gas output, and on the other hand, a higher ER provides an increase in the amount of combustion products in the reactor, which leads to reducing the amount of flammable gases. It has been determined that with an increase in SOMR from 2 to 2.5, the volume fraction of H_2 in the synthesis gas increases, and CO_2 decreases. Hydrogen obtained from biomass gasification processes is one of the promising methods for alternative hydrogen production from fossil fuels.

KEYWORDS: electrodeless plasmatron, gasification, steam plasma reactor, biomass, CFD modeling

INTRODUCTION

Research into plasma gasification of biomass is being conducted as a response to the need for more efficient use of biomass to produce energy and various products. The growing production of advanced bioenergy carriers and biomaterials is increasing competition for various applications of biomass. Biomass is an umbrella term that includes many sources such as agricultural, aquatic, and land waste. In order to develop the use of biomass in a sustainable manner, the status and prospects of biomass value chains for heat, power, fuel and materials production are reviewed, their current and long-term levelized production costs and avoided emissions are assessed. Currently, the economically and environmentally preferred options are the combustion of wood chips and pellets in district heating systems and large-scale fermentation. The key technologies for biomass processing are large-scale gasification (bioenergy and biomaterials) and fermentation (biofuels and biomaterials). However, both methods require improvement of technological and economic indicators. In the last decade, the use of biomass to produce modern bioenergy and biomaterials has increased significantly to counter the depletion of fossil resources and reduce greenhouse gas emissions. This growth is expected to continue or even accelerate [1]. The growing demand for biomass will increase competition between biomass feedstocks and applications. Thus, to ensure sustainable expansion of biomass use, it is necessary to know which pathways (biomass value chains) are the most promising for the production of heat, electricity, fuels and materials in terms of their technological, economic and environmental performance. Among the various thermochemical processes for processing biomass, the most developed are pyrolysis and gasification.

In this regard, the production of low-carbon hydrogen for use as a clean energy carrier is an important step

towards a decarbonized economy. Plasma pyrolysis is an emerging technology that has great potential for large-scale production of low-carbon, affordable hydrogen. Achieving the ambitious emissions reduction targets set in the Glasgow COP26 agreement [2] will ensure the transition to a zero-carbon circular economy. Today, 96 % of hydrogen is produced from fossil fuels through reforming. The most common processes include steam methane reforming (48 %), petroleum and heavy oil reforming (30 %), and coal gasification (18 %). All these processes result in the release of large amounts of CO_2. Low-carbon (or zero-carbon) methods of hydrogen production are needed to create a sustainable and clean hydrogen economy. One of the attractive methods for processing hydrocarbons is the use of plasma. The plasma system can be adapted to work with various hydrocarbons. Today, due to the high demand for energy consumption, limited fossil fuel resources, staggering energy costs and negative environmental impacts, scientists are constantly looking for innovative and low-cost methods to transition from fossil fuel consumption to sustainable, efficient, green and renewable energy sources. In this regard, the conversion of biomass to hydrogen (H_2) using plasma is increasingly attracting attention due to its advantages over traditional energy sources [3]. Currently, biomass provides about 14 % of global energy demand. However, the cost of producing hydrogen from biomass remains relatively high and ranges from $1.21 to $2.42/kg for gasification and $1.21–2.19/kg for pyrolysis, which is three times the cost of steam methane reforming (0. 75 $/kg) [4].

The emergence of new plasma technologies in thermochemical conversion methods may open new routes to the cost-effective production of H_2 and value-added products. Plasma pyrolysis is an emerging technology that has great potential for large-scale production [5–7]. Despite all the unique advantages of plasma technologies for H_2 production, it is necessary to eliminate the weaknesses and gaps that hinder their application on a large scale [8]. These are incomplete conversion, low energy efficiency, unwanted by-products and lack of scalability, which are the main obstacles in H_2 production using plasma technologies.

Microwave discharge is one of the techniques used to produce nonequilibrium plasma, in which, even at atmospheric pressure, the temperature of electrons is approximately 4000–6000 K, while the temperature of heavy particles is about 2000 K. When using steam as a plasma-forming gas in microwave discharge, radicals such as H, OH and O are generated, as well as high-energy electrons. Due to the high electron density, the working gas in a microwave plasma is highly dissociated and therefore chemically very reactive. The plasma creates both reducing and oxidizing conditions, which indicates the effectiveness of steam plasma for various types of material processing. Microwave gasification is a new technology, but it is certainly a promising technology for achieving a sustainable bioeconomy [7]. Although this technology shows enormous potential that can be fully realized in the near future, the selectivity and efficiency of biohydrogen production and gas synthesis still require improvement and further research to ensure cost-effective and energy-saving industrialization.

Three different types of advanced thermal plasma technologies such as DC atmospheric plasma torches, RF plasma torches and microwave plasma torches are considered for small and industrial scale waste treatment. The authors of [9] conducted a comparative study of all three plasma torches for use in the energy sector and waste recycling. Simulation modeling and experimental results of indirect DC plasma torch and high frequency plasma torch were presented. The results show that DC plasma torches and high frequency plasma torches are economical and beneficial for large-scale waste treatment and energy recovery. At the same time, when processing waste on a small scale, a microwave plasma torch can be used. Overall, minimizing environmental impact and process economics are the most important parameters to improve the feasibility and sustainability of plasma waste treatment plants. High-frequency plasma torches with plasma power from 15 kW to 200 kW are designed for more than 10,000 hours of non-stop operation [11]. They are widely used in the chemical and metallurgical industries due to their high reliability and long service life without replacing parts (within 2–3 months).

The use of thermal plasma torches for waste treatment is gaining momentum worldwide due to their suitable basic characteristics [9]. Plasma gasification has so far been developed commercially, typically using DC plasma discharge technology [10]. However, DC burners suffer from short electrode life in the presence of oxidizing gases, resulting in high operating costs associated with their replacement. An alternative is to use electrodeless plasma torches.

PURPOSE AND OBJECTIVES OF THE STUDY

The goal of this study was to generate atmospheric pressure plasma (a mixture of water vapor and oxygen) using an electrodeless discharge for the processing of biomass to produce hydrogen.

To achieve this goal, it is necessary to solve the following tasks:

1. Conduct CFD modeling of the process of plasma gasification of biomass using a mixture of water vapor and oxygen.

2. Develop and implement a special reactor system that allows for environmentally friendly and complete plasma-thermal gasification of biomass.

3. Investigate the efficiency of producing synthesis gas with a high hydrogen content using the developed reactor system.

METHODS OF RESEARCH

Considering the knowledge gaps in scaling up steam plasma gasification technology, this study developed a microwave-assisted and induction-assisted continuous steam-oxygen gasification system and explored the feasibility of using them to produce hydrogen-enriched synthesis gas. A review of the literature shows that there is currently no information about such technology in the open literature.

The main part of the process plant for the continuous production of hydrogen-rich synthesis gas is the steam-plasma gasification reactor. Synthesis gas consists mainly of CO, H_2, CO_2 and H_2O. The reactor being developed by the authors is intended exclusively for gasification of biomass, namely sunflower husks. Sunflower husks contain of 81 % volatile substances, which means they are suitable for various thermochemical processes. Structurally, the reactor is designed to be scalable. The operation of the reactor is based on the principle of gasification using plasma of a mixture of water vapor and oxygen. In the reactor, the biomass is converted into synthesis gas, the composition of which reflects thermodynamic equilibrium at a temperature in the upper part of the reactor of about 1000–1200 °C. An effective gasification process requires achieving high temperatures, which are provided by plasma heating and reducing the proportion of ballast through the use of steam-oxygen blast. Gasification using oxygen-enriched blast leads to an increase in the temperature and speed of the process, which brings it closer to the conditions of thermodynamic equilibrium. The energy supplied with the plasma is spent on maintaining the tempera-ture of the process, compensating for the decrease in heat generation from the oxidation of the raw material. The shaft-type reactor is shown in Figure 1, *a*. It consists of a gasification chamber (removal of volatile substances) and gasification of fixed carbon in the coke residue after removal of volatile substances. The composition of the synthesis gas at the outlet of the reactor is considered as the sum due to the conversion of solid carbon and pyrolysis gases. At the bottom of the chamber there are tangential channels for supplying a mixture of water vapor and oxygen at a temperature of about 2000 °C. Gasification of husks is carried out in a vortex chamber in a rotating high-temperature flow. The chamber has a shape close to the cylindrical one.

The vortex plume (Figure 1, *b*) uniformly fills and heats the surface of the chamber. Thus, the speed and completeness of gasification increase. The entire internal surface of the reactor is made of special heat-resistant ceramics designed to operate in aggressive conditions. The design of the reactor is based on CFD modeling (Figure 2, *a*, *b*).

The synthesis gas leaving the reactor (see Figure 1) has a very high temperature (about 1000 °C). Heat recovery from synthesis gas using a radiative/convective heat exchanger increases the overall efficiency of the process. The heat is used to produce process steam and energy recovery. The use of a thermally insulated reactor reduces losses and entrainment of fly ash residues. This allows the reactor to be put into long-term operation without stopping for cleaning. The location of the vortex in the chamber promotes self-cleaning of the chamber walls from deposits with a flow of fresh steam-oxygen mixture. Ash is removed through a movable grate. Through it, oxygen is supplied to the gasification zone. This allows the process to be carried out in conditions below the temperature at which the ash begins to deform (1140 °C) and to
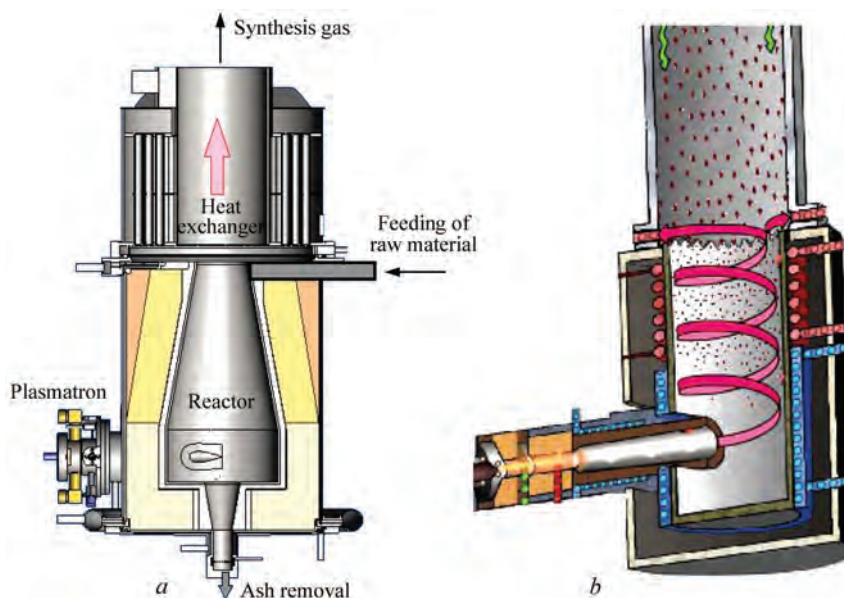

Figure 1. Reactor for steam plasma gasification of biomass: *a* — general layout; *b* — organization of vortex flow
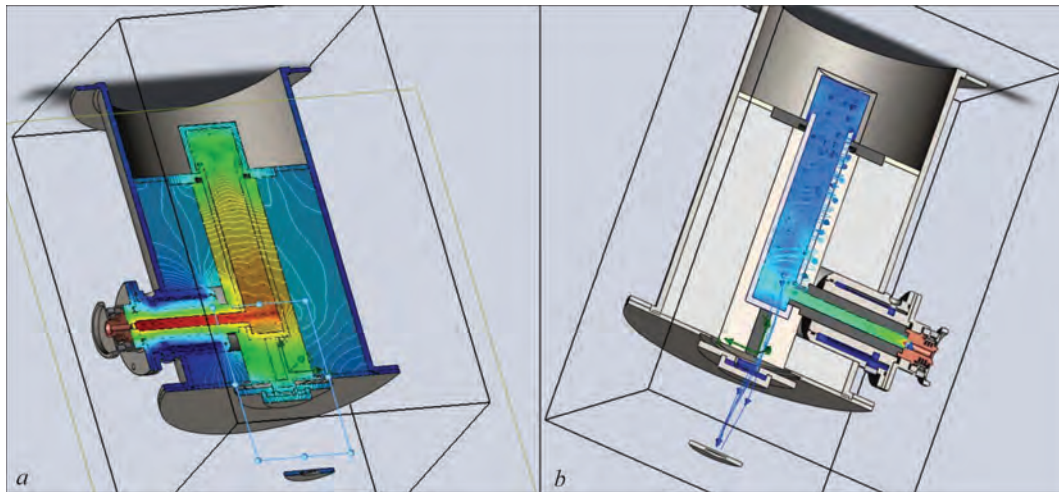
Figure 2. Simulation of a steam plasma reactor: *a* — temperature fields; *b* — velocity fields

build a gasification regime with the removal of solid slag. At the first stage of the process, raw materials are unloaded into a storage hopper. The volume of the hopper is sufficient to dampen fluctuations in waste reception cycles. From the hopper, waste is fed into the upper part of the reactor using a screw feeder.

The most important aspect in developing technologies for the production and use of synthesis gas is the relationship between its composition and energy cost. Since we strive for the highest productivity, which is also the most economical option, the method developed by the authors to reduce specific power consumption is based on the use of the plasma-autothermal principle of gasification of biomass (sunflower husks, corn cobs, etc.). First, gasification of the biomass occurs with the release of volatile products under steam-oxygen plasma conditions and subsequent combustion of part of the gasification products to CO_2. Here, 33173 kJ/kg of carbon is released. This heat, together with the plasma heat, is sufficient to compensate for the endothermic effect (10875 kJ/kg of carbon) of the water-gas reaction ($H_2O + C = C + H_2$) of biomass gasification, which occurs in a steam environment and amounts to 8 kW·h/kg of carbon.

The results obtained by the authors [12] indicate that the gasification process provides ideal thermodynamic conditions for gasification reactions with various fuels. The process can operate in a quasi-equilibrium state without the use of catalysts at a temperature of 1273 K. An important overall result is the fact that the concentrations of H_2 and CO increase with increasing O_2 consumption until the O_2/fuel ratio becomes equal to 0.60–0. 70. At the same time, the concentrations of H_2 and CO have maximum values (44 and 24 mol.%), respectively (Figure 3, *a*).

An increase in O_2 consumption promotes exothermic combustion reactions and, therefore, leads to an increase in temperature in the reactor (Figure 3, *b*). Therefore, to obtain richer synthesis gas, low oxygen consumption and acceptable reactor temperature, it is better to choose an O_2 flow rate at which the O_2/fuel ratio is in the optimal region.

The effect of steam supply on the composition of the synthesis gas and the temperature in the reactor in the absence of additional heating is shown in Figure 4. Figure 4, *a* shows that an increase in steam flow leads to a moderate decrease in the concentrations of H_2 and CO. When the H_2O/O_2 ratio increases by 200 %, the H_2 and CO concentrations decrease from 3 to 9 %,
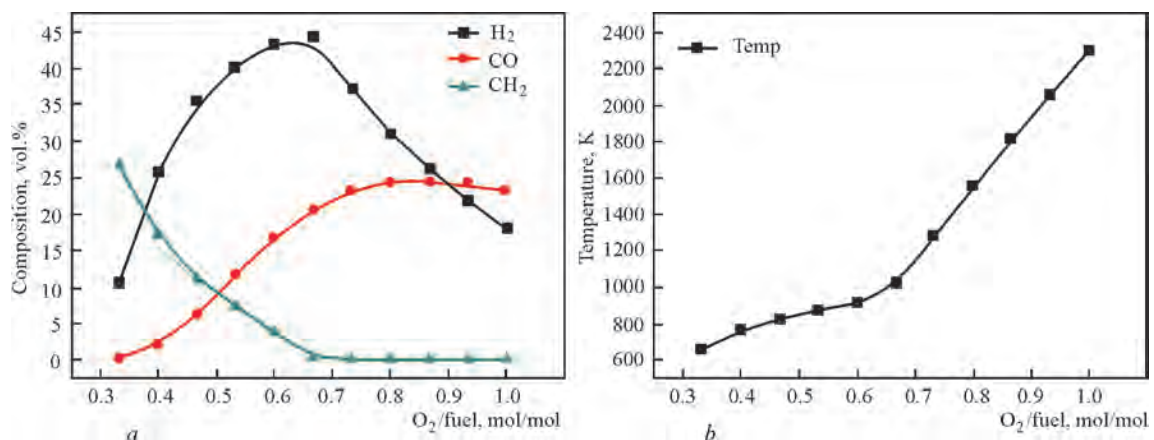

Figure 3. The influence of the oxygen content in the mixture with the processed raw materials on the composition of the synthesis gas (*a*) and temperature (*b*) in the reactor
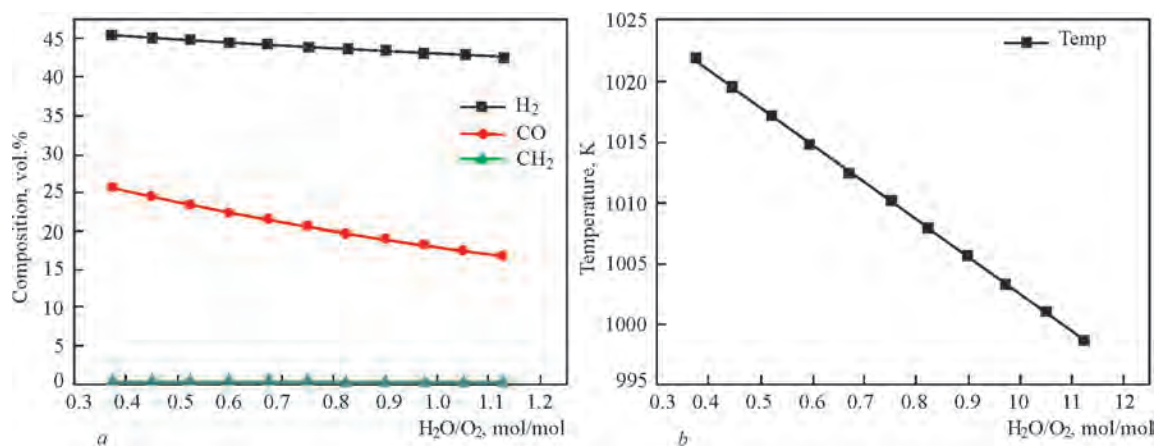
Figure 4. The influence of steam content in the feedstock on the composition (*a*) of synthesis gas and temperature (*b*) in the reactor

respectively. This may be due to the fact that the increased amount of steam takes away some of the heat and reduces the temperature of the reactor, as shown in Figure 4, *b*, thereby preventing the endothermic reactions of steam reforming and gasification.

The main role of additional plasma heating of the working mixture in the reactor during gasification becomes clear from Figures 3 and 4.

RESEARCH RESULTS

Atmospheric pressure plasma jets are the main tool for gasification. However, the small size of atmospheric pressure plasma jets limits their use to small-scale processes in materials processing. To solve this problem, the authors have developed a method for increasing plasma volume without additional power supplies or circuits. In this case, additional gas flows are located orthogonal to the direction of jet propagation, which leads to the formation of new plasma regions along these flows. This approach increases the volume of the plasma, which also increases the effective area available for interaction with surfaces. The resulting expanded plasma flows are recorded using methods of visualization and optical emission spectroscopy with time integration, as well as by calculation. This method is attractive for effective exposure of large areas to plasma. Figure 5 shows the results of modeling and full-scale tests of increasing the volume of plasma jet flows.

The main processes in the reactor (see Figures 1 and 2) are as follows. The carbon residue from the pyrolysis zone meets and reacts with gasifying agents. At the same time, homogeneous reactions occur in the gas phase. When high-temperature steam is supplied to this section, as we did during testing, the reaction system becomes more complex. First, injection of high temperature steam activates the water shift reaction, which significantly affects the chemical equilibrium in this section. Secondly, the introduction of additional mass and energy affects the mass and energy balances inside the reactor. It is impossible to accurately model all the reactions that occur in this zone. High-temperature plasma injection of oxygen and steam is a critical component of the process. Plasma power affects the energy balance of the entire gasification process and directly affects the temperature profile, synthesis gas composition, tar yield suppression and stability of the gasification process.

The experimental test was carried out in a laboratory gasifier (Figure 6), developed in accordance with CFD modeling (Figure 2). Thermal insulation of the reactor ensures an efficiency of more than 75 %. The useful power of the plasma torch is 10–30 kW. Husk consumption is up to 50 kg/hour: it contains: ash —
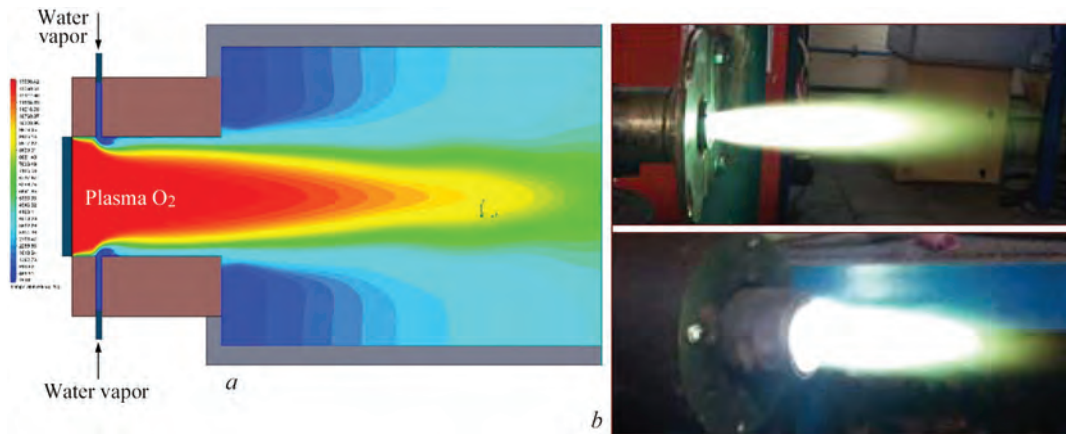

Figure 5. Increasing the volume of plasma jet flows: *a* — modeling; *b* — full-scale tests
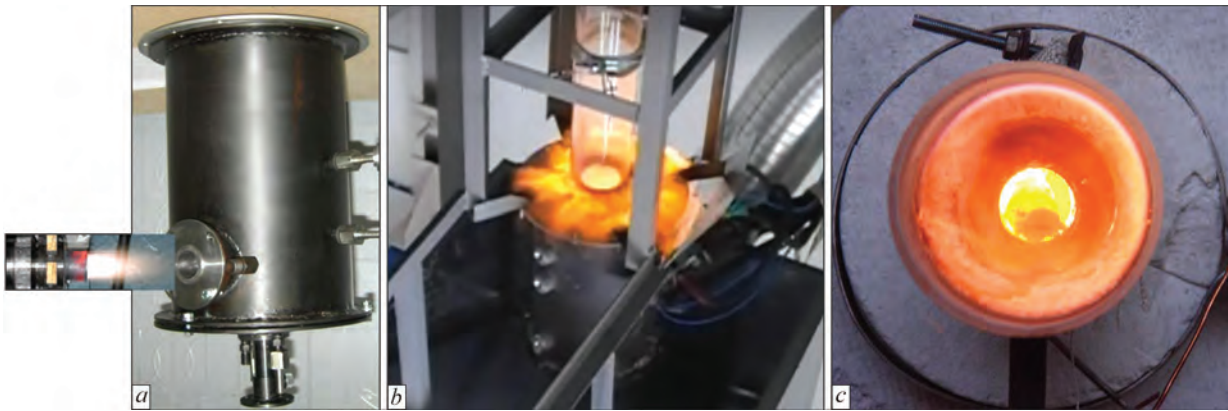
Figure 6. Demonstration vortex vapor-plasma reactor: *a* — external view; *b*, *c* — reactor in operation. Test materials: sunflower husks and corn cobs

up to 1.5 kg/hour, nitrogen — up to 1.5 kg/hour, moisture — up to 3.5 kg/hour. The lowest calorific value of sunflower husk is 17–19 MJ/kg or up to 5 kW/h. Bulk density is 100–150 kg/m³. Steam consumption is 2–7 kg/hour, oxygen consumption is 1–3 kg/hour. Stoichiometry is 1.45 kg O_2 per 1 kg of husk.

The peculiarity of sunflower husk is its high yield of volatile substances ($\approx$ 80 %), it is well gasified. Fixed carbon is 22.8 %. However, the composition of husk ash contains an increased amount of alkali metal oxides, calcium oxides (CaO), silicon (SiO_2), aluminum (Al_2O_3), etc. The presence of low-melting eutectics in the dust and slag causes increased slagging of both radiation and convective heating surfaces. This imposes serious restrictions on the organization and parameters of the process. The slag capacity of the ash should be taken into account. It increases with temperature. The softening temperature of ash, due to the presence of up to 15 % CaO and alkali metal oxides in the composition, is quite low and already at a tem-

perature of 850–900 °C, slagging of heating surfaces becomes avalanche-like. Therefore, gasification of husks requires a low-temperature regime [13].

In this study, by analogy with work [14], test materials (sunflower husks) and dimensionless characteristic numbers were used to characterize the operating parameters of oxygen-steam plasma gasification. The plasma flow (Figure 5) provides heat for gasification in the reactor (Figure 6). The amount of plasma heat is characterized by the ratio of plasma energy to waste energy (sunflower husk) (PER), which is defined as:

$$PER = \frac{P_{pla}}{LHV_w \cdot \dot{m}_w},$$

where P_{pla} is the plasma power; LHV_w is the lower calorific value of raw materials; $\dot{m}_w$ is mass flow of raw materials.

Equivalence Ratio (ER) is used to quantify the degree of combustion in gasification/processes:

Table 1. Measurement results

| Experiment number	1	2	3	4	5	6	7
Operating parameters							
PER	0.12	0.08	0.04	0.12	0.12	0.12	0.12
ER	0.06	0.06	0.06	0.04	0.08	0.06	0.06
SOMR	2.26	2.26	2.26	2.26	2.26	2.0	2.5
Steam temperature, °C	1500	1100	800	1800	1300	1600	1250
Measurement results							
Synthesis gas output, nm³/kg waste	1.67	1.4	1.2	1.57	1.77	1.66	1.7
H_2 volume fraction, %	55	45	30	57	52	50	55
CO volume fraction, %	32	30	25	35	30	30	35
CO_2 volume fraction, %	10	18	30	6	16	8	8
N_2 volume fraction, %	2	2	2	2	2	2	2
CH_4	0	5	13	0	0	0	0
H_2/CO	1.72	1.5	1.2	1.63	1.73	1.67	1.57
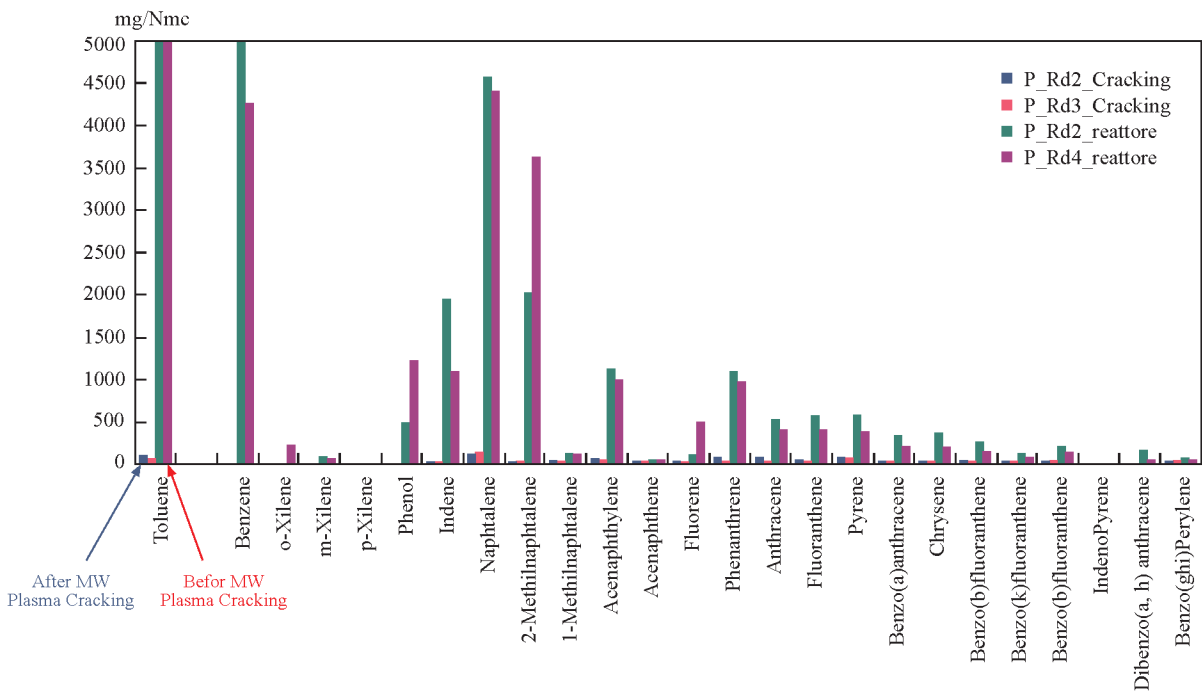
Figure 7. Gas chemical analysis of wood chip pyrolysis. Amounts of components before and after plasma molecular cracking [17]

$$ER = \frac{\left(\dot{m}_{O_2} / \dot{m}_w \right)}{\left(\dot{m}_{O_2} / \dot{m}_w \right)_{stoik}},$$

where $\dot{m}_{O_2}$ is the oxygen consumption; $\dot{m}_{O_2} / \dot{m}_w$ is the ratio of oxygen and raw material consumption; $\left(\dot{m}_{O_2} / \dot{m}_w \right)_{stoik}$ is the stoichiometric ratio of oxygen and raw material consumption.

The steam to oxygen mass ratio (SOMR) is a dimensionless parameter, which is used to characterize the steam flow rate in the oxygen-steam gasification process. In this work, it was used as the third dimensionless parameter:

$$SOMR \quad \frac{steam}{}$$

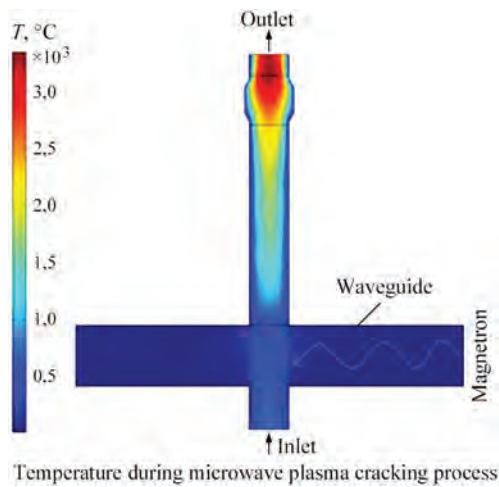Temperature during microwave plasma cracking process

Figure 8. Simulation of microwave plasma. Gas temperature distribution inside the plasmatron

The results of measurements of plasma steam-oxygen gasification of sunflower husks in a demo reactor (Figure 6) are given in Table 1.

High-temperature plasma blasting is the most important component of the process. Plasma power affects the energy balance of the entire gasification process, and it also directly affects the temperature profile, synthesis gas composition, resin yield and stability of the gasification process. Several cases were simulated to investigate the influence of PER on gasification performance. In these cases, the ER and SAMR values are set to 0.06 and 2.26, respectively. These values have been verified as "optimal" values for oxygen and steam gasification. The PER value ranges from 0.04 to 0.12. Increasing PER increases the average temperature of the steam-oxygen feed mixture and increases the heat input for gasification. The volume fractions of all combustible gases increase with increasing PER, while the opposite trend is observed for CO_2. However, it should be noted that the positive effect of increasing PER is not unlimited. The temperature inside the reactor also increases with increasing PER. Too high a temperature compromises the thermal stability of the reactor walls, and low-melting ash components may melt in the gasification section. An average wall temperature in the gasification section of more than 1300 °C is already too high for engineering applications.

In traditional gasifiers, the energy required for heating the feedstock, pyrolysis and gasification of the feedstock is generated mainly through partial combustion. The equivalence ratio (ER) for a traditional gasifier is around 0.3 to meet the energy demand. In the case under study, heat is introduced by plasma and high-temperature steam, so the ER val-
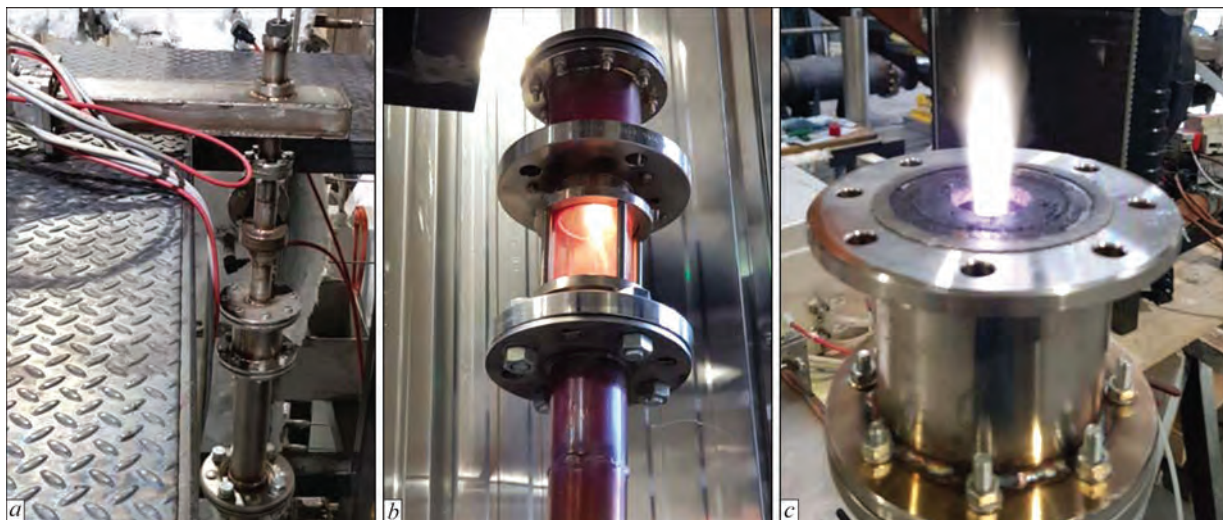
Figure 9. Microwave plasma system (*a*) on a pyrolysis reactor (*b*), microwave plasmatron in the laboratory (*c*) [17]

ue will be much lower (about 0.06). The effect of ER on the gasification process is twofold. On the one hand, a higher ER provides more chemical heat during combustion, which has a beneficial effect on both the synthesis gas yield and the LHV value, so this ER effect is positive. On the other hand, a higher ER means more combustion products in the reactor, resulting in less combustible gases. When air is used, increasing the amount of N_2 entering the reactor dilutes the combustible gas content. From this point of view, ER also has a negative impact on synthesis gas production. The final impact of ER on the gasification process is a combination of these two aspects. The supply of high-temperature steam affects the gasification process from two sides. Firstly, steam is involved in chemical reactions such as the water-gas reaction and the water gas shift reaction. In this case, it affects the chemical equilibrium in the system. Secondly, high-temperature steam changes the overall flow of mass and energy within the reactor and affects the energy balance of the system. As SOMR increases from 2 to 2.5, the volume fraction of H_2 in the synthesis gas increases, and CO_2 decreases. Similar trends were noted by other researchers [14–16]. This phenomenon is the result of stimulating the water-gas shift reaction ($CO + H_2O \rightarrow H_2 + CO_2$) by increasing the steam supply. As a result of the additional heat input from high-temperature steam, the synthesis gas yield and LHV slowly increase with increasing SOMR.

Pyrolysis gas formed during biomass gasification in traditional gasifiers is highly contaminated and contains resins and many other heavy hydrocarbons (Figure 7). The direct use of pyrolysis gas is complicated by the presence of aromatic substances in its composition. This gas is not suitable for combustion (due to environmental regulations) or as fuel for electric generators (due to engine failure).

The traditional purification (cracking) of such gas (pyrolysis gas from wood chips or sunflower husks) is thermal cracking, but this method requires high energy consumption (about 360 kW/h per 1000 N·m³/h), which is not economically feasible [17].

Therefore, for this task there is a new cracking technology — microwave plasma cracking.

Gas pyrolysis cracking processes will make it possible to prepare raw gas to power heating and hot water boilers or use it as fuel for gas generating stations in accordance with modern environmental requirements.

An important task is the cracking of pyrolysis gas and the conversion of resinous substances (resins, tars, aromatic molecules) into a gaseous state, thereby increasing the energy value of the gas. The results of the microwave plasma simulation are shown in Figure 8.

According to the results obtained by the Italian company Plasma Dynamics SRL [17], energy consumption during microwave plasma cracking of pyrolysis gas from wood chips is about 75–80 kW/h per 1000 N·m³/h), which is economically acceptable. The microwave plasma system is shown in Figure 9.

Synthesis gas by components (vol.%) after plasma cracking has the following composition: hydrogen (H_2) — 45; carbon monoxide (CO) — 20; carbon dioxide (CO_2) — 14.5; methane (CH_4) — 12; aqueous phase (H_2O) — 6.3; nitrogen (N_2) — 0.99; ethane (C_2H_6) — 0.5; ethylene (C_2H_4) — 0.5; acetylene (C_2H_2) — 0.2; oxygen (O_2) – 0.01.

CONCLUSIONS

1. A new model of biomass gasification using electrodeless HF and microwave plasmatrons and steam-oxygen blast has been developed and studied.

2. The influence of three dimensionless operating parameters PER, ER and SOMR is discussed:

● PER has a positive effect on both synthesis gas yield and LHV synthesis of gas with suppression of tar formation.

● ER has two contradictory effects on LHV synthesis of gas: a positive effect due to the increase in

chemical heat and a negative effect due to the combustion of synthesis gas.

● SOMR mainly affects the equilibrium of the water-gas shift reaction during the gasification process.

Superheated steam supplies some heat for pyrolysis, so SOMR also has a small positive effect on synthesis gas and LHV yields. There is a relationship between PER and ER. The available degree of PER and ER is determined under oxygen-steam plasma gasification conditions. The possible range for PER under the conditions studied is 0.04–0.12. The available range of SOMR and ER is defined at PER = 0.06. Increasing SAMR expands the available ER range. The optimal gas synthesis rate can be obtained at SAMR = = 2.26 and ER = 0.06.

It has been established that all three parameters have a positive effect on the efficiency of steam-oxygen plasma gasification of biomass without the formation of tars.

3. A new method for increasing plasma volume without additional power sources or circuits for effective plasma exposure over large areas has been proposed and tested.

REFERENCES

1. Gerssen-Gondelach, S.J., Saygin, D., Wicke, B. et al. (2014) Competing uses of biomass: Assessment and comparison of the performance of bio-based heat, power, fuels and materials. *Renewable and Sustainable Energy Reviews, Elsevier*, 40(**C**), 964–998. DOI: https://doi.org/10.1016/j.rser.2014.07.197

2. Glasgow Climate Pact (2021) In: *Report of Conf. of the Parties Serving as the Meeting of the Parties to the Paris Agreement on its third Session, Held in Glasgow from 31 October to 13 November 2021*. https://unfccc.int/sites/default/files/resource/cma2021_10_add1_adv.pdf

3. Zhovtyanskij, V., Ostapchuk, M. (2022) Plasma technologies in the problem of producing "more than green hydrogen". *Gorenie i Plazmohimiya*, 20(**1**), 11–32 [in Russian]. DOI: https://doi.org/10.18321/cpc478

4. Elhambakhsh, A., Van Duc Long, N., Lamichhane, P., Hessel, V. (2023) Recent progress and future directions in plasma-assisted biomass conversion to hydrogen. *Renewable Energy*, **218**, 119307. DOI: https://doi.org/10.1016/j.renene.2023.119307

5. Valizadeh, S., Hakimian, H., Farooq, A. et al. (2022) Valorization of biomass through gasification for green hydrogen generation: A comprehensive review. *Bioresource Technology*, **365**, 128143. DOI: https://doi.org/10.1016/j.biortech.2022.128143

6. Chen, G., Tu, X., Homm, G., Weidenkaff, A. (2022) Plasma pyrolysis for a sustainable hydrogen economy. *Nature Reviews Materials*, 7(**5**), 333–334. DOI: https://doi.org/10.1038/s41578-022-00439-8

7. Vecten, S., Wilkinson, M., Bimbo, N. et al. (2021) Hydrogen-rich syngas production from biomass in a steam microwave-induced plasma gasification reactor. *Bioresource Technology*, 337(**2**), 125324. DOI: https://doi.org/10.1016/j.biortech.2021.125324

8. Gomez, E., Amutha Rani, D., Cheeseman, C.R. et al. (2009) Thermal plasma technology for the treatment of wastes: A critical review. *J. of Hazardous Materials*, 161(**2–3**), 614–626. DOI: https://doi.org/10.1016/j.jhazmat.2008.04.017

9. Gabbar, H.A., Darda, S.A., Damideh, V. et al. (2021) Comparative study of atmospheric pressure DC, RF, and microwave thermal plasma torches for waste to energy applications. *Sustainable Energy Technologies and Assessments*, **47**, 101447. DOI: https://doi.org/10.1016/j.seta.2021.101447

10. Petrov, S.V., Zhovtyansky, V.A. (2019) *Energy efficient steam-plasma technologies for waste processing*. Kyiv, Naukova Dumka [in Russian].

11. *Applied Plasma Technologies. More Products: Plasma Torches*. https://www.plasmacombustion.com/product-torches.html

12. Yuehong, Z., Hao, W., Zhihong, X. (2006) Conceptual design and simulation study of a co-gasification technology. *Energy Conversion and Management*, 47(**11–12**), 1416–1428. DOI: https://doi.org/10.1016/j.enconman.2005.08.024

13. Gorbatenko, V.Ya., Danilin, E.A., Kolosov, M.V. (2007) Combustion device for burning husks. *Energeticheskie i Teplotehnicheskie Processy i Oborudovanie*, **2**, 159–163.

14. Zhang, Q., Dor, L., Zhang, L. et al. (2012) Performance analysis of municipal solid waste gasification with steam in a plasma gasification melting reactor. *Applied Energy*, **98**, 219–229. DOI: https://doi.org/10.1016/j.apenergy.2012.03.028

15. Lucas, C., Szewczyka, D., Blasiaka, W., Mochidab, S. (2004) High-temperature air and steam gasification of densified biofuels. *Biomass Bioenergy*, 27(**6**), 563–575. DOI: https://doi.org/10.1016/j.biombioe.2003.08.015

16. Blasiak, W., Szewczyk, D., Lucas, C. (2002) Reforming of biomass wastes into fuel gas with high temperature air and steam. In: *Proc. of Conf. on Pyrolysis and Gasification of Biomass and Waste, Strasbourg, France, 2002*.

17. *Plasma dynamics. Research and development in plasma technology*. https://plasma-dynamics.it/

ORCID

S. Petrov:0000-0003-0373-8003,
P. Stukhlyak: 0000-0001-9067-5543
S. Bondarenko: 0000-0001-9590-4747,
Shahram Roshanpour: 0000-0002-4272-9217
M. Ganczarski: 0009-0002-2967-6795

CONFLICT OF INTEREST

The Authors declare no conflict of interest

CORRESPONDING AUTHOR

S. Petrov
The Gas Institute of the NASU
39 Degtyarivska Str., 03113, Kyiv, Ukraine.
E-mail: vizana.sp@gmail.com

SUGGESTED CITATION

JOURNAL HOME PAGE

https://patonpublishinghouse.com/eng/journals/tpwj

EFFECTIVENESS OF THE INFLUENCE OF SOLID-STATE LASER RADIATION ON THE PROCESS OF PULSED-ARC WELDING OF ALUMINIUM ALLOY 1561

Y. Zhao, X. Wang, Z. Liu, V.Yu. Khaskin

Guangdong Provincial Key Laboratory of Advanced Welding Technology, China-Ukraine Institute of Welding, Guangdong Academy of Sciences, Guangzhou, 510650, China

ABSTRACT

The results of consumable electrode pulsed-arc welding of 1561 aluminium alloy of 6 mm thickness (P-MIG) with and without addition of focused radiation of the Nd:YAG laser were analyzed. During laser-P-MIG welding, the influence of the arc energy source improves absorption of laser radiation and promotes high-quality formation of the weld reinforcement, and the influence of the laser source leads to an increase in the depth of penetration due to the formation of a vapour-gas channel (keyhole) and to a decrease in the current density of the anode region of the arc on the electrode wire, which reduces emissions of welding aerosols. Factors influencing the effectiveness of laser radiation during laser-P-MIG welding were determined. It is shown that an increase in laser power leads to an increase in arc voltage with a simultaneous decrease in welding current. Formation of high-quality welds by P-MIG welding of 1561 alloy requires an energy input of 4.5–5.0 kJ/cm. Here, a regular structure of the weld metal with the dendritic parameter of 13–15 μm and joint strength of 90–92 % of the strength of the base metal is formed. Introduction of focused radiation of a 3.0 kW Nd:YAG laser into the welding process allows reducing the energy input by approximately half, due to which the dendritic parameter decreases to 10 μm, and the strength of the joints increases to 93–96 % of base metal strength.

KEYWORDS: aluminium alloy, consumable electrode pulsed arc welding (P-MIG), Nd:YAG-laser radiation, modes, welding aerosols, structures, strength.

INTRODUCTION

ANALYSIS OF PUBLISHED DATA AND PROBLEM DEFINITION

The question of welding aluminium alloy structures is becoming ever more urgent in connection with increasing demand for lightweight vehicles and technical facilities, instruments, etc. [1]. This is also promoted by application of a wide range of building structures from aluminium alloys [2]. In particular, the researchers are interested in application of aluminium alloys of the fourth, fifth and sixth series as building and structural materials [3]. These alloys are attractive not only due to such characteristics as wear- and corrosion resistance, a combination of low density with an acceptable strength, but also due to sufficiently good weldability [4]. Technologies of welding structures from such materials have been optimized for a rather long time [5]. With emergence of modern welding processes, however, in particular laser-arc and laser-plasma [6], there comes the question of improvement of the effectiveness of joining the already well-known materials.

Application of laser-MIG process can be more advantageous for welding aluminium alloys than use of laser-TIG and laser-plasma processes, due to a higher adaptability-to-fabrication of feeding additional material at weld formation and simpler controllability

of its structure formation. However, the laser-MIG welding process has its features. So, in this process of welding 5 mm 5083 alloy with application of fiber-laser radiation, a susceptibility to formation of coarse porosity in the welds was revealed [7]. It was related to disturbance of the vapour-gas channel (keyhole) stability. Transition to heat conduction welding mode, which prevents keyhole formation, can help eliminate this drawback [8]. It, however, lowers the effectiveness of laser radiation application. Another variant for improvement of the quality of laser-MIG welding of 5083 alloy can be the process of welding from two sides, which is more suitable for joining thicknesses greater than 10 mm [9].

Thus, there is an urgent task of studying the features of the process of welding the known structural aluminium alloys is particular, of fifth series, with application of a consumable electrode arc and laser radiation. Here, it is important to consider the factors of improvement of the efficiency of application of radiation with wave length of the order of 1.06 μm. The 5083 alloy or 1561 alloy of up to 10 mm thickness close to it can be considered as the studied alloys [10].

PURPOSE AND OBJECTIVE OF THE STUDIES

The purpose of the work is to analyze the possibilities of improvement of process effectiveness and reduction of the specific energy input into the metal in

Table 1. Chemical composition of 1561 alloy, wt.%

Al	Mn	Si	Fe	Cu	Zn	Zr	Mg	Be
Base	0.8–1.1	≤0.4	≤0.4	≤0.1	≤0.2	0.02–0.12	5.5–6.5	0.0001–0.0003

consumable electrode pulsed-arc welding of 1561 aluminium alloy (P-MIG), due to involvement of laser radiation of the near infrared spectrum range in the process.

Solving the following tasks is proposed to achieve this purpose:

1. Analyze the interaction of arc and laser energy sources during welding of 1561 alloy and the influence of laser radiation on the features of P-MIG welding.

2. Analyze the influence of the change of laser radiation power on weld formation, change of the weld cross-sectional area and other parameters of P-MIG process of welding 1561 alloy.

3. Compare the obtained results of P-MIG welding of 1561 alloy without application of laser radiation and with its application.

MATERIALS, EQUIPMENT AND METHODS OF INVESTIGATION

The following investigation procedure was selected to achieve the defined purpose of the work: selection of parameters of the mode of P-MIG welding of 1561 aluminium alloy 6 mm thick by the criterion of satisfactory formation of the weld, investigation of the influence of addition of focused laser radiation (wave length $\lambda = 1.06$ μm) on the process of P-MIG welding, comparison of penetration of 1561 alloy plates ($\delta = 6$ mm) at P-MIG welding with and without addition of laser radiation, selection of parameters of the mode of laser-P-MIG welding of 1561 alloy ($\delta = 6$ mm) by the criterion of satisfactory formation of the weld, analysis of the obtained results by macrosections of weld cross-section, determination of the prospects of application of focused laser radiation

($\lambda = 1.06$ μm) together with consumable electrode pulsed arc in welding alloys of Al–Mg system.

In order to conduct the experiments, samples of 1561 alloy of 300×100×6 mm size were used in the work. Chemical composition of 1561 alloy is given in Table 1. Wire from the same alloy of 1.2 mm diameter was used as the consumable electrode.

Experiments were conducted by the scheme proposed in work [11]. According to this scheme, a laboratory facility was selected, based on a three-co-ordinate manipulator, which was used to conduct P-MIG and laser-P-MIG welding (Figure 1). Used for this purpose was an original welding head, which integrated the laser and arc components. During performance of studies on P-MIG welding the arc torch was installed upright on the sample, and in the studies of laser-P-MIG welding the axis of the focused laser beam was directed normal to the sample, and the arc torch was located ahead in the direction of welding at a certain angle (Figure 1, *a*). Used as the shielding gas was argon with flow rate of 12–20 l/min. Radiation of up to 4.0 kW power was supplied from Nd:YAG laser, using optical fibre of 400 μm diameter (up to 0.5 mm diameter of focusing spot). Fronius TPS-2700 power source with reserved polarity current of about 300 Hz was used as the power source for P-MIG process.

Sample welding was performed without edge preparation. The angle of inclination of the axis of focused laser radiation to the metal being welded was equal to 81°, and the angle of inclination of the arc torch was 55°. The weld root was formed on a variable backing from stainless steel with a forming groove of 1.5–2.1 mm depth.

Figure 1. Facility (*a*) for conducting experiments on laser-P-MIG welding and clamp (*b*) with the sample after welding
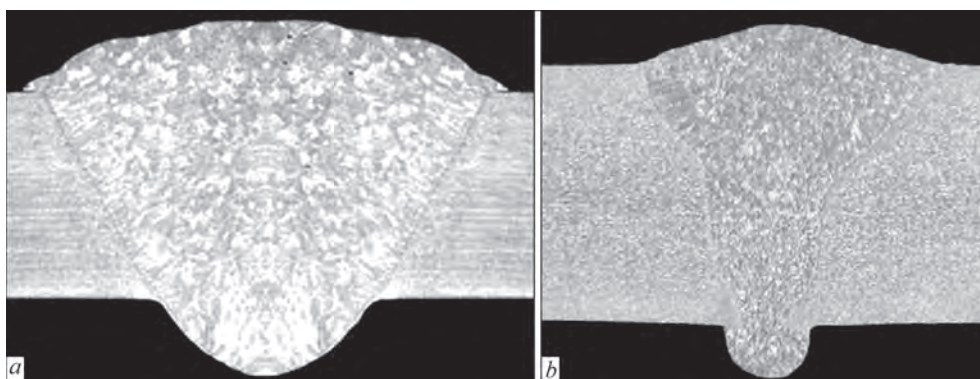
Figure 2. Macrostructure of welds produced by different processes of welding 1561 alloy (δ = 6 mm): a — P-MIG ($I \approx 200$ A; $U =$ = 22.5 V; $V = 0.42$ m/min; $E_{MIG} \approx 4.8$ kJ/cm); b — laser-P-MIG welding ($P = 3.0$ kW; $I = 75$ A; $U = 17$ V; $V = 1.0$ m/min; $E_{\Sigma} = 2.4$ kJ/cm)

Welding was followed by making transverse sections of the samples, which were used further on to prepare macrosections. The geometrical parameters of the welds (width B, reinforcement height a, penetration depth h, cross-sectional area S) was determined on these macrosections with the accuracy of ±0.1 mm. The number and diameter of pores and voids in the welds were also assessed. When preparing the macrosections, the weld structure was revealed by chemical etching in the solution, which consisted of three acids — $HCl:HNO_3:HF$ in the proportion of 18:4:1. The weld microstructures were revealed in keeping with the recommendations of work [12]. The produced structures were studied in Neophot-32 microscope with the magnifications of ×50–1000. Mechanical testing for static uniaxial tension was conducted in keeping with the requirements of GOST 6996–66 with application of universal servohydraulic test system MTS 318.25 (Material Test System, USA) with the maximal force of 250 kN.

RESULTS OF INVESTIGATION OF ALUMINIUM ALLOY WELDING

Investigations were conducted by butt welding without edge preparation of 1561 aluminium alloy sam-

ples of the selected size. Here, the following ranges of welding mode parameter variation were chosen:

• P-MIG welding — welding current $I = 100$– = 200 A, arc voltage $U = 16$–24 V, process speed $V =$ = 0.42; 0.5; 0.75; 1.0 m/min, filler wire feed rate $V_w =$ = 4–12 m/min;

• laser-P-MIG welding — radiation power P = = 1–4 kW; process speed $V = 0.5$; 0.75; 1.0 m/min, ranges of other mode parameters are similar to P-MIG welding.

Values of energy inputs of the processes of metal welding from one side were calculated by the following formulas:

• P-MIG welding $E_{MIG} = 0.72IU/V$, kJ/cm, where 0.72 is the effective efficiency of a consumable electrode arc in argon [13, 14];

• laser welding $E_{las} = 0.75P/V$, kJ/cm, where 0.75 is the effective efficiency of welding by Nd:YAG laser [15];

• laser-P-MIG welding $E_{\Sigma} = E_{las} + E_{MIG}$.

First, the criterion of weld formation quality was used to select the mode of P-MIG welding (Figure 2, a). After that the mode of laser-P-MIG welding was selected in a similar way (Figure 2, b). Comparison of these welds showed that in the case of application
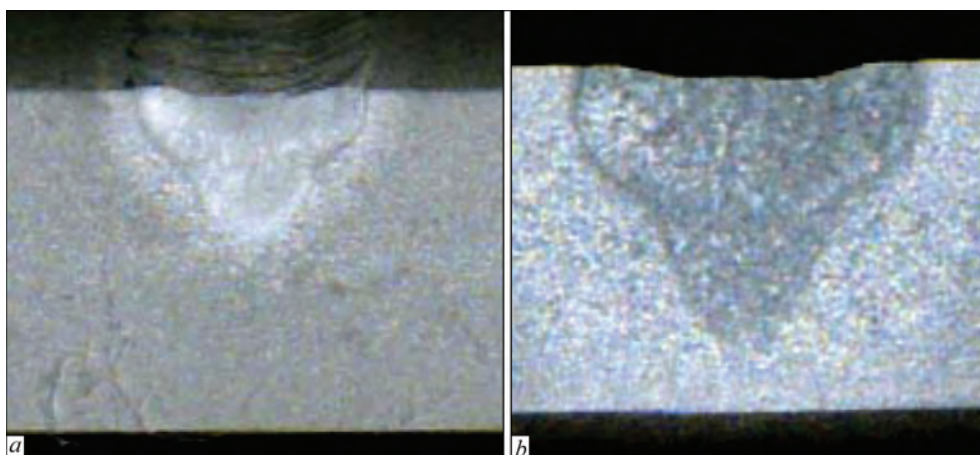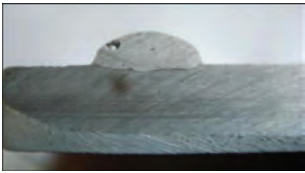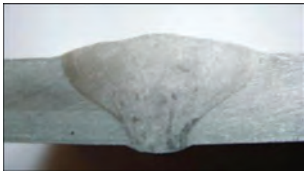

Figure 3. Macrostructure of weld deposits produced by laser welding of 1561 alloy (δ = 6 mm): a — $P = 3.0$ kW; $V = 0.6$ m/min; $E_{las} \approx 2.3$ kJ/cm; b — $P = 4.0$ kW; $V = 0.5$ m/min; $E_{las} \approx 3.6$ kJ/cm

Table 2. Geometrical shape of weld deposits in 1561 alloy (δ = 6 mm), depending on welding speed and electrode wire feed rate in P-MIG and laser-P-MIG processes

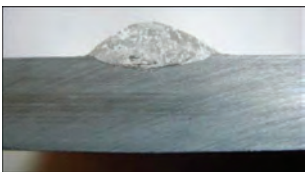| Welding modes		P-MIG welding	Laser-P-MIG welding (P = 4 kW)
Welding speed, m/min	Wire feed rate, m/min		
0.5	7.5		
0.5	8.3		
0.75	8.3		
0.75	9.3		
1.0	10.9		
1.0	12.2		

of laser-P-MIG welding the welds is narrowed ~1.7 times. Further studies revealed that the welds are narrowed 1.5–2.0 times on average. Here, the welding energy input decreases approximately 2 times, compared to P-MIG welding, and the welding speed is increased more than 2 times. Such a result is indicative of the good prospects for replacement of P-MIG welding by laser-P-MIG welding and the need for a more detailed comparison of these processes.

An attempt to perform laser welding of 1561 alloy (δ = 6 mm) revealed problems with achievement of complete penetration, related to insufficient power density of the used Nd:YAG-laser, the radiation of which was focused into a spot of approximately 0.5 mm diameter. More over, the need to use filler material to eliminate weld sagging and to form upper reinforcement was determined (Figure 3).

It was found that under the conditions of P-MIG process in the range of welding speeds of 0.5–0.7 m/h and of wire feed rates of 7.5–9.3 m/min, it was not possible to achieve complete penetration of 6 mm 1561 alloy. At the same time, at the same modes the hybrid process of laser-P-MIG welding allows achieving complete penetration of the welded metal due to the availability of focused laser radiation of 4 kW power (Table 2).

More over, in addition to the obvious influence of laser radiation on the penetration depth and weld formation, its influence on the arc voltage and welding current was established during performance of technological studies. It was found that irrespective of the wire feed rate (in the range from 7.5 to 13.2 m/min) laser radiation of 4 kW power increases the arc voltage by 1–2 V (and the arc length, accordingly), and
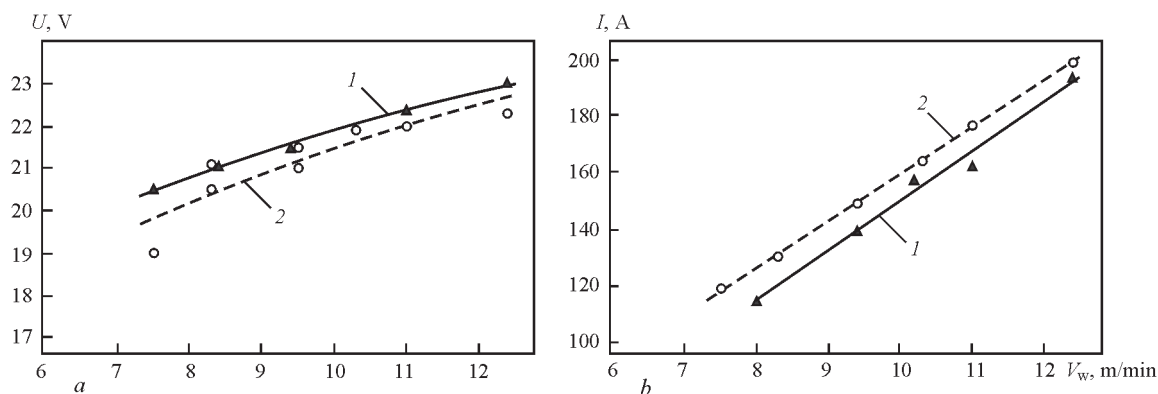
Figure 4. Dependencies of the change in arc voltage U, V and welding current I, A on electrode wire feed rate V_w, m/min at laser-P-MIG (*1*) welding with 4 kW laser radiation and at P-MIG welding (*2*)

reduces the welding current by 10–15 A (Figure 4). With increase of laser radiation power from 1 up to 4 kW at unchanged electrode wire feed rate, the same dependence of increase of arc voltage and decrease of welding current (Table 3) is also observed. Here, an increase of the total $h + a$ value (penetration depth h + weld reinforcement height a) and weld width B at laser-P-MIG welding is found compared to P-MIG welding (Figure 5).

Preliminary studies, conducted at PWI showed [16] that with current increase in inert-gas consumable electrode welding the average temperature of

Table 3. Macrostructures of weld deposits, produced at P-MIG and laser-P-MIG welding of 1561 aluminium alloy ($\delta = 6$ mm) ($V = 0.5$ m/min; $V_w = 8.3$ m/min)

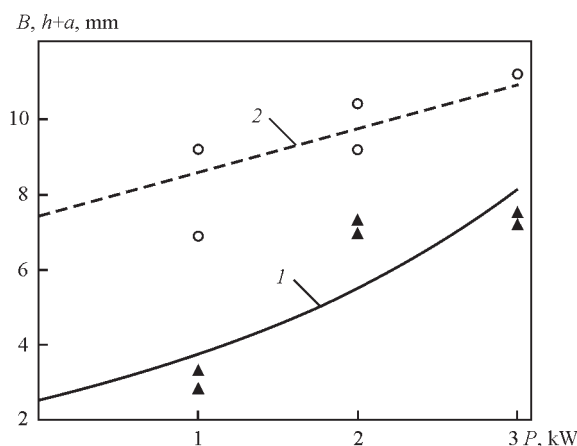| Welding current, I, A	Arc voltage U, V	Radiation power, P, kW	Result
135	18.7	0	
135	18.7	1	
126	18.6	2	
130	20.0	3	
128	20.5	4	

33

Figure 5. Influence of the change of laser power *P*, kW at laser-P-MIG welding (*V* = 0.5 m/min; *V*$_w$ = 8.3 m/min) of 1561 alloy (δ = 6 mm) on increase of the total value of penetration depth *h* with reinforcement height *a* (*1*) and weld width *B* (*2*)

electrode metal drops is increased, reaching the values of boiling temperature of the aluminium alloy, from which the wire is made. Here, evaporation of metals with a comparatively low temperature of vapour formation, such as magnesium, lithium, zinc, etc occurs. Lowering magnesium content in the weld metal by one percent leads to decrease of the joint strength by 10–20 MPa. Conducted investigations showed that at P-MIG welding in the studied current range magnesium content in the weld metal can decrease by up to 25 % compared to the data in Table 1, and in the case of laser-P-MIG welding — by up to 15 %. It is probable that this is related to a considerable (up to 3 times) reduction of the weld pool volume.

The high average temperature of electrode metal drops in welding with consumable electrode of 1561 grade (irrespective of shielding gas composition) leads to evaporation of alloying elements and working zone contamination by welding aerosols of a complex chemical composition, which contain a number of toxic solid-phase components, namely Al_2O_3, MgO and MnO_2. Determination of the quantity of aerosols was performed by the following procedure. Air from

Figure 6. Influence of energy input *E*, kJ/cm of the processes of welding 1561 alloy (δ = 6 mm) on the total value of penetration depth *h* with reinforcement height *a* (*1*, *2*) and weld width *B* (*3*, *4*): *1*, *3* — laser-P-MIG (*P* = 4 kW); *2*, *4* – P-MIG

the welding zone at 20 cm distance from the arc was sampled with electric aspirator of 822 model with 12–15 l/min rate through preloaded AFA-VP-20 filters. The quantity of solid aerosols in the working zone air was measured by the gravimetric method. Al_2O_3, MgO and MnO_2 content was determined by the procedure described in work [17].

The total quantity of aerosols at P-MIG welding depends, primarily, on the density of welding current on the electrode wire. The higher the current density, the greater the quantity of aerosols formed around the weld pool. In the studied mode range, the current density was 50–90 A/ mm², here the concentrations of the respective welding aerosols were as follows: $K_{Al_2O_3}$ = = 125–145 mg/m³, K_{MgO} = 14–17 mg/m³, K_{MnO_2} = 1.9–2.2 mg/m³. In laser-P-MIG welding no changes in the concentration of the above-mentioned welding aerosols were found.

In hybrid laser-MIG process the manifestation of the glow of focused laser radiation in the concentrated aerosol environment around the area of welding arc impact is very well observed. With increase of the wire melting rate (welding current), the number of electrode metal drops and volume of products evaporating from them become greater. It increases the density of gas environment in the near-cathode region. More over, the weld pool on aluminium alloys has the form of a kind of mirror, which increases in size with increase of welding current. It causes greater losses of laser radiation in a heterogeneous drop-aerosol environment around the pool and enhances its reflection from the pool proper. This results in reduction of the fraction of absorbed laser radiation and effective laser power, which acts directly on the metal being welded, i.e. the efficiency of the laser component of laser-P-MIG welding process is decreased. It leads to reduction of the penetration depth and change of geometrical parameters of the formed welds, accordingly.

Investigations of the influence of electrode wire feed rate on the geometrical parameters of weld deposits in P-MIG and laser-P-MIG welding showed the following. At the same welding speeds (*V* = 0.5 m/min) and wire feed rates (*V*$_w$ = 7.5–9.3 m/min) the hybrid laser-P-MIG process allows increasing the weld width by 50–60 % compared to P-MIG at simultaneous reduction of reinforcement height by 10–60 % (in keeping with increase of *V*$_w$ value). Similar dependencies are observed also at high welding speeds, but at smaller absolute values of the geometrical parameters of welds.

As shown by the conducted studies, introduction of laser radiation of power *P* into P-MIG process leads to increase of penetration depth (Figure 5). However, comparison of energy inputs of P-MIG and laser-P-
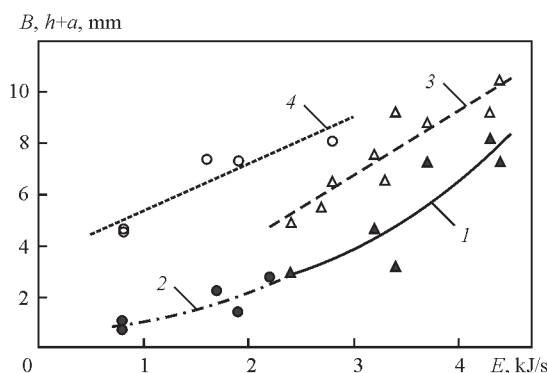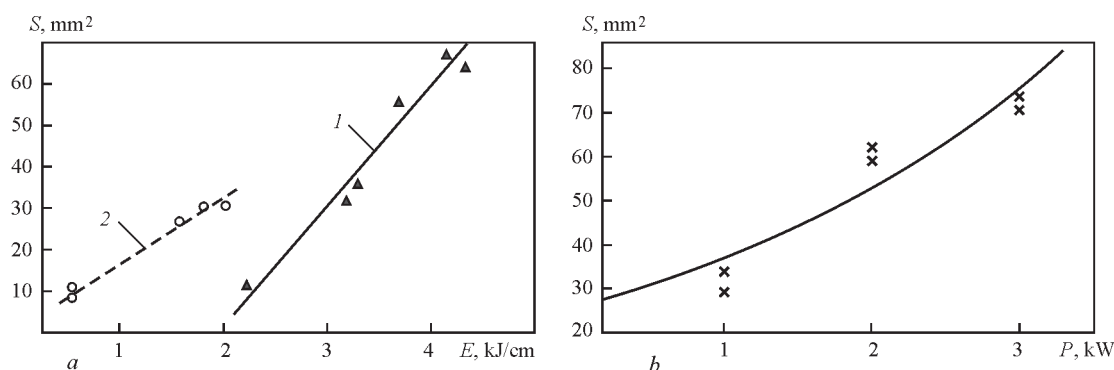
Figure 7. Influence of energy input E, kJ/cm (a) and laser radiation power P, kW (b) on area S, mm^2 of weld cross-section at laser-P-MIG welding of 1561 alloy ($\delta = 6$ mm)

MIG welding shows that the process of increase of penetration depth (more exactly total $h + a$ value) is continuous and has a common tendency (Figure 6). In keeping with this tendency, increase of $h + a$ value is directly proportional to the welding energy input. Instead, the change of width of the welds and their cross-sectional area depends on the availability of laser radiation. So, at laser-MIG-welding with the same energy input the weld width decreases by 30–40 %, compared to weld width at P-MIG welding (Figure 6), which accounts for approximately three times reduction of the remelted metal area in this case (Figure 7, a). At the same time, increase of the remelted metal area with increase of laser power P at laser-P-MIG welding (Figure 7, b) is indicative of increase of penetration depth due to radiation impact.

As regards the characteristic weld defects in the form of inner pores and voids, it is not difficult to reduce their quantity and dimensions to acceptable level in the case of application of preliminary scraping of the edges and chemical etching of the electrode wire, as well as ensuring a reliable gas protection of the weld pool. Under the conditions of conducting the experiments, inner pores of 0.2–0.8 mm diameter were observed in the quantity of the order of 5–10 pcs/100 mm of the weld. Cracking susceptibility when producing the joints by the studied welding processes was not established. Investigations of microstructures of welds produced by laser, P-MIG and laser-P-MIG welding showed the dependence of weld

structure on the welding process, which can be determined through the dendritic parameter (Figure 8). In the case of laser welding, the dendritic parameter is equal to 8 μm (Figure 8, a), at laser-P-MIG welding is it increased to 10 μm, and at P-MIG welding it is equal to 13–15 μm (Figure 8, c).

Microstructure of weld metal with all the studied welding processes predominantly depends on the welding method and mode. The weld metal structure is determined by grain shape and dimensions and their inner structure, as well as the shape, dimensions and location of chemical compounds, precipitating during crystallization. At close dimensions of the grains produced by laser-P-MIG and P-MIG welding, the dendrite branches can be both thin (in the case of laser-P-MIG, Figure 8, b), and thick (at P-MIG, Figure 8, c), and eutectic inclusions can be fine or coarse, respectively.

The formed structure influences the mechanical properties of the produced joints in an appropriate way. Static tensile testing showed that P-MIG welding allows reaching values of temporary fracture resistance of 314–323 MPa, and laser-P-MIG welding — 327–336 MPa. In all the cases, fracture occurred through the zone of weld fusion with base metal. Taking into account base metal strength (~350 MPa) it can be assumed that P-MIG welding ensures joint strength at the level of 90–92 %, and laser-P-MIG — at the level of 93–96 %.
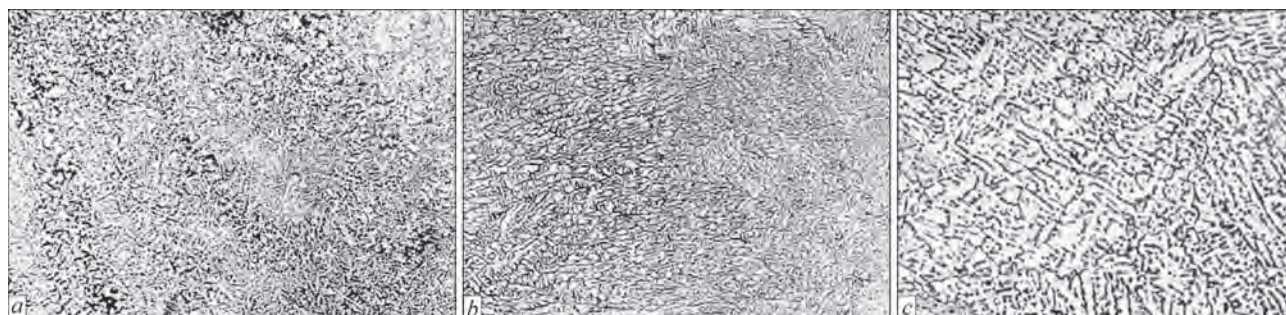

Figure 8. Microstructure of the metal of 1561 alloy welds, produced by the following welding processes (×250): a — laser; b — laser-P-MIG; c — P-MIG

DISCUSSION OF THE RESULTS
OF STUDYING THE ALUMINIUM ALLOYS

Experiments show that at combination of the laser and P-MIG welding processes into one common process, the influence of focused laser radiation is primarily realized through creation of the keyhole, and the influence of consumable electrode arc — through improvement of absorption of laser radiation, creating a pool of a certain width, adding metal and formation of welds with certain geometrical parameters. With increase of the power of laser and arc components of the common process the density of evaporation from the weld pool and of spatter ejection from it are increased. It leads to increase of concentration of harmful welding aerosols and lowering of laser radiation efficiency due to its scattering, reflection from the pool and other power losses. In its turn, P-MIG welding is characterized by two times higher energy input and approximately 2–3 times greater weld width than laser-P-MIG welding (Figure 2), which may lead to greater values of the parameters of residual stress-strain state of welded structures. However, correct selection of the mode parameters can ensure acceptable results at application of each of the considered processes.

One of the most important factors, influencing the penetration depth at laser-P-MIG welding, is the ratio of powers of the laser and arc components and the process speed. So, in welding with the speed of 60 m/h, increase of electrode wire feed rate from 10.9 to 12.2 m/min (from $I = 162$ A, $U = 22.4$ V to $I = 194$ A, $U = 23$ V, respectively) almost did not influence the increase of penetration depth, but increased the weld width from $B = 10.1$ mm to $B = 13.5$ mm (Table 2). This is associated with filling of the keyhole with electrode wire liquid metal, which is performed by the drop method and is an antiphase self-oscillation of the keyhole. In other cases, for instance, at laser-P-MIG welding at the speed of 45 m/h, drop transfer of electrode metal coincides with self-oscillation of the keyhole and promotes a considerable increase of penetration depth at increase of electrode wire feed speed from 8.3 ($I = 123$ A, $U = 21.1$ V) up to 9.3 ($I = 142$ A, $U = 21.1$ V) m/min (Table 2).

Increase of arc voltage with simultaneous reduction of welding current under the influence of laser radiation at P-MIG welding (Figure 4), is, primarily, associated with increase of ionization of the near-cathode region of the welding arc by radiation and with the respective change of the arc volt-ampere characteristics. Moreover, deepening of the weld pool due to formation of a keyhole by focused laser radiation leads to a certain elongation of the arc, causing an increase of arc voltage (to 0.5–1.0 V). At the same time, additional ionization of the zone of arc column impact can lead to a certain (~10 A) lowering of welding current. This tendency is directly proportional to increase of laser radiation power, and it becomes noticeable at its value above 1 kW at arc power of the order of 2 kW.

Absence of increase of welding aerosol evolution at transition from P-MIG to laser-P-MIG welding can be associated with two processes, occurring under the impact of laser radiation. On the one hand, the influence of laser radiation power promotes increase of evaporation of aluminium, magnesium and other elements and formation of such aerosols as Al_2O_3, MgO and MnO_2. On the one hand, under the impact of laser radiation reflected from the weld pool the anode region of electrode wire is additionally heated and becomes larger (i.e. the surface of the metal drop formed at the electrode wire tip, which is covered by the arc discharge, becomes greater). Here, the current density decreases, lowering the intensity of welding aerosol formation at the same time.

The main factor, which determines the type of weld microstructure, is the cooling rate at crystallization. Therefore, to assess the structure, the dendritic parameter was selected as the main index of the process of change of weld metal crystallization rate (Figure 8). The dimensions of the dendritic parameter depend on the ratio of laser and arc powers. In the studied case, the dendritic parameter of laser-P-MIG welding (10 μm) was somewhat closer to the case of laser welding (8 μm), than to that of P-MIG process (13–15 μm), which was attributable to higher welding speed (1.0 m/min), lower energy input (~ 2.4 kJ/cm). Such a decrease of the dendritic parameter can account for increase of the level of mechanical properties of the joints produced by laser-P-MIG welding (increase of power by 3–4 %).

CONCLUSIONS

1. It was established that at laser-P-MIG welding of 1561 alloy the influence of the arc energy source promotes improvement of laser radiation absorption and sound formation of weld reinforcement, and the laser source influence leads to increase of penetration depth due to keyhole formation, and to lowering of current density in the arc anode region on electrode wire that reduces welding aerosol evolution. Here, the effectiveness of laser radiation can be decreased because of power losses with spattering of metal drops from the weld pool and keyhole filling with electrode wire liquid metal, which can be prevented by selection of the ratio of welding speed and laser and arc powers.

2. The action of focused laser radiation on P-MIG process of welding 1561 alloy becomes noticeable

starting from 1 kW, and it is manifested in exponential increase of penetration depth and cross-sectional area of welds with power increase. Increase of laser radiation power leads to arc voltage rising from 1–2 V at 2 kW up to 0.1–0.3 V at 4 kW with simultaneous decrease of welding current from 13–15 A to ~6 A, respectively, at welding speed of 0.5 m/min.

3. It was established that application of P-MIG process for welding 6 mm 1561 alloy requires energy input of 4.5–5.0 kJ/cm and allows formation of a regular structure of weld metal with dendritic parameter of 15 μm and joint strength equal to 90–92 % of base metal strength. Introduction of focused radiation of 3 kW Nd:YAG laser into the welding process enables reducing the energy input two times, resulting in dendritic parameter lowering to 10 μm, and joint strength increasing to 93–96 % of base metal strength.

REFERENCES

1. Benedyk, J.C. (2010) 3 — Aluminium alloys for lightweight automotive structures. In: *Woodhead Publishing Series in Composites Science and Engineering, Materials, Design and Manufacturing for Lightweight Vehicles*, 79–113. Ed. by P.K. Mallick. Woodhead Publishing. DOI: https://doi.org/10.1533/9781845697822.1.79

2. Sun, Y. (2023) The use of aluminium alloys in structures: Review and outlook. *Structures*, 57(**5**), 105290. DOI: https://doi.org/10.1016/j.istruc.2023.105290

3. Hung, F.-S. (2020) Design of lightweight aluminium alloy building materials for corrosion and wear resistance. *Emerging Materials Research*, 9(**3**), 750–757. DOI: https://doi.org/10.1680/jemmr.19.00177

4. Ambriz, R.R., Mayagoitia, V. (2011) *Welding of aluminium alloys*. In: *Recent Trends in Processing and Degradation of Aluminium Alloys*, 516, 63–86. Ed. by Prof. Zaki Ahmad. DOI: https://doi.org/10.5772/18757

5. Khaskin, V.Y. (2013) Development of laser welding of aluminium alloys at the E.O. Paton Electric Welding Institute. *The Paton Welding J.*, **5**, 51–55.

6. Bushma, A.I. (2015) State-of-the-art of hybrid laser-plasma welding (Review). *The Paton Welding J.*, **8**, 18–25. DOI: https://doi.org/10.15407/tpwj2015.08.04

7. Bunaziv, I., Akselsen, O. M., Salminen, A., Unt, A. (2016) Fiber laser-MIG hybrid welding of 5 mm 5083 aluminium alloy. *J. Materials Proc. Technology*, **233**, 107–114. DOI: https://doi.org/10.1016/j.jmatprotec.2016.02.018

8. Sánchez-Amaya, J. M., Pérez, T. D., Rovira, L. G., Botana, J. (2009) Laser welding of aluminium alloys 5083 and 6082 under conduction regime. *Appl. Surface Sci.*, 255(**23**), 9512–9521. DOI: https://doi.org/0.1016/j.apsusc.2009.07.081

9. Jiang, Z., Hua, X., Huang, L. et al. (2018) Double-sided hybrid laser-MIG welding plus MIG welding of 30-mm-thick aluminium alloy. *Int. J. Adv. Manuf. Technol.*, **97**, 903–913. DOI: https://doi.org/10.1007/s00170-018-1997-7

10. Babych, O.A., Korzhyk, V.M., Grynyuk, A.A. et al. (2020) Hybrid welding of aluminium 1561 and 5083 alloys using plasma-arc and consumable electrode arc (Plasma-MIG). *The Paton Welding J.*, **7**, 11–22. DOI: https://doi.org/10.37434/tpwj2020.07.02

11. Krivtsun, I.V., Khaskin, V.Yu., Korzhik, V.N., Luo, Ziyi (2015) Industrial application of hybrid laser-arc welding (Review). *The Paton Welding J.*, **7**, 41–46. DOI: https://doi.org/10.15407/tpwj2015.07.07

12. (2018) *Encyclopedia of aluminium and its alloys*. 2 Vols Ed. by G.E. Totten et al., 1st Ed. Boca Raton, CRC Press. DOI: https://doi.org/10.1201/9781351045636

13. DuPont, J.N., Marder, A.R. (1995) Thermal efficiency of arc welding processes. *Welding J.*, **74**, 406–416.

14. Hälsig, A., Mayr, P. (2013) Energy balance study of gas-shielded arc welding processes. *Welding in the World, Le Soudage dans le Monde*, 57(**5**). DOI: https://doi.org/10.1007/s40194-013-0073-z

15. De Oliveira, A.F.M., dos S. Magalhães, E., dos S. Paes, L.E. et al. (2023) A thermal analysis of laser beam welding using statistical approaches. *Processes*, 11(**7**). DOI: https://doi.org/10.3390/pr11072023

16. Levchenko, O.G., Mashin, V.S. (2003) Sanitary-hygienic characteristic of process of consumable electrode inert-gas welding of AMg6 aluminium alloy. *The Paton Welding J.*, **1**, 46–48.

17. Cole, H., Epstein, S., Peace, J. (2007) Particulate and gaseous emissions when welding aluminium alloys. *J. of Occupational and Environmental Hygiene*, 4(**9**). DOI: https://doi.org/10.1080/15459620701516162

ORCID

Y. Zhao: 0000-0001-9471-4490,
X. Wang: 0009-0003-3423-2547,
Z. Liu: 0000-0002-0074-9666,
V.Yu. Khaskin: 0000-0003-3072-6761

CONFLICT OF INTEREST

The Authors declare no conflict of interest

CORRESPONDING AUTHOR

V.Yu. Khaskin

Guangdong Provincial Key Laboratory of Advanced Welding Technology, China-Ukraine Institute of Welding, Guangdong Academy of Sciences, Guangzhou, 510650, China.
E-mail: khaskin1969@gmail.com

JOURNAL HOME PAGE

https://patonpublishinghouse.com/eng/journals/tpwj

PRODUCING OF COAXIAL JOINTS OF DISSIMILAR METALS BY EXPLOSION

A.G. Bryzgalin[1], E.D. Pekar[1], S.D. Ventsev[1], M.O. Pashchin[1], P.S. Shlyonskyi[2]

[1]E.O. Paton Electric Welding Institute of the NASU
11 Kazymyr Malevych Str., 03150, Kyiv, Ukraine
[2]Liaoning Xin Huayang Weiye Equipment Manufacturing Company Ltd No. 1 Road,
Tieling high-tech industrial development zone, Liaoning provice, China

ABSTRACT

Explosive welding allows joining metals and alloys in almost any combinations unlike various types of fusion welding. It provides the ability of manufacturing products with a combination of service properties of applied materials with a high level of strength, tightness, fatigue strength, etc. In addition to bimetals produced in fairly large volumes for chemical and oil equipment, explosive welding is used to manufacture products with special characteristics for different industries. Producing coaxial joints (welding is performed along generatrices of axisymmetric coaxial tubes) can be attributed to a special class of tasks, since they are more economical than alternative methods of their production. In some cases, a permanent joint can be created by explosion compression without welding of elements to be joined. This work presents a number of technological processes for manufacturing coaxial products developed at the PWI, which use both welding and explosive compression. The presented developments testify that a wide range of practical tasks can be solved with the help of explosion.

KEYWORDS: coaxial joints, explosive welding, bimetal, adapter, rod, coupling, permanent joint

INTRODUCTION

Coaxial explosive welding (EW) of cylindrical products is used in a smaller volume compared to EW of sheet metal on a parallel flow chart, but it is used to solve very important practical tasks. First of all, it deals with corrosion-resistant bimetallic tubes of chemical and oil engineering, in which strength is provided by a tube of carbon steel, and resistance to the medium is provided by appropriate metals or alloys (stainless steel, copper, brass, aluminium, niobium, etc.).

Bimetallic tubes and adapters are also used in cryogenic, space, aircraft engineering, elementary particle accelerators and other high-tech industries. Analysis of publications on the topic shows that from

Figure 1. Explosive welding of coaxially arranged tubes

the moment when EW was discovered as a technology for bimetal production (1959), a large volume of research on coaxial welding was conducted in the USA and the USSR, the main flow charts of welding were proposed and tested, the features and differences from EW of plane sheets were determined. An overview of flow charts of coaxial explosive welding of tubes and tubes with tube plates of units for chemical production apparatuses is given in [1, 2]. However, since the mid-1960s, a number of publications has shortened sharply and began to bear mostly an informational nature with references to previously published works. This is probably associated with the development of industrial technologies and, accordingly, the lack of interest from producers to publishing their technological developments.

At the same time, it is worth noting some publications that differ in a new technical approach to solving tasks of coaxial welding.

In [3], it was proposed to perform EW with the use of water as a medium that transmits working pressure (Figure 1).

A mixture of hexogen with potassium nitrate was used as an explosive substance (ES). The mixture was placed in a cylindrical aluminium shell. The charge detonation velocity varied depending on the shell diameter but was always close to 7000 m/s. Considering that the detonation velocity in EW is 2000–3000 m/s, the mentioned chart is of interest to research. The works [4, 5] propose the method of theoretical prediction of the collision velocity of the metal of tubes to be
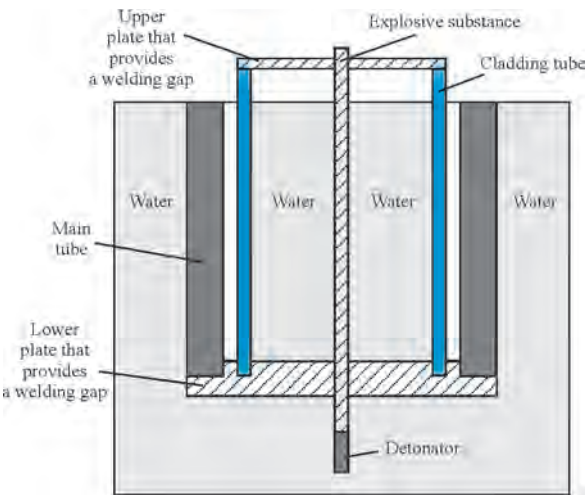
welded — the main EW parameter, which determines the power parameters of the process in underwater explosive welding and welding in air, respectively.

However, determination of coaxial EW modes is a rather difficult problem and it is currently realized for each type of joints separately by using the calculation-experimental method. The methods of producing permanent joints (which are not disassembled on components without their partial fracture) with explosion without mandatory welding are also of interest.

In this work, technological solutions for various tasks are presented, which use the methods for producing coaxial joints developed at the PWI.

PRODUCTION OF COAXIAL COPPER-ALUMINIUM RODS BY EXPLOSIVE WELDING AND DRAWING

The conductive busses of a critical electrical equipment are made of copper, which has high electrical conductivity and at the same time high density [6]. In case of its operation at high current frequency (for example, in aircraft engineering), replacement of solid copper busses with aluminium, which are cladded with a thin layer of copper, provides a significant reduction of mass of products while maintaining their electrical conductivity.

At the PWI, the technology for manufacturing bimetal copper-aluminium rods by explosive joining of a copper shell with an aluminium rod and subsequent drawing was developed [7].

The margin of the joint did not exhibit a wave formation characteristic of explosive welding, which indicates that welding was performed on the lower limit of admissible modes, that is, with a minimum energy input [8]. This allowed minimizing (by an order of 10 % along the joint length) the amount of intermetallics formed during welding.

Producing rods with the required diameter of 8.0 and 9.0 mm was carried out by drawing bimetallic billets with a diameter of 26 mm. Here, heat treatment of billets at all stages of drawing operation is not required.

The specific electrical resistance of a bimetal rod to direct current in terms of the temperature of 20 °C amounted to $0.027 \cdot 10^{-6}$ Ohm/m.

The air in the gap forms a shock wave, the front of which moves at a speed higher than the detonation velocity, the speed of this front is constantly reduced due to an increase in the resistance of the air in the gap. At some length of coaxial elements assembled for welding, the rate of air leakage from the gap becomes lower than the detonation velocity. A certain volume of air remains between the elements to be welded, forming bubbles. The movement of the shock wave leads to a significant heating of the element surfaces [9] to be welded, up to boiling aluminium. This has a significant impact on the quality of produced welded joints. In order to prevent this, it was suggested to vacuum a welding gap. Experiments with similar, but longer specimens on the same modes with vacuuming and without a welding gap were conducted. The final pressure at vacuum was 1 Pa [10].

After explosive welding without vacuuming was performed at a distance of approximately 250 mm from the edge of a billet, which is closer to the initiation point, a beginning of defects in the form of a cladding layer tear and a damage to the aluminium surface is observed, which acquires a torn form, there are also defects in the form of bubbles that appear at a distance of 100 mm from the specimen edge. On the specimen with vacuuming, a similar picture is observed, but defects appear at a distance of about 500 mm. The formation of defects in the specimen with vacuuming is explained by the presence of air in the gap, though more rarefied.

A typical feature of both specimens is that most bubbles and all defects in the form of tears are concentrated on a one generatrix. Obviously, this is associated with the fact that as a result of the uneven detonation front, it will always lag behind on one of the generatrix. Such unevenness will depend, first of all, on the shift of the charge initiation center of an explosive substance (ES) from the center of the welding assembly, as well as on the uneven detonation velocity and the charge thickness along the specimen length. It should be noted that in welding with vacuuming, the formed intermetallics had a smaller size. Apparently, this is associated with the fact that in welding with vacuum, there is no heating due to the air flowing from the gap (Figure 2).

It can be concluded that vacuuming of the gap in explosive welding of coaxial billets by external charge improves the quality of welded joint, which consists in an increase in the length of welded billets, on which defects of the type of bubbles and external layer tear are absent, as well as a decrease in the size and amount of intermetallics during welding of copper + aluminium pair. It should be noted that in welding of more strength materials with a higher melting point, no visible defects are formed, the integrity of materials is preserved, the rod produced by explosive welding has less deformation in length. Figure 3 shows a photo of a steel-copper rod for manufacture of a copper refining cathode, produced at the PWI.

TUBE ADAPTERS OF BIMETALS

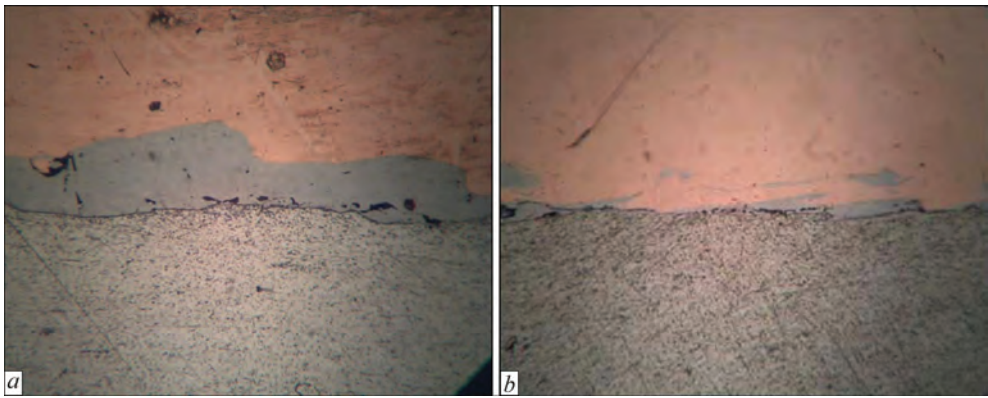are widely used in shipbuilding, metallurgy, pipeline transport and nuclear power engineering.

Figure 2. Intemetallics on the copper-aluminium joint interface after explosive welding: *a* — without vacuuming; *b* — with vacuuming
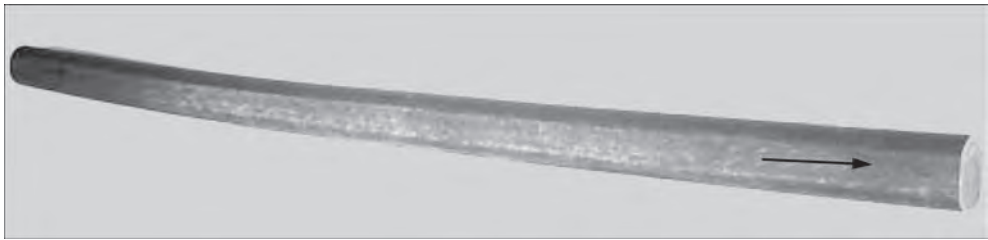

Figure 3. Bimetallic rod produced by explosive welding of copper base with steel tube

At the PWI, the technology for manufacturing the so-called quasi-butt tube transitional element was developed [11]. It represents a branch-pipe with the same geometry of the cross-section along its entire length, but has different materials at its ends, which are joined with each other by explosion (Figure 4).

The further attachment of the pipeline elements to the adapter is performed by fusion welding of similar materials, which allows achieving the high service properties of welded joints. The adapter length is almost unlimited and allows preventing the thermal impact from the arc butt welding of the pipeline extension for the joint produced by explosive welding.

The variants of joining almost any metals are possible with explosive welding. At the PWI, adapters from the following metals: aluminium + copper; copper + steel; stainless steel + steel 20 are manufactured.

The layer adhesion strength was studied by tensile tests of bimetallic tube specimens and those that were cut out along the adapter generatrix. The specimen width was 5–10 mm, depending on its diameter. The length was equal to the adapter length. The clamps of the tensile machine were mounted so that the distance from them to the closest butt edge was at least 20 mm. From each adapter, 3 tensile specimens were cut out.

In all cases, the specimen fracture occurred on weaker metal. There were no cases when a specimen fractured in the joint zone.

The general appearance of steel-copper tube adapters is presented in Figure 5.

Adapters successfully passed tensile tests, high pressure resistance and vacuum and helium tightness.

Such a butt joining of tubes by explosive welding was produced for the first time in the world practice.

In the electrotechnical industry, joining of copper and aluminium conductive elements is quite frequently used. A direct contact of such elements without welding is accompanied by electrochemical corrosion and burnout of expensive materials, resulting in an increase in the transitional resistance, growing during operation. Any kind of welding of these materials
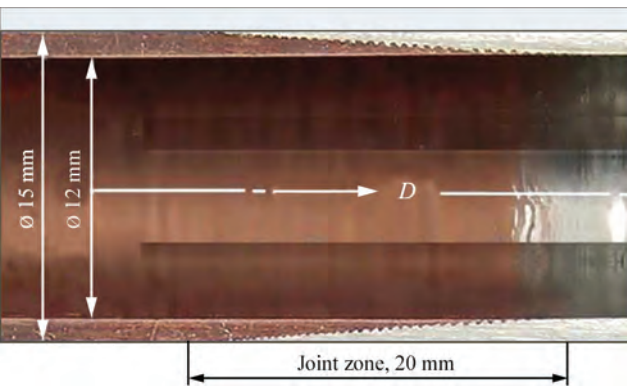

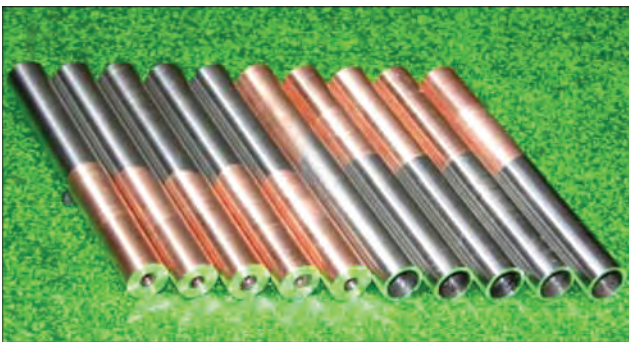**Figure 4.** Quasi-butt tube adapter

Figure 5. General appearance of tube Cu-steel adapters

Figure 6. Joining of copper and aluminium cables by crimped couplings

leads to the formation of Al_nCu_m type intermetallics, which can affect electrotechnical properties of a joint. Explosive welding is the most effective method of producing copper-aluminium electrical conductors with increased service properties. The efficiency of introducing designs of composite conductive assemblies produced by explosive welding is confirmed by 1.7–2.5 times decrease in the transitional resistance and by 5–7 times increase in the service life [8].

In particular, bimetallic couplings are used to join copper and aluminium multiconductor cables. They represent a hollow aluminium cylinder, half of which length is cladded with an explosion of copper layer from the inside. The copper cable is inserted into the coupling on the side of cladding and aluminium one is on the back side. Joining is performed by mechanical crimping of the coupling (Figure 6).

From the technological point of view, in some cases, explosive welding has to be performed by an external charge. Therefore, in this case, thicker aluminium is cladded, which is not characteristic of explosive welding [12]. A thin copper tube is a supporting one and should be reinforced from the inside to avoid its deformation during the explosion.

Studies of different variants of the copper tube reinforcement showed that the most rational option is the following: a rigid, for example, steel rod, is inserted inside a vertically mounted copper tube. A gap between the rod and the tube wall is filled with the Wood alloy, which has a melting point of approximately 70–90 °C. Such a rod at room temperature is not deformed by external pressure of detonation products. To remove the support from the copper tube after EW, it is enough to heat the produced billet to 80–90 °C, for example, in boiling water.

Microstructure of a copper-aluminium joint has a slight wave profile with a small quantity of intermetallic inclusions.

Since standard procedures for evaluation of the tear strength of the layers of the bimetallic ring, cut out from the tube billet are absent, a well-known procedure of testing bimetallic rings for flattening was used to qualitatively evaluate the adhesion strength of the layers [13]. The tests were conducted to detect cracks and delaminations in the joint zone under the action of loading.

The lack of delaminations at the joint interface indicates a high quality of EW and the preservation of plastic properties of both metals at the high level.

In the manufacture of products of complex configuration, a combination of EW with fusion welding can be used. The creation of a linear collider adapter can be a typical example [13, 14].

An adapter serves for joining separate cryomodules into one whole. Cryomodule elements to be joined is a niobium supra-conducting resonator, that has to be welded-on by electron beam welding to a niobium adapter branch-pipe, and the casing coaxially arranged to a niobium resonator of stainless steel has to be welded-on to the adapter disc manufactured of the same stainless steel. A niobium resonator is located inside a stainless steel casing, a vacuum is created in it and a liquid helium is poured under the casing. Thus, an adapter should provide the vacuum and helium tightness and operability of the unit in the conditions of high-frequency electromagnetic loads at cryogenic temperatures. The scheme and photo of an adapter is shown in Figure 7.
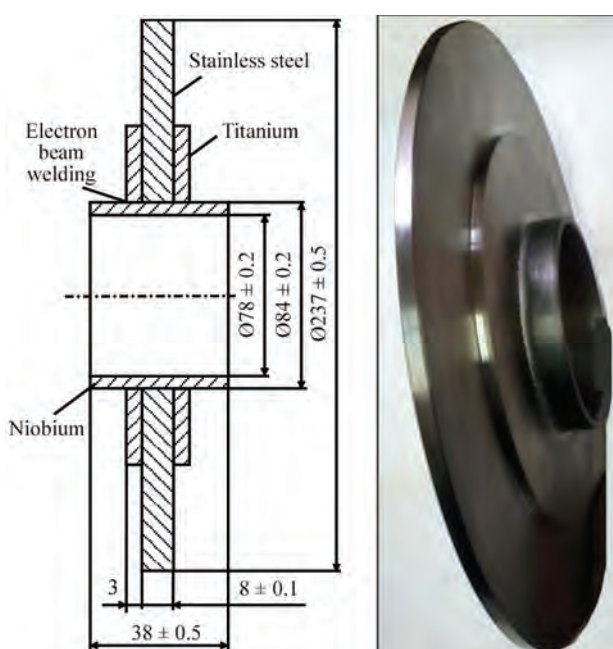

Figure 7. Design of adapter, which ensures the absence of niobium intermetallics formation during welding
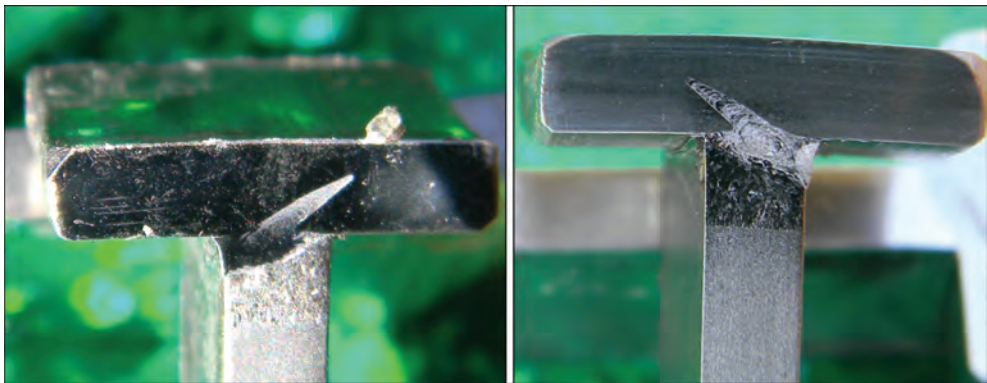
Figure 8. Sections of place of joining niobium with titanium by electron beam welding

It is known that welded joints of the highest quality are produced during welding of similar materials. I.e., an adapter should provide producing of welded joints of niobium with niobium, and stainless steel with stainless steel. Therefore, an adapter should be composed of at least two metals — niobium and stainless steel. The use of any methods of fusion welding to produce a joint of niobium with stainless steel, including electron beam welding, is unacceptable for solving the specified task due to the formation of Nb_xFe_y type intermetallics, which do not allow providing the required tightness of a joint. Manufacture of an adapter by explosive welding of a niobium tube with a steel disc appeared to be a fairly expensive process due to high consumption of niobium at subsequent mechanical treatment.

Previously conducted experiments showed that in electron beam welding of niobium with titanium, no intermetallics are formed and the required tightness of joints is provided on helium and vacuum. In this regard, the following option of manufacturing an adapter was proposed.

The stainless steel disc is first cladded with titanium on both sides by explosive welding, then, after rendering the required shape to the produced trimetal (by straightening and turning in size), a hole for a niobium tube is cut out. The branch-pipe is inserted into the hole and welded-on to titanium by electron beam welding. The possible formation of intermetallics in joining of titanium with steel, which is produced by explosive welding, does not affect the adapter service-ability, because helium cannot get into the cavity of the niobium tube through the adapter.

Mechanical tests of the produced EW joints on tear of layers showed satisfactory strength (375 MPa), the bending of bimetal at 180° did not detect the formation of delaminations or cracks. The optimal modes of electron beam welding of titanium with niobium (Figure 8) were experimentally selected.

The specimens produced by combined technology were cooled with liquid helium to a temperature of 4.2 K, and then quickly heated to room temperature with dryers. The specimens after thermal cycling carried out in such a way provided a helium and vacuum tightness [15].

The existing methods of joining rebars when constructing reinforced concrete objects [16] have a number of disadvantages. Development of high-performance, economic and ergonomic methods of joining thermal reinforced rebars, providing strength properties of joints at the level of the base metal, is a very urgent task for today.

One of such methods can be joining of rebars by couplings crimped by explosion. The advantages of explosive technology are absence of strength loss of the base metal, ability to join metals that cannot be welded by fusion methods without deterioration of service properties, for example, thermally strengthened or bimetal rebars, coated with an external anti-corrosion layer, lack of need in using special equipment, independence of power supply sources, ability to conduct works with high performance.

Figure 9. Principal scheme and macrosection of rebar joint made by explosion: *1* — rebar; *2* — charge shell; *3* — initiating detonating cord; *4* — coupling; *5* — explosive substance
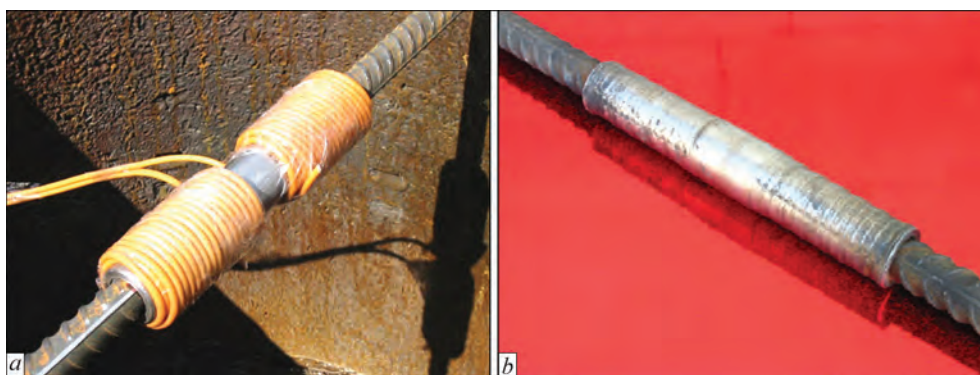
Figure 10. Example of coupling compressed by a charge from the detonating cord before charge explosion (*a*) and after explosion (*b*)
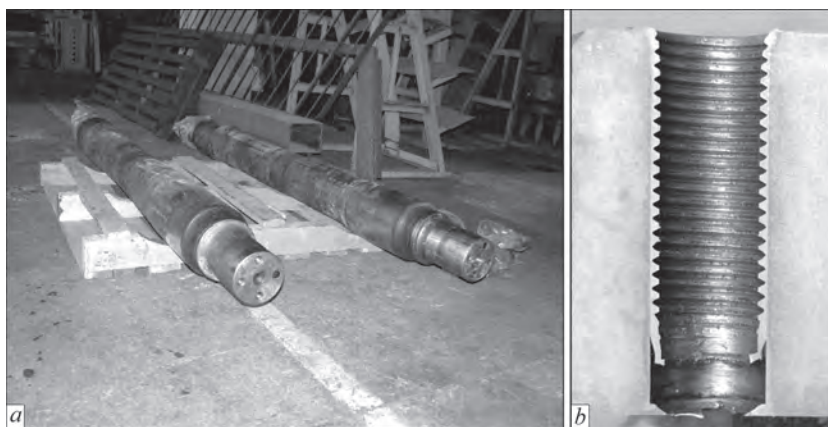

Figure 11. Repair of threaded holes by means of explosive welding: *a* — general appearance of wheel pair axle with four threaded holes; *b* — macrosection of threaded hole restored by explosion

The essence of the technology consists in the fact that a steel coupling (tube) with a charge of explosive substance located on its outer surface is put on the ends of the joined rebars symmetrically relative to the butt. The pressure created by the charge explosion, crimps the coupling metal so that it tightly touches with the bar metal. The presence of transverse projections on the bar surface ensures the formation of a permanent mechanical joint (Figure 9).

The strength of a joint when adding tensile load will be determined by the strength of the coupling metal, the strength of transverse projections of the rebar, working for creasing, and the strength of the rebar itself. The method of calculating the coupling and charge parameters that provide an equal strength of the joint and rebar metal was developed.

The tests on tear and cyclic fatigue life of the bar joints of different sizes and strength class were conducted. The couplings were compressed with charges from a detonating cord that was wound on a coupling in several layers (Figure 10).

All specimens that were tested on tear fractured on the base metal.

The fatigue tests were performed in accordance with the requirements of DSTU [17] in the laboratory conditions of the PWI at the mode of the axial harmonic tension in the area of multicyclic fatigue life at a frequency of 5 Hz and a stress ratio of 0.4. The criterion for completion of the tests was a complete fracture of the specimen. The specimens were fractured inside the coupling at a distance of 10–35 mm from its edge.

Analysis of the obtained data shows that in terms of fatigue resistance, such joints are not inferior to other methods of joining rebars widely used in industry.

Wheel pairs of cars are subjected to increased wear of threaded holes for fixing bearing caps in the axles of wheel pairs [18]. The existing methods of their restoration with the use of arc welding are either unacceptable because of inadmissible thermal deformations (sealing of holes by fusion and application of new thread) or not reliable due to the dynamic nature of working loads (inserting of the tube into the hole, its welding with the base metal along the upper edge and cutting new thread). At the PWI, it was proposed to weld-on a repair tube to the base metal of the axle in the worn threaded holes by the method of explosive welding and cutting new thread (Figure 11).

As ES, a mixture of ammonite with nitrate was used. Lack of fusion on the edge, characteristic of EW, was absent at the upper part, and at the lower part, it did not affect the quality of the joint in general, since the length of a newly cut thread exceeded the length of the working turns of the bolt. Gas formation

from the explosion did not affect the quality of welding and did not create defects in the hole.

The minimum value of the cyclic fatigue life of the axles with threaded holes, restored by the method of explosive welding, amounted to 122,000 load cycles, which is only by 4 % lower than the basic value for new axles.

Two wheel pairs with the holes restored by explosion were mounted on a car and passed working tests at the test site of Ukrzaliznytsia. After the run of 100,000 km without defect formation, the tests were stopped.

CONCLUSIONS

1. The strength and fatigue life of coaxial joints made by explosive welding is usually not lower than that of the same joints produced by other methods.

2. Manufacturing of complex products by combination of explosive and fusion welding allows avoiding the formation of undesired intermetallics and providing the necessary service properties of a product.

3. Explosive technologies can be effectively used to create coaxial joints of different purposes.

REFERENCES

1. Crossland, B. Bahrani, A.S. Willia, J.D. Shribman, V. (1967) Explosive welding of tubes to tubeplates. *Welding and Metal Fabrication*, **35**, 88–94.

2. Harry, J. Addison, Jr. James, F. Kowalick, Winston W. Cavtll (1969) Explosion welding of cylindrical shapes. In: *Report A69-3 of the Department of the Army Frankford Arsenal, Philadelphia*.

3. Yong, Yu, Honghao, Ma, Kai, Zhao et al. (2017) Study on underwater explosive welding of Al-steel coaxial pipes. *Central European J. of Energetic Materials*, 14(**1**), 251–265. DOI: https://doi.org/10.22211/cejem/68696

4. Moujin, Lin, Junjie, Liao, Bing, Xue et al. (2023) Expansion velocity of metal pipe in underwater explosive welding. *J. Mater. Proc. Technol.*, **319**, 118071. DOI: https://doi.org/10.1016/j.jmatprotec.2023.118071

5. *Sina Gohari* Rad, Siamak Mazdak, Ali Alijani (2023) Proposing an analytical model for predicting the dimensions of interfacial waves produced in the explosive welding of coaxial cylinders. *Thin-Walled Structures*, **190**, 110982. DOI: https://doi.org/10.1016/j.tws.2023.110982

6. DSTU EN 13601:2010: *Copper and copper alloys. Copper rod, bar and wire for general electrical purposes. Specifications.*

7. Bryzgalin, A.G., Dobrushin, L.D., Shlensky, P.S. et al. (2015) Manufacture of coaxial copper-aluminium rods using explosion welding and drawing. *The Paton Welding J.*, **3–4**, 69–73. DOI: https://doi.org/10.15407/tpwj2015.04.10

8. Lysak, V.I., Kuzmin, S.V. (2005) *Explosion welding*. Moscow, Mashinostroenie [in Russian].

9. Pervukhin, L.B., Shishkin, T.A., Pervukhina, O.L. (2012) Specificity of explosive welding in marginal zones. In: *Proc. of Symp. on Explosive Production of New Materials: Science, Technology, Business, and Innovations*. Moscow, Torus Press Ltd.

10. Pashchin, M.O., Shlonskyi, P.S., Bryzgalin, A.G. et al. (2021) Features of formation of structure of coaxial joints of copper and aluminium in explosion welding with vacuuming of welding gap. *The Paton Welding J.*, **2**, 2–7. DOI: https://doi.org/10.37434/as2021.02.01

11. *Method of manufacturing of bimetal pipe adapters using explosion welding*. Appl. for invent. No. 2022 02799 from 05.08.2022.

12. Shlyonskyi, P.S. (2020) Explosion welding of copper-aluminium pipes by the "reverse scheme". *The Paton Welding J.*, **8**, 51–53. DOI: https://doi.org/10.37434/as2020.08.08

13. Bryzgalin, A.G., Pekar, E.D., Shlensky, P.S. et al. (2017) Application of explosion welding for manufacture of trimetallic transition pieces of cryomodules of linear collider. *The Paton Welding J.*, **12**, 34–39. DOI: https://doi.org/10.15407/as2017.12.04

14. Basti, A., Bedeschi, F., Bryzgalin, A. et al. (2020) *Upgrade of the ILC cryomodule*. arXiv.org > physics > arXiv:2004.05948

15. Sabirov, B., Basti, A., Bedeschi, F. et. al. (2016) High technology application to modernization of international electron-positron linear collider (ILC). In: *Proc. of Inter. Conf. on New Trends in High-Energy Physics, Montenegro*.

16. Bryzgalin, A.G., Shlyonskyi, P.S., Pekar, E.D. et al. (2022) Joining building rerebars using couplings compressed by explosion. *The Paton Welding J.*, **11**, 35–38. DOI: https://doi.org/1037434/as 2022.11.05

17. DSTU B V. 2.6-169:2011L: *Welded joints of rerebars and embedded products of concrete structures.*

18. Lobanov, L.M., Illarionov, S.Yu., Dobrushin, L.D. et al. (2012) Repair explosion cladding of threaded channel of car axles. *The Paton Welding J.*, **2**, 42–46.

ORCID

A.G. Bryzgalin: 0000-0001-5886-3069,
E.D. Pekar: 0000-0001-5025-4445,
S.D. Ventsev: 0000-0003-4753-5259,
N.A. Pashchin: 0000-0002-2201-5137,
P.S. Shlyonskyi: 0000-0002-3566-1752

CONFLICT OF INTEREST

The Authors declare no conflict of interest

CORRESPONDING AUTHOR

P.S. Shlyonskyi
E.O. Paton Electric Welding Institute of the NASU
11 Kazymyr Malevych Str., 03150, Kyiv, Ukraine.
E-mail: shlensk@ukr.net

JOURNAL HOME PAGE

https://patonpublishinghouse.com/eng/journals/tpwj

INFLUENCE OF HEAT TREATMENT ON THE STRUCTURE AND PROPERTIES OF Ti–28Al–7Nb–2Mo–2Cr TITANIUM ALUMINIDE AND ITS WELDED JOINTS

S.V Akhonin, V.Yu. Bilous, A.Yu. Severyn, R.V. Selin, I.K. Petrichenko

E.O. Paton Electric Welding Institute of the NASU
11 Kazymyr Malevych Str., 03150, Kyiv, Ukraine

ABSTRACT

The influence of furnace annealing on the structure of cast metal in ingots of 200 mm diameter of the intermetallic Ti–28Al–7Nb–2Mo–2Cr titanium alloy produced by the method of electron beam melting and its welded joints produced by the method of electron beam welding was determined. It was determined that the EBM metal produced from the ingots of 200 mm diameter is satisfactorily welded under the conditions of applying such additional technological measures as preheating and local heat treatment. It is shown that annealing at the temperature of 1260 °C for 10 h led to the formation of a uniform microstructure in the base metal, HAZ and weld metal, decomposition of the duplex structure and absence of regions with a two-phase $(\gamma+\alpha_2)$-lamellar structure. The room temperature strength of welded joints after annealing is equal to 746 MPa or 98 % of the base metal strength.

KEYWORDS: titanium aluminide, electron beam welding, welded joints, duplex structure, lamellar structure, strength

INTRODUCTION

Intermetallic alloys based on Ti–Al system have high indices of heat-resistant properties and are designed for operation in different structures at temperatures of 600–900 °C [1, 2]. In such alloys, two intermetallic phases are formed: α_2-phase (Ti$_3$A1), which has a hexagonal densely-packed crystalline lattice, and γ-phase (TiAl), which has an ordered tetragonally distorted face-centered structure. Gamma-alloys are divided into two large groups: single-phase γ-alloys with the aluminium content of 50–52 mol.% and two-phase $(\alpha_2+\gamma)$ alloys with the aluminium content of 42–49 mol.%. Most common alloying elements in such alloys are Nb, Cr, Mo, Zr, Mn, W [3–6]. Gamma-alloys are considered to be the most promising materials for aerospace and engine-building areas [7–11].

The prospects for the use of intermetallics are based on the following features of intermetallics: intermetallics preserve their strength to high temperatures [12–14]; the modulus of elasticity of intermetallics is less intensively reduced with an increase in the temperature unlike that of industrial heat-resistant alloys; the self-diffusion coefficient in intermetallics is by several orders of magnitude lower than that in disordered alloys at comparable temperatures, which affects the lower creep rate [15, 16].

The use of alloys based on titanium intermetallics for the manufacturing of turbine blades, as well as hot gas tract parts such as combustion chambers, diffusers, exhaust systems, will allow increasing the operating temperature of gas turbine engines (GTE) by 100–150 °C, reducing mass and increasing the ser-

vice life of engine. In Ukraine, in nowadays conditions, the manufacturing and application of this class of materials for the aircraft and power engineering is of great demand [16].

The main tasks to be solved in the development of structural materials based on intermetallics are an increase in the low-temperature ductility and fracture toughness [18].

To produce alloys based on titanium aluminides, the use of electron beam melting (EBM) is promising, which allows minimizing the liquation processes during ingot solidification by dividing the process of melting billet and ingot solidification, producing high-quality homogeneous ingots with a fine-grained structure and removing high- and low-density inclusions, which is very important for producing ingots of critical purpose [17, 18].

Also, an important problem affecting the possibility of using alloys based on titanium aluminide is their weldability. The thermal cycle of electron beam (EBW) and argon-arc welding (AAW) leads to the formation of cold cracks in joints [19]. To prevent the formation of cracks, it is necessary to apply additional technological measures — local heat treatment (LHT), preheating and annealing after welding [20–24]. The impact of heat treatment on the properties of welded joints, produced by EBW with LHT is also a poorly-studied issue.

The aim of this work is to determine the impact of furnace annealing on the base metal structure of the intermetallic Ti–28Al–7Nb–2Mo–2Cr titanium alloy, produced by the EBM method, and its welded joints produced by the method of electron beam welding.
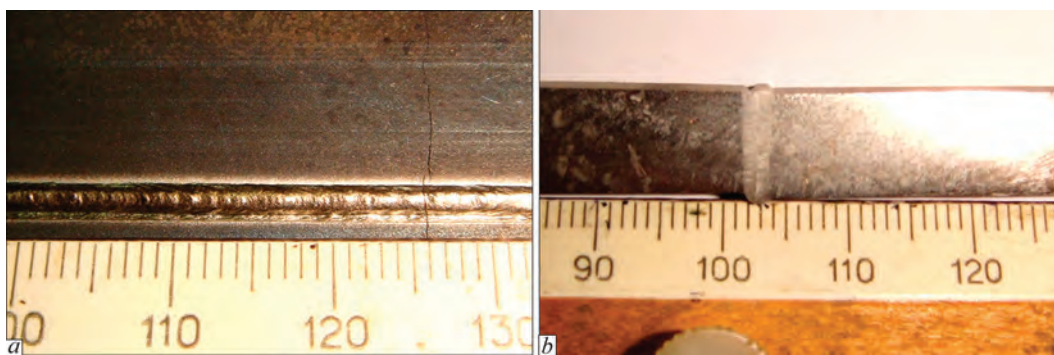
Figure 1. Welded joint of alloy based on Ti–28Al–7Nb–2Mo–2Cr titanium aluminide, produced by EBW without using preheating and LHT (*a*) and in the state after LHT (*b*): I_b = 90 mA (*a*), V_w = 7 mm/s (*a*, *b*), LHT temperature is 750 °C, 10 min (*b*)

MATERIALS AND RESEARCH METHODS

Smelting of experimental ingots with a diameter of 200 mm from the alloy based on Ti–28Al–7Nb–2Mo–2Cr titanium aluminide was carried out in the multipurpose laboratory electron beam installation UE-121.

Examination of the specimen structure of the alloys based on titanium aluminide was carried out in the Neophot-32 optical microscope at various magnifications. The photos of microstructures were taken with a digital camera C-3000 of the OLYMPUS Company.

EBW was carried out in the modernized welding unit UL-144, equipped with ELA 60/60 power source, TsF-19 welding gun and SU-220 beam control device [25].

EBW allows applying such additional technological measures as preheating and postweld local heat treatment directly in a vacuum chamber that prevents oxidation and saturation of the weld metal and heat-affected zone (HAZ) by gas impurities [26–28]. To determine weldability of the specimens from the metal based on Ti–28Al–7Nb–2Mo–2Cr titanium aluminide, welding of 120×60×8 mm specimens was performed. For electron beam welding, billets for the specimens were cut out of the cast ingot of 200 mm diameter. The specimens of butt joints were assembled without a gap and edge preparation.

One of the advantages in electron beam welding technology concerning titanium and Ti-based alloys, in addition to providing reliable protection of welded joints, is the ability to carry out local preheating and further heat treatment in a vacuum chamber [29]. Preheating of welded joints is a quite effective technological measure used in welding of high-strength titanium alloys to prevent the formation of cold cracks [26, 30].

EBW parameters are the following: speed — 7 mm/s; current — 80 mA. Temperature of specimen preheating was 400 °C, temperature of postweld LHT in the vacuum chamber — 900 °C. The use of preheating and local electron beam heat treatment allowed producing high-quality welded joints without cracks. The temperatures of preheating of 400 °C and postweld LHT in the vacuum chamber of 900 °C were chosen in accordance with the experience of welding 47XD alloy based on titanium aluminide [31].

Welded joints of the alloy based on Ti–28Al–7Nb–2Mo–2Cr titanium aluminide, produced without LHT, are prone to the formation of cold cracks (Figure 1, *a*). When applying such additional technological measures as preheating and LHT, the metal of Ti–28Al–7Nb–2Mo–2Cr titanium aluminide is welded satisfactorily. The weld formation in EBW of Ti–28Al–7Nb–2Mo–2Cr titanium aluminide with preheating and LHT is good, undercuts, pores and cracks are not formed.

An example of the welded joint transverse macrosection of the alloy based on Ti–28Al–7Nb–2Mo–2Cr titanium aluminide, produced by EBW with preheating and postweld LHT is shown in Figure 1, *b*. It was determined: the width of the weld above is 2.2 mm and on the back side it is 1.8 mm, the height of the reinforcement above is 0.5 mm and on the back side it is 0.8 mm. The weld formation in EBW with preheating and postweld LHT is good, undercuts, pores and cracks are not formed.

STRUCTURE OF BASE METAL OF ALLOY BASED ON Ti–28Al–7Nb–2Mo–2Cr TITANIUM ALUMINIDE

γ-TiA1 intermetallic, on the base of which an experimental intermetallic Ti–28Al–7Nb–2Mo–2Cr alloy was produced, has an ordered tetragonally distorted face-centered structure L10, in which planes filled with titanium atoms alternate with planes occupied by aluminium atoms [32]. The homogeneity region of this intermetallic in the Ti–Al system is quite large [33].

Microstructure of the base metal of the intermetallic alloy based on Ti–28Al–7Nb–2Mo–2Cr titanium aluminide is shown in Figure 2. In the middle zone of the ingot, the cast metal is characterized by the fact that the linear phase is an ordered cubic B2-phase forming a mesh structure with different sizes of meshes from 30 to 100 μm (Figure 2, *a*), sometimes against
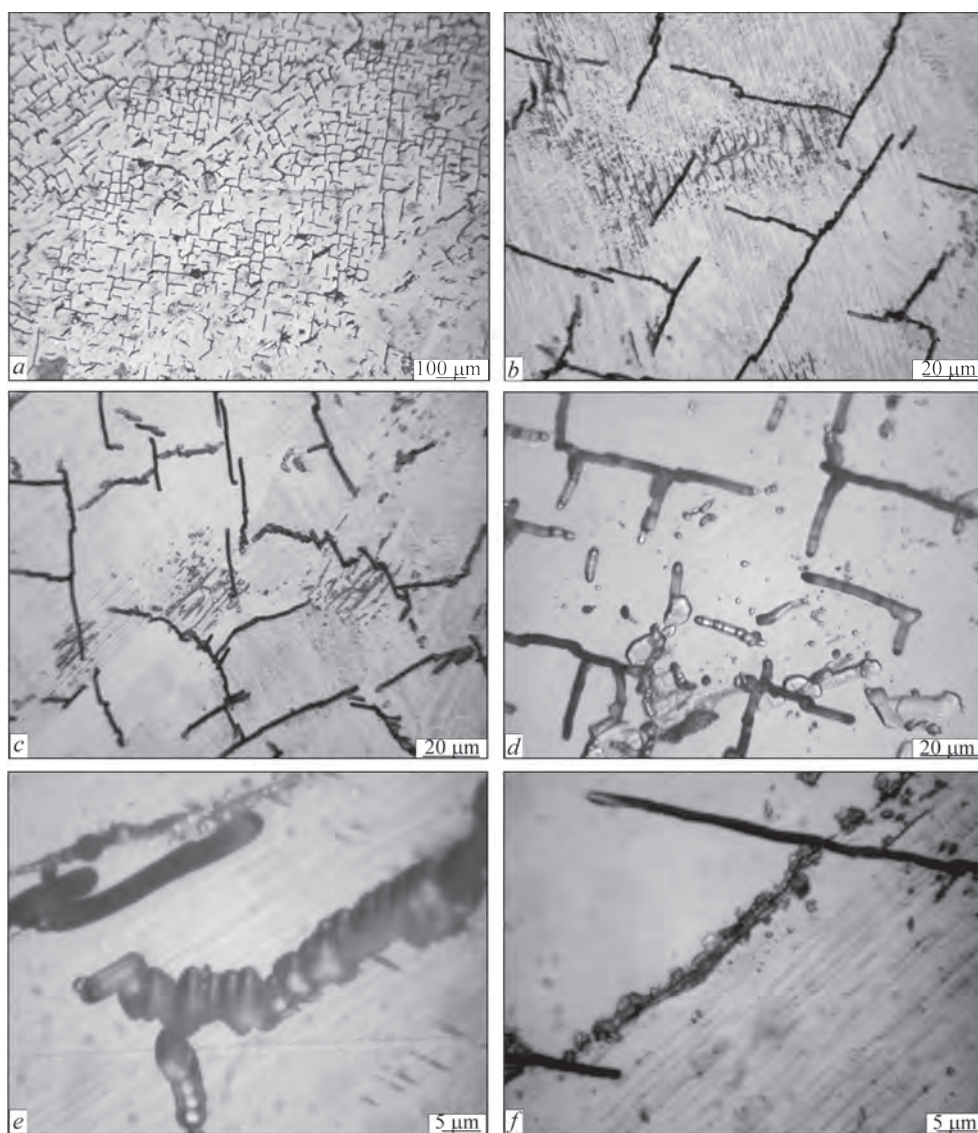
Figure 2. Microstructure of base metal of alloy based on Ti–28Al–7Nb–2Mo–2Cr titanium aluminide

the background (Figure 2, *b*) of lamellar structure with lamellae twinning (Figure 2, *f*). In some places, a light phase containing other particles is observed (Figure 2, *b*). The phase forming a mesh structure includes both rectilinear and curvilinear regions (Figure 2, *c*) and looks dark or light in the photo (Figure 2, *d*). Often, such particles have a transverse substructure (Figure 2, *e*). Dispersed precipitations (probably, precipitations of B2-phase) are located both against the background of the matrix phase (Figure 2, *d*), as well as decorate other components of the structure: grain boundaries, lamellae (Figure 2, *c*). The thickness of the linear phase forming a mesh ranges from 1 to 5 μm (Figure 2, *e*).

To determine the influence of additional furnace heat treatment, namely annealing, on the structure of the base metal of Ti–28Al–7Nb–2Mo–2Cr titanium aluminide, a part of the metal was subjected to furnace annealing. Annealing was performed in the vacuum chamber, its temperature was 1260 °C, the time

was 10 h, cooling of the joints occurred with the furnace. The BM structure after annealing is represented by a light matrix phase, which is γ-titanium aluminide (Figure 3, *a*). Against the background of the matrix, a dark linear phase is clearly revealed, which forms a mesh with nuclei of 50–100 μm. The thickness of the linear phase elements is 1.5–2.5 μm.

After annealing, the structure also contains dispersed particles of up to 1.0–1.5 μm, forming clusters (Figure 3, *b*) in the matrix phase, as well as chains decorating other structural elements (boundaries of lamellae and other particles) (Figure 3, *c*, *d*). In the structure, also separated dark (Figure 3, *d*) and light particles of 2–15 μm long and about 2 μm thick are present.

Thus, all structural elements inherent in the metal of Ti–28Al–7Nb–2Mo–2Cr titanium aluminide after annealing were observed in the metal structure before annealing as well. A significant difference of annealed BM from non-annealed is a significant reduction in the fraction of a lamellar structure. Thus, as
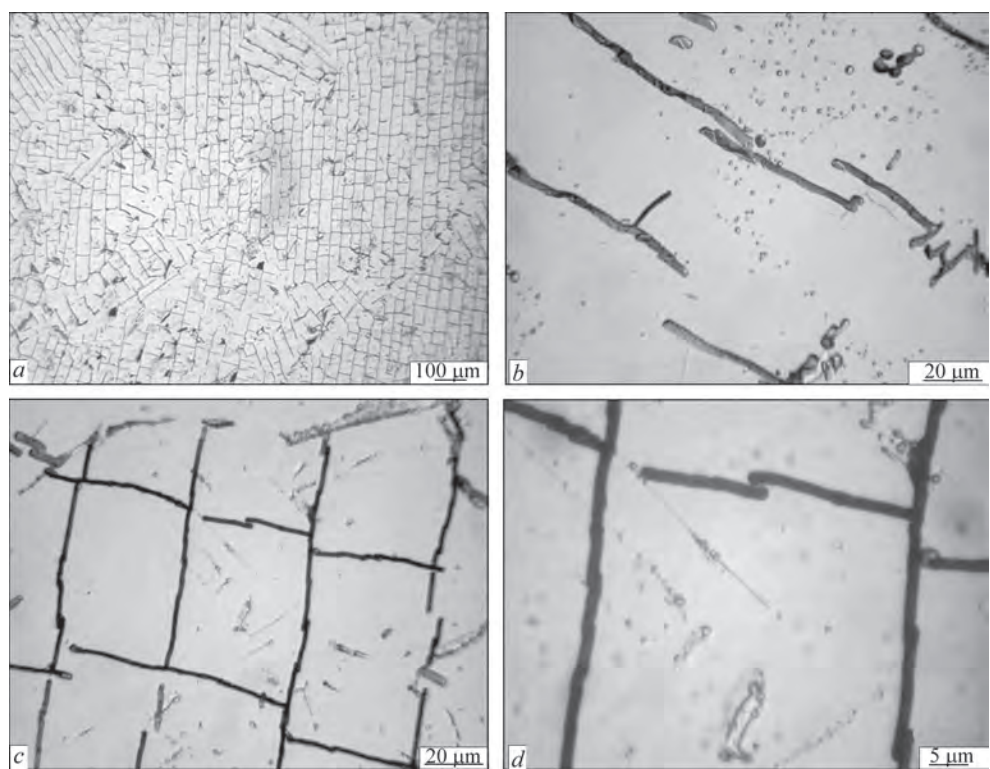
Figure 3. Microstructure of base metal of alloy based on Ti–28Al–7Nb–2Mo–2Cr titanium aluminide, after annealing at 1260 °C

a result of annealing at 1260 °C, in the base metal of Ti–28Al–7Nb–2Mo–2Cr titanium aluminide, transformation namely of the duplex structure occurred.

MICROSTRUCTURE OF WELD METAL

The weld metal, produced by EBW with preheating and LHT, consists mainly of coarse grains, elongat- ed in the direction of heat removal. Only along the weld axis, finer equiaxial grains of 100–200 μm are formed. The linear dark phase forming a mesh is located in the form of bands transverse to the weld axis in the weld part of medium height. The intragranular metal structure of the middle weld part consists of small (not more than 20 μm) regions with a lamel-
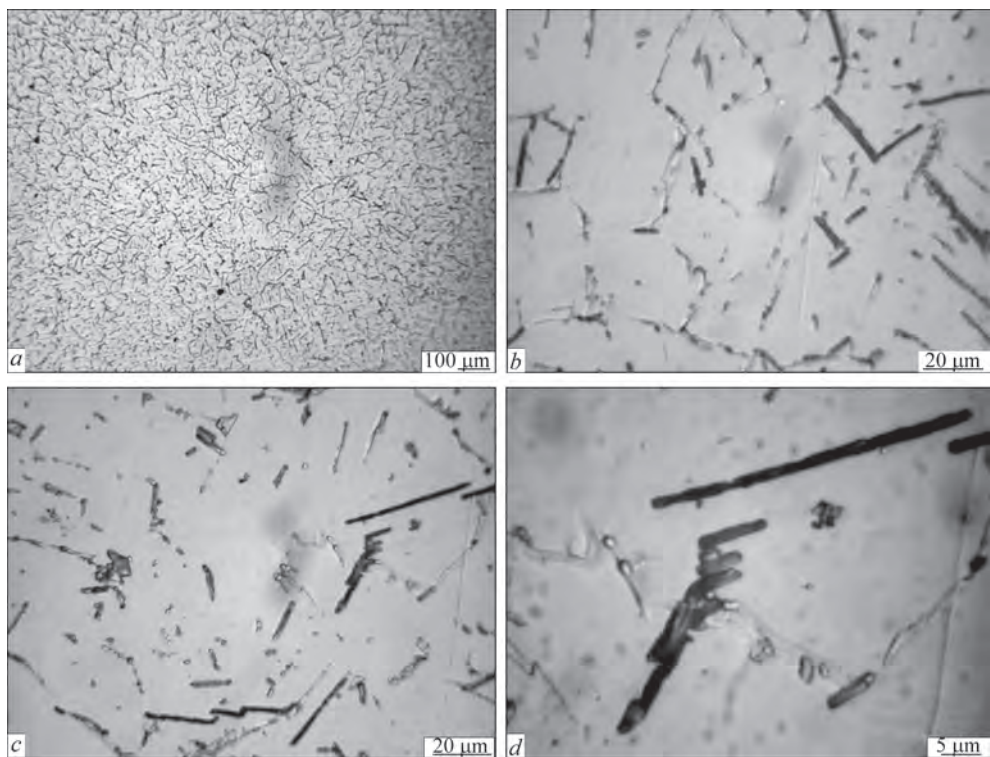

Figure 4. Microstructure of welded joint weld metal of alloy based on Ti–28Al–7Nb–2Mo–2Cr titanium aluminide, produced by EBW, after annealing at 1260 °C

lar structure against the background of a light matrix phase. Here, the thickness of lamellae in the weld metal is about 1 μm. In addition, in the structure, linear particles forming a mesh are present. They have a length of 3–80 μm and a thickness of 1–3 μm, can be homogeneous and fragmented. In many linear particles, dispersed phase precipitations are concentrated, which are arranged also against the background of the matrix phase. The weld metal structure contains also micropores, their size is 1–2 μm.

MICROSTRUCTURE OF WELD METAL AFTER HEAT TREATMENT

In the weld metal against the background of the light matrix phase, linear dark and light structural elements are revealed (Figure 4). Dark particles, mostly rectilinear of up to 50 μm long and 1.5–2.5 μm thick are located in the volume of grains (Figure 4, *b*, *c*). Light rectilinear particles are often decorated with dispersed precipita-tions, along the grain boundaries, light fringing can be observed (Figure 4, *d*). Dispersed particles of up to 2 μm are present both in the volume of grains as well as in the form of boundary fringes or other structural elements. In the weld metal, micropores are present.

In the weld metal, produced by EBW after 10-hour annealing at 1200 °C as well as in the base metal, lamellar structure observed before annealing, is absent.

MICROSTRUCTURE OF HAZ METAL

HAZ microstructure of the welded joint of Ti–28Al–7Nb–2Mo–2Cr titanium aluminide unlike BM in HAZ is represented by a lamellar structure with a small length of lamellae of up to 10 μm and a thickness of about 1 μm. From the weld metal, the metal of the near-weld zone differs by much lower density of region location with a lamellar structure. Other structural HAZ components are identical to similar elements of the weld metal structure except of
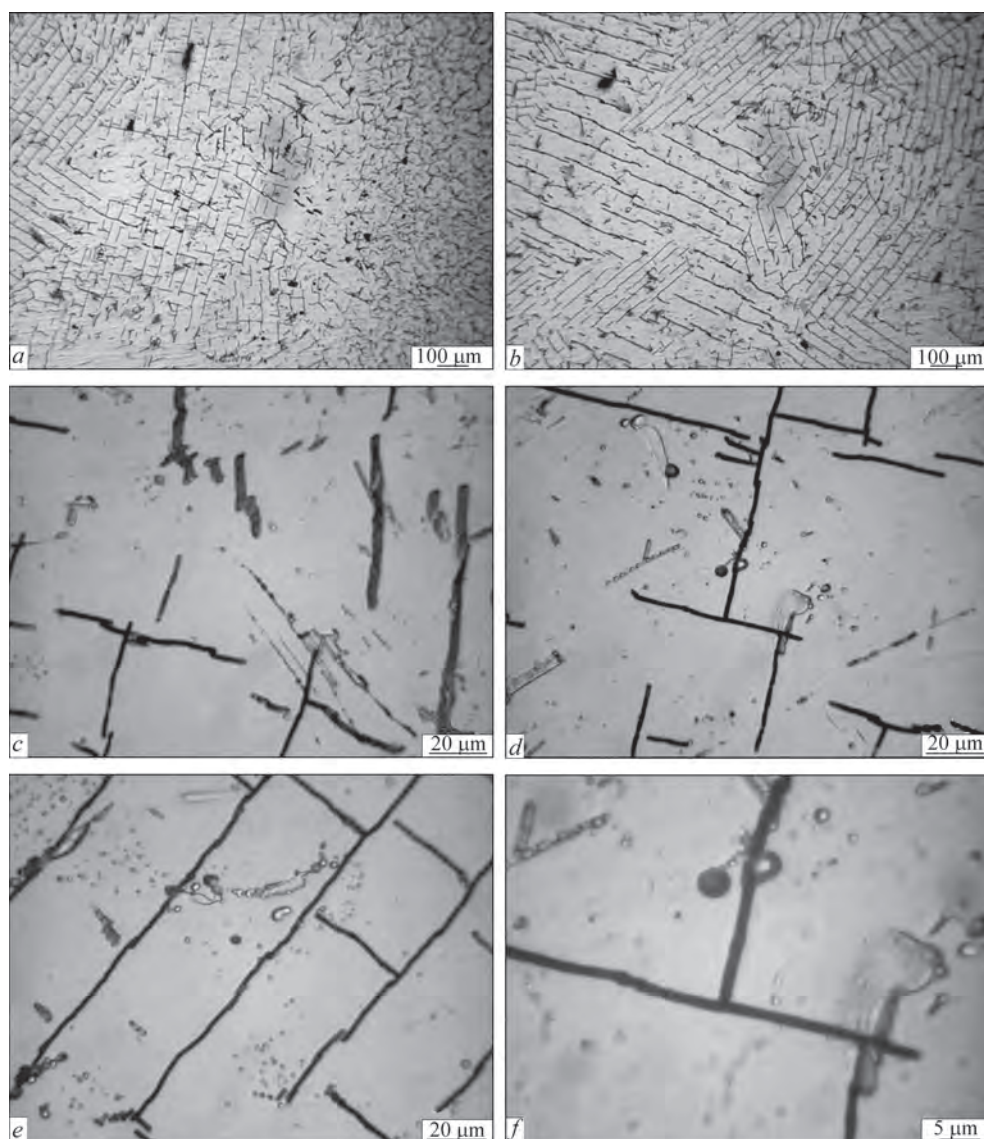

Figure 5. Microstructure of HAZ metal of welded joint of alloy based on Ti–28Al–7Nb–2Mo–2Cr titanium aluminide, produced by EBW, in the state after annealing at 1260 °C

Table 1. Mechanical properties of base metal and welded joints of alloy based on Ti–28Al–7Nb–2Mo–2Cr titanium aluminide, produced by EBW with preheating and LHT

Specimen	σ_t, MPa	σ_{02}, MPa	KCV, J/cm^2
Base metal	754	570	12.9
EB welded joint after annealing at 1260 °C during 10 h	746	566	9.8

the fact that in HAZ, the phase forming a mesh structure does not form bands transverse to the weld axis and, most probably, inherits the nature of the phase location forming a mesh in BM.

Microstructure of the HAZ metal after annealing at 1260 °C is presented in Figure 5. Analysis of the obtained images showed that in HAZ, up to the very fusion zone, a formation of a linear dark phase of a mesh pattern is observed, which in some places changes into a banded pattern. The parameters of the mesh and bands nuclei are the same as in BM. The thickness of the linear phase is 1.0–2.5 μm. In the HAZ metal, light particles of up to 20 μm long are encountered (Figure 5, *d*, *b*), which are often decorated with dispersed particles. In addition, single dispersed particles and their clusters are observed (Figure 5, *e*, *f*).

Thus, the main difference of the HAZ metal structure of the welded joint of the intermetallic Ti–28Al–7Nb–2Mo–2Cr alloy after annealing consists in the absence of regions with a lamellar structure that were present in HAZ after welding.

Therefore, the carried out 10-hour annealing of the electron beam welded joint of the intermetallic alloy based on γ-phase at a temperature of 1260 °C led to the formation of relatively homogeneous microstructure in the base metal, HAZ and weld metal. As a result of annealing, in the metal of all zones of the welded joint, decomposition of a duplex lamellar structure occurred. In the metal of all areas of the welded joint, regions with a lamellar structure are almost absent.

The obtained mechanical properties of welded joints of the alloy based on Ti–28Al–7Nb–2Mo–2Cr titanium aluminide allowed making a conclusion that at 20 °C, the strength of welded joints after annealing at 1260 °C is at the level of 746 MPa or 98 % from the strength of the base metal (Table 1). The indices of impact toughness are at the level of 9–13 J/cm^2.

Thus, the cast metal of ingots based on Ti–28Al–7Nb–2Mo–2Cr titanium aluminide, produced by the EBM method is satisfactorily welded by EBW when applying preheating and LHT. After 10-hour annealing of the base metal and welded joint metal of the intermetallic alloy at a temperature of 1260 °C in the base metal, weld metal and HAZ, rela-

tively uniform microstructure was formed. As a result of annealing, in the metal of all zones of the welded joint, decomposition of a duplex lamellar structure occurred. In general, the maximum fracture toughness is typical of alloys with a lamellar structure, but after heat treatment, welded joints have indices of the room temperature strength at the level of the base metal. In the metal of all areas of the welded joint, regions with a lamellar structure are almost absent.

CONCLUSIONS

1. The metal produced from the ingots based on Ti–28Al–7Nb–2Mo–2Cr titanium aluminide is satisfactorily welded by EBW under the conditions of applying such additional technological measures, as preheating and LHT. The weld formation in EBW with preheating and postweld LHT is good, undercuts, pores and cracks were not detected.

2. The intragranular structure of the weld metal after AAW and EBW with LHT is different from the structure of the base metal. Thus, in EBW it is composed of small (not more than 20 μm) regions with a (γ+ α$_2$)-lamellar structure against the background of a light matrix of the γ-phase with a mesh from linear particles of 3–80 μm long and 1–3 μm thick, in AAW — from a single-phase γ-structure, alternating with the regions of a two-phase (γ+ α$_2$)-lamellar structure of up to 50 μm.

3. Annealing of the welded joint of Ti–8Al–7Nb–2Mo–2Cr alloy, produced by EBW, at a temperature of 1260 °C during 10 h led to the formation of a homogeneous microstructure in the base metal, HAZ and weld metal, as a result of annealing in all zones of the welded joint, decomposition of a duplex structure occurred and the regions with a two-phase (γ+α$_2$)-lamellar structure are absent.

4. The strength of welded joints, produced by EBW with LHT of the intermetallic alloy based on Ti–28Al–7Nb–2Mo–2Cr titanium aluminide after annealing at 1260 °C is at the level of 746 MPa or 98 % from the strength of the base metal.

REFERENCES

1. Peters, M., Kumpfert, J., Ward, C.H., Leyens, C. (2003) Titanium alloys for aerospace applications. *Adv. Eng. Mater.*, **5**, 419–427.
2. Williams, J.C., Boyer, R.R. (2020) Opportunities and issues in the application of titanium alloys for aerospace components metals. *Metals*, 10(**6**), 705.
3. Burtscher, M., Klein, Y., Lindemann, J. et al. (2020) An advanced TiAl alloy for high-performance racing applications. *Materials*, **13**, 4720.
4. Hu, D. (2001) Effect of composition on grain refinement in TiAl-based alloys. *Intermetallics*, **9**, 1037–1043.
5. Xia, Q., Wang, J.N., Yang, J., Wang, Y. (2001) On the massive transformation in TiAl-based alloys. *Intermetallics*, **9**, 361–367.

6. Bewlay, B.P., Nag, S., Suzuki, A., Weimer, M.J. (2016) TiAl alloys in commercial aircraft engines. *Materials at High Temperatures*, **33**, 549–559.

7. Iliin, A.A., Lolachev, B.A., Polkin, I.S. (2009) *Titanium alloys. Composition, structure, properties:* Refer. Book. VILS-MATI [in Russian].

8. Clemens, H., Mayer, S. (2016) Intermetallic titanium aluminides in aerospace applications — processing, microstructure and properties. *Materials at High Temperatures*, **33**, 560–570.

9. Kim, Y.W., Kim, S.L. (2018) Advances in gammalloy materials–processes–application technology: Successes, dilemmas, and future. *JOM*, **70**, 553–560.

10. Hu, D., Botten R.R. (2002) Phase transformations in some TiAl-based alloy. *Intermetallics*, **10**, 701–715.

11. Kim, Y.-W., Dimiduk, D.M. (2002) Designing gamma TiAl alloys: Fundamentals, Strategy and Productions. *Intermetallics*, **10**, 531.

12. Cobbinah, P.V., Matizamhuka, W.R. (2019) Solid-state processing route, mechanical behaviour, and oxidation resistance of TiAl alloys. *Adv. Mater. Sci. and Eng*., **1**, 4251953.

13. Kenel, C., Leinenbach, C. (2016) Influence of Nb and Mo on microstructure formation of rapidly solidified ternary Ti–Al–(Nb, Mo) alloys. *Intermetallics*, **69**, 82–89.

14. Kim K.W., Klemens H.et al. (2003) *Gamma titanium aluminides*. TMS, Warrendale, PA, USA.

15. (2003) *Titanium and titanium alloys. Fundamentals and applications*. Eds by Leyens and M. Peters. Weinheim. WILEY-VCH Verlag GmbH & Co, KGaA, Germany.

16. Burtscher, M., Klein, T., Mayer, S. et al. (2019) The creep behavior of a fully lamellar γ-TiAl based alloy. *Intermetallics*, **114**, 106611.

17. Hu, D. (2001) Effect of composition on grain refinement in TiAl-based alloys. *Intermetallics*, **9**, 1037–1043.

18. Xia, Q., Wang, J.N., Yang, J., Wang, Y. (2001) On the massive transformation in TiAl-based alloys. *Intermetallics*, **9**, 361–367.

19. Santos, D.S., Bououdina, M., Fruchart, D. (2002) Structural and thermodynamic properties of the pseudo-binary $TiCr_2$–xV_x compounds with $0.0 \leq x \leq 1.2$. *J. of Alloys and Compounds*, 340(**6**), 1–2, 101.

20. Chen, G.Q., Zhang, B.G., Liu, W., Feng, J.C. (2011) Crack formation and control upon the electron beam welding of TiAl-based alloys. *Intermetallics*, 19(**12**), 1857–1863. DOI: https://doi.org/10.1016/j.intermet.2011.07.017

21. Chaturvedi, M.C., Xu, Q., Richards, N.L. (2001) Development of crack-free welds in a TiAl-based alloy. *J. Materials Proc. Technology*, 118(**1**), 74–78. DOI: https://doi.org/10.1016/S0924-0136(01)00870-6.

22. Biamino, S., Penna, A., Ackelid, U. et al. (2011) Electron beam melting of Ti–48Al–2Cr–2Nb alloy: Microstructure and mechanical properties investigation. *Intermetallics*, 19(**6**), 776–781. DOI: https://doi.org/10.1016/j.intermet.2010.11.017

23. Reisgen, U., Olschok, S., Backhaus, A. (2010) Electron beam welding of titanium aluminides — Influence of the welding parameters on the weld seam and microstructure. *Materialwissenschaft und Werkstofftechnik*. DOI: https://doi.org/10.1002/mawe.201000683Citations: 10

24. Cao, J., Qi, J., Song, X., Feng, J. (2014) Welding and joining of titanium aluminides. *Materials*, **7**, 4930–4962.

25. Akhonin, S.V., Bilous, R.V., Selin, I.K. et al. (2022) Argon-arc welding of high-temperature titanium alloy doped by silicon. *The Paton Welding J.,* **5**, 26-33. DOI: https://doi.org/10.37434/tpwj2022.05.04

26. Liu, P., Zhang, G.M., Zhai, T., Feng, K.Y. (2017) Effect of treatment in weld surface on fatigue and fracture behavior of titanium alloys welded joints by vacuum electron beam welding. *Vacuum*, **141**, 176–180.

27. Huang, J.L., Warnken, N., Gebelin, J.C. et al. (2012) On the mechanism of porosity formation during welding of titanium alloys. *Acta Materialia*, 60(**6–7**), 3215–3225.

28. Li, Y.J., Wu, A.P., Quan, L.I. et al. (2019) Effects of welding parameters on welds hape and residual stresses in electron beam welded Ti_2AlNb alloy joints. *Transact. of Non Ferrous Metals Society of China*, 29(**1**), 67–76.

29. Pederson, R., Niklasson, F., Skystedt, F., Warren, R. (2012) Microstructure and mechanical properties of friction- and electron-beam welded Ti–6Al–4V and Ti–6Al–2Sn–4Zr–6Mo. *Materials Sci. and Eng., A*, **552**, 555–565.

30. Tsai, C.J. (2014) Improved mechanical properties of Ti–6Al–4V alloy by electron beam welding process plus annealing treatments and its microstructural evolution. *Materials & Design*, **60**, 587–598. DOI: http://dx.doi.org/10.1016/j.matdes.2014.04.037

31. Zamkov, V.N., Sabokar, V.K., Vrzhizhevsky, E.L. et al. (2005) Electron beam welding of titanium gamma-aluminide. In: *Proc. of CIS Conf. Ti-2005, Ukraine, Kyiv, 22–25 May*, 157–164.

32. Grigorenko, S.G., Grigorenko, G.M., Zadorozhnyuk, O.M. (2017) Intermetallics of titanium. Peculiar features, properties, application (Review). *Suchasna Elektrometal.,* **3**, 51–58. DOI: https://doi.org/10.15407/sem2017.03.08.

33. Chandra, U., Hartwig, I., Ulrich, K. (1973) Einsatz elektrisch erzeudneter Gasplasmen in der metallurgischen Verfanrenstechnik Umschmelzen von Titan-und Eisen- Schwamm zu Blocken in einen Plasmaofen. *Techn. Mitt. Krupp Forschugsber*, BA31, H.1, 1–7.

ORCID

S.V Akhonin: 0000-0002-7746-2946,
V.Yu. Bilous: 0000-0002-0082-8030,
A.Yu. Severyn: 0000-0003-4768-2361,
R.V. Selin: 0000-0002-2990-1131

CONFLICT OF INTEREST

The Authors declare no conflict of interest

CORRESPONDING AUTHOR

V.Yu. Bilous
E.O. Paton Electric Welding Institute of the NASU
11 Kazymyr Malevych Str., 03150, Kyiv, Ukraine.
E-mail: titan.paton@gmail.com

JOURNAL HOME PAGE

https://patonpublishinghouse.com/eng/journals/tpwj

SUBSCRIPTION–2025

If You are interested in making subscription directly via Editorial Board, fill, please, the coupon and send application by Fax or E-mail.

12 issues per year, back issues available.

$384, subscriptions for the printed (hard copy) version, air postage and packaging included.

$312, subscriptions for the electronic version (sending issues of Journal in pdf format or providing access to IP addresses).

Institutions with current subscriptions on printed version can purchase online access to the electronic versions of any back issues that they have not subscribed to. Issues of the Journal (more than two years old) are available at a substantially reduced price.

Subscription Coupon Address for Journal Delivery			
Term of Subscription Since	20	Till	20
Name, Initials			
Affiliation			
Position			
Tel., Fax, E-mail			

The archives for 2009–2023 are free of charge on
www://patonpublishinghouse.com/eng/journals/tpwj

ADVERTISING
in "The Paton Welding Journal"

Address
11 Kazymyr Malevych Str., 03150, Kyiv, Ukraine
Tel./Fax: (38044) 205 23 90
E-mail: journal@paton.kiev.ua
www://patonpublishinghouse.com/eng/journals/tpwj